

Carbon balance of a rain-fed maize field

Inauguraldissertation
zur
Erlangung der Würde eines Doktors der Philosophie
vorgelegt der
Philosophisch-Naturwissenschaftlichen Fakultät
der Universität Basel

von

Irene Lehner
aus Lüterkofen-Ichertswil (SO)

Basel, 2008

Genehmigt von der Philosophisch-Naturwissenschaftlichen Fakultät auf Antrag von
Prof. Dr. Eberhard Parlow, Basel und Prof. Dr. Christian Bernhofer, Dresden.

Basel, den 16. Juni 2008

Prof. Dr. Hans-Peter Hauri
Dekan

Acknowledgements

First, I would like to thank Prof Dr Eberhard Parlow who gave me the opportunity to work in his motivating group. His confidence enables a large degree of freedom and facilitates own thoughts and ideas and their realisation. He supported me in my activities and let me participate in several workshops and conferences and enabled my stay at CSIRO.

I would like to thank my co-referee Prof Dr Christian Bernhofer for his disposition and his encouragement in the final stage of this thesis.

That I once started with the PhD was also due to the motivation of Dr Roland Vogt and his infecting verve for micrometeorology. With his rich experience and knowledge he supported me in every respect from conceptual to detail questions. He fetched uncountable hints during uncountable discussions. A big thank you!

There was a lot of field work to do and Dominik Michel provided sedulous commitment. Thanks!

Max Soder did not always understand what the mad scientists were doing on his field, but he was very cooperative and supported us.

The discussions with Dr Christian Feigenwinter gave me many insights in the domain of CO₂ advection. Björn Lietzke joined us during the last vegetation period for his master's thesis about this subject and he did a great job. The advection experiment was only possible with the support of Prof Dr Dieter Scherer (Technical University of Berlin) and Prof Dr Andrea Pitacco (University of Padova) who contributed with additional instrumentation and Dr Andreas Christen (University of British Columbia) who developed a LabView based software for the corresponding data acquisition.

Thomas Kleiber shared the office with me and was confronted with the ups and downs during my PhD. Thanks for his support, and as we know "Eins kann mir keiner ...". I did not always understand what Günter Bing and Kaspar Bucher-Studer were talking about computers, but they provided an excellent sup-

port. For administrative and other problems Josette Pfefferli-Stocky always found a solution rapidly.

This study is part of the INTERREG IIIa project Nr. 3c.10 "Impacts of climate change on vegetation in the Upper Rhine Valley". The collaboration with the project partners was pleasant. Special thanks go to Dr Jutta Holst (University of Freiburg i.Br.) for many valuable discussions.

Dr Eva van Gorsel, Dr Helen Cleugh and Dr Ray Leuning made my research stay at CSIRO in Canberra to become true. I enjoyed the time working with their team and the stay in the famous place Tumbabloody-rumba. Special thanks go to Dr Eva van Gorsel for her friendship, her hospitality and many fruitful discussions from the very beginning of this work.

As a scientist working in the air, I greatly appreciate the help of Dr Rainer Weissshaidinger and Heidi Strohm for soil analysis. Heidi Strohm and Marianne Caroni were also tolerating the smell of popcorn in their lab during two vegetation periods - thanks! Paul Müller did many valuable jobs for technical assistance.

The seco (Swiss State Secretariat for Economic Affairs) provided funding of this study for three years. The successful end of this thesis was only possible by a three month prolongation by the Institute of Meteorology, Climatology and Remote Sensing at the University of Basel and by the financial support of the Freiwillige Akademische Gesellschaft, Basel.

Finally, I would like to thank the whole team at the Institute of Meteorology, Climatology and Remote Sensing at the University of Basel. It was a pleasure to be a part of it! And I am indebted to my parents and my friends who support and accompany me since many years.

Zurich, April 2008

Abstract

This thesis analyses micrometeorological measurements carried out from June 2004 until October 2006 in the framework of the INTERREG IIIa Project Nr. 3c.10 "Impacts of climate change on vegetation in the Upper Rhine Valley".

The study addresses the exchange processes of carbon, water and energy of a rain-fed field under maize-fallow rotation. Measurements with an ultrasonic anemometer-thermometer, an open-path CO₂/H₂O infra-red gas analyser and of the meteorological drivers such as photosynthetic photon flux density (PPFD), temperature and precipitation give insight in the interaction between atmosphere, soil and vegetation.

Energy balance considerations show similar patterns of the energy flux densities for vegetation periods and bare field conditions. Energy balance closure is 80 % and 52 %, respectively. A closer look shows a clear diurnal pattern with bad closure during nighttime and an increasing closure fraction during daytime, in fact resulting in an overshooting in late afternoon.

Evapotranspiration shows a clear seasonal pattern with maximum values of $\sim 3.5 \text{ mm d}^{-1}$ reached in mid-July. The total water need for the three subsequent years is 321, 397, and 422 mm per kg kernels (yield). The water use efficiency shows a strong relationship with PPFD and the amount of biomass.

The focus of the study is on carbon balance. During the three subsequent vegetation periods 930, 785, and 841 g C m⁻² are sequestered, respectively. The yield is 455, 417, and 340 g C m⁻². About 40 % of the biomass remaining on the field at harvest are decomposed during the dormant season. The resulting numbers for the carbon balance show a "yearly" sink of this agroecosystem of $\sim 250 \text{ g C m}^{-2}$. Besides unlimited photosynthetic active radiation the combination of the optimal temperature range with the needed precipitation amount corresponding to the need of the actual growth stage are essential for optimal maize growth.

Zusammenfassung

Diese Arbeit analysiert mikrometeorologische Messungen, welche von Juni 2004 bis Oktober 2006 im Rahmen des INTERREG IIIa Projekts Nr. 3c.10 "Auswirkungen von Klimaänderungen auf Pflanzenbestände am Oberrhein" durchgeführt wurden.

Die Studie behandelt die Austauschprozesse von Kohlenstoff, Wasser und Energie eines nicht bewässerten Feldes mit Mais-Brache-Rotation. Die Messungen mit einem Ultrasonic Anemometer-Thermometer und einem open-path CO₂/H₂O Infrarotgasanalysator und von meteorologischen Steuergrößen wie der photosynthetisch aktiven Strahlung (PAR), der Temperatur und des Niederschlags ermöglichen Einblicke in das Zusammenspiel von Atmosphäre, Boden und Vegetation.

Die Energiebilanz zeigt ein ähnliches Muster für die Vegetationsperiode und die Brache. Die Schliessung der Energiebilanz beträgt 80 % resp. 52 %. Eine nähere Betrachtung zeigt einen eindeutigen Tagesgang mit einer schlechten Schliessung während der Nacht und einer steigenden Schliessung während des Tages, welche am späten Nachmittag sogar in einer Überschliessung resultiert.

Die Verdunstung zeigt einen eindeutigen saisonalen Verlauf mit den Maximalwerten von $\sim 3.5 \text{ mm d}^{-1}$ Mitte Juli. Der Wasserverbrauch in den drei Jahren ist 321, 397 und 422 mm pro kg Mais. Die Wassernutzungseffizienz zeigt einen starken Zusammenhang mit der PAR und der vorhandenen Biomasse.

Der Schwerpunkt der Studie ist die Kohlenstoffbilanz. In den drei Vegetationsperioden werden 930, 785 und 841 g C m⁻² gebunden. Der Ernteertrag beträgt 455, 417 und 340 g C m⁻². Gegen 40 % der bei der Ernte auf dem Feld verbleibenden Biomasse werden während der Brache abgebaut. Die resultierenden Werte der Kohlenstoffbilanz zeigen eine jährliche Senke von $\sim 250 \text{ g C m}^{-2}$. Neben der PAR ist die Kombination der optimalen Temperatur und der benötigten Niederschlagsmenge entsprechend der aktuellen Wachstumsphase grundlegend für ein optimales Wachstum.

Contents

List of Figures	ix
List of Tables	xiii
List of Symbols	xv
List of Abbreviations	xvii
1 Introduction	1
2 Theory	5
2.1 Net ecosystem exchange	5
2.1.1 Definitions	5
2.1.2 C4 photosynthesis	5
2.1.3 Respiration	6
2.1.4 Controlling factors	6
2.2 Atmospheric boundary layer	8
2.2.1 Outer layer	8
2.2.2 Inner layer	8
2.3 Eddy covariance method	11
2.4 Mass conservation equation	13
3 Methods	15
3.1 Site description	15
3.2 Instrumentation	17
3.2.1 Long-term measurements	17

3.2.2	Advection experiment	19
3.3	Data processing	20
3.3.1	Turbulence measurements	20
3.3.2	Quality control of turbulence measurements	21
3.3.3	Corrections of turbulent flux densities	23
3.3.4	CO ₂ storage term	25
3.3.5	Radiation measurements	26
3.3.6	Soil measurements	26
3.3.7	Temperature / humidity sensors	28
3.3.8	Closed-path gas analyser	28
3.3.9	Advective terms	28
3.4	Gap filling	31
3.4.1	Periods of assimilation	31
3.4.2	Periods of respiration	33
3.4.3	Long gaps	34
3.4.4	Examples	34
3.4.5	Error estimation	35
3.4.6	Gap filling of latent heat flux densities	36
4	Results and Discussion	39
4.1	Meteorological conditions	39
4.2	Energy balance	42
4.2.1	Energy balance components	42
4.2.2	Energy balance closure	44
4.3	Water balance	46
4.4	Carbon balance	48
4.4.1	Seasonal pattern and inter-annual variability	48
4.4.2	Driving forces	51
4.4.3	Examples	52

4.4.4	Advection	54
5	Summary and Conclusions	59
5.1	Methodology	59
5.2	Synthesis	60
5.3	Outlook and future research	61

List of Figures

2.1	Overview of the CO ₂ fluxes resulting in net ecosystem exchange.	5
2.2	Light attenuation within a maize canopy.	6
2.3	Mature maize plant.	7
2.4	Scheme of the structure of the atmosphere.	8
3.1	Map of the surrounding of the experimental site in Eimeldingen.	15
3.2	Aerial view of the site southbound.	15
3.3	Development of canopy height from emergence in May until final canopy height is reached in August for vegetation periods 2004, 2005 and 2006.	15
3.4	Schematic view of the main tower.	17
3.5	Schematic top view of the advection set-up.	19
3.6	Photo of the southern advection tower and the main tower with the cup profile.	19
3.7	Wind direction vs normalised mean vertical wind component w_* for time period June to November 2005 (a) before and (b) after the coordinate rotation.	20
3.8	Comparison of $\overline{w'c'}$ derived from double rotation and planar fit method for vegetation periods and for bare field conditions.	21
3.9	Definitions of the tilt angles α, β and γ for the xyz convention.	21
3.10	Mean of the footprint during vegetation periods for unstable and stable conditions.	23
3.11	Available energy vs turbulent heat flux densities during vegetation periods.	23
3.12	Comparison of estimates of the CO ₂ storage term by the profile method and single-level method.	26
3.13	Set-up for the radiation comparison.	26
3.15	Set-up for the comparison of the PPFD sensors.	26
3.14	Signal of the reference sensor vs the difference between the CNR1 and the reference sensor for: (a) R_{sd} , (b) R_{su} , (c) R_{ld} , (d) R_{lu} and (e) R_n . In graph (f) R_n of the sensor combination vs R_n of the CNR1 are displayed.	27

3.16	Final mean vertical wind profile. The original shape is derived from cup anemometer measurements and linearly adapted to mean sonic measurements.	29
3.17	PPFD _{net} vs NEE for some days representing different growth stages during vegetation period 2005.	31
3.18	Measured vs modelled daytime NEE during vegetation periods.	33
3.19	Measured vs modelled respiration during night-time or bare field conditions.	34
3.20	Daily sums of NEE: Measured or gapfilled by parametrisation vs modelled with an ANN for the whole measurement period.	35
3.24	Measured vs modelled Q_E for vegetation periods.	36
3.21	Course of NEE measured and parametrised from 2005/06/01 until 2005/08/02.	37
3.22	Course of NEE measured and parametrised from 2005/12/01 until 2006/02/01.	37
3.23	Course of daily totals of NEE for the whole measurement period: measured and parametrised values and output by an ANN.	37
4.1	Daily averages of (a) air temperature and soil temperature in 5 cm depth, (b) air temperature and VPD, (c) soil moisture in 10 cm depth and daily total of precipitation, (d) daily total of net PPFD and (e) daily mean albedo of short-wave radiation and PPFD.	40
4.2	Wind rose with 10° sectors of daytime situations on the left and of night-time situations on the right based on half hourly data from the whole measurement period.	41
4.3	Mean diurnal course of the energy balance components for vegetation periods and bare field conditions based on half hourly values: (a) net radiation R_n , (b) soil heat flux density G , (c) storage term ΔS , (d) energy used by photosynthesis Q_P , (e) sensible heat flux density Q_H , (f) latent heat flux density Q_E , (g) available energy and turbulent heat flux densities and (h) mean diurnal course of closure fraction (CF).	43
4.4	Daily sums of energy consumed by photosynthesis during vegetation period 2005.	44
4.5	Mean diurnal pattern of the partitioning of R_n into Q_H , Q_E and G during vegetation periods.	44
4.6	Bowen ratio (β) vs closure fraction (CF) for vegetation periods and bare field conditions, separated for unstable and stable conditions.	45
4.7	Friction velocity (u_*) vs closure fraction (CF) for vegetation periods and bare field conditions, separated for unstable and stable conditions.	45
4.8	Daily sums of evapotranspiration for the whole measurement period.	47
4.9	Cumulative curves of evapotranspiration and precipitation for each vegetation period and period of bare field conditions, respectively.	47
4.10	Pattern of the water use efficiency WUE over the whole measurement period.	47
4.11	Daily sums of NEE for the three subsequent years.	49

4.12	Cumulative curve of NEE, separating vegetation periods and bare field conditions.	50
4.13	Cumulative curve of NEE.	50
4.14	Cumulative curve of NEE for the three "years".	50
4.16	Daily quantum yield as a function of VPD of all three vegetation periods.	51
4.15	Pattern of the quantum yield over the whole measurement period.	52
4.17	Mean Q_{10} values as a function of soil temperature.	52
4.18	Course of (a) NEE, (b) quantum yield, (c) $PPFD_{net}$, (d) air temperature and (e) precipitation and soil moisture from July 10 to July 20 2005.	53
4.19	Course of (a) NEE, (b) quantum yield, (c) $PPFD_{net}$, (d) air temperature and (e) precipitation and soil moisture during October 2005.	53
4.20	Course of (a) NEE, (b) quantum yield, (c) $PPFD_{net}$, (d) air temperature and (e) precipitation and soil moisture from July to August 2006.	54
4.21	Course of (a) NEE, (b) air and soil temperature and (c) precipitation and soil moisture from November 2004 to March 2005.	54
4.23	Median vertical velocity \bar{w} for different classes of stability parameter ζ	55
4.24	Mean daily course of mean CO_2 concentration profile within the control volume from August 1 st to October 1 st 2006.	56
4.22	Mean diurnal course of different parameters concerning the CO_2 fluxes according to the mass conservation equation: (a) eddy flux F_c , (b) storage term S_c , (c) mean vertical wind velocity \bar{w} , (d) friction velocity u_* , (e) difference in CO_2 concentration between the top measurement level at 4.55 m and the mean concentration below ΔCO_2 , (f) horizontal advection F_{HA} and (g) vertical advection F_{VA} . Graph (h) shows the difference of total NEE according to $(F_c + S_c + F_{HA} + F_{VA})$ and NEE according to $(F_c + S_c)$	57
4.25	Mean diurnal course of F_{HA} depending on height. Top: total F_{HA} in the control volume. Right: mean daily profile.	58

List of Tables

3.1	Soil carbon content.	16
3.2	Overview of the instrumentation at the Eimeldingen site.	18
3.3	Rotation angle α and roll angle β for planar fit.	21
3.4	Applied limits to fast data.	22
3.5	Average impact of spectral loss correction to Q_H , Q_E , and F_c for stable and unstable conditions.	24
3.6	Average impact of humidity and density correction on Q_H , Q_E , and F_c for stable and unstable conditions.	25
3.7	Instrumentation during radiation comparison.	28
3.8	Parameter for Michaelis-Menten equation (Eq. 3.24) to fill daytime data gaps during vegetation periods 2004–2006.	32
3.9	Error estimation for the different gap-filling methods by the absolute and relative root mean square error (aRSME, rRSME), the mean absolute error (MAE) and the bias error (BE).	36
4.1	Monthly values of mean air temperature, total precipitation and total $PPFD_{net}$	41
4.2	Sums of the terms of the water balance for each vegetation period and period of bare field conditions, respectively.	47
4.3	Carbon balance.	49

List of Symbols

a'	quantum yield (= LUE)	$\mu\text{mol } \mu\text{mol}^{-1}$
a, b	regression coefficients	
b_0, b_1, b_2	regression coefficients	
c	CO ₂ concentration	ppm, mmol m^{-3}
c	speed of sound	m s^{-1}
CF	closure fraction	
c_p	specific heat of moist air at constant pressure	$\text{J kg}^{-1} \text{K}^{-1}$
c_v	volumetric heat capacity	$\text{J m}^{-3} \text{K}^{-1}$
Co_{wx}	cospectrum	
d	displacement height	m
F	vertical flux density	
F_c	vertical flux density of CO ₂	$\text{mmol m}^{-2} \text{s}^{-1}, \text{mg m}^{-2} \text{s}^{-1}$
F_{HA}	horizontal advection of CO ₂	$\text{mmol m}^{-2} \text{s}^{-1}, \text{mg m}^{-2} \text{s}^{-1}$
F_{VA}	vertical advection of CO ₂	$\text{mmol m}^{-2} \text{s}^{-1}, \text{mg m}^{-2} \text{s}^{-1}$
f	normalised frequency	s^{-1}
G	soil heat flux density	W m^{-2}
g	acceleration due to gravity	m s^{-2}
h_c	canopy height	m
i	index variable	
k	von Karman number	
L	Monin-Obukhov length	m
L_s	canopy shear length scale	m
l_v	latent heat of vaporisation	J kg^{-1}
LUE	light use efficiency (= a')	$\mu\text{mol } \mu\text{mol}^{-1}$
m	molar mass of air	g mol^{-1}
m_a	molar mass of dry air	g mol^{-1}
m_v	molar mass of water vapour	g mol^{-1}
N	number of values	
NEE	net ecosystem exchange	$\text{mmol m}^{-2} \text{s}^{-1}, \text{mg m}^{-2} \text{s}^{-1}$
p	pressure	Pa
PPFD_{in}	incoming photosynthetic photon flux density	$\text{mmol m}^{-2} \text{s}^{-1}$
PPFD_{out}	reflected photosynthetic photon flux density	$\text{mmol m}^{-2} \text{s}^{-1}$
PPFD_{net}	net photosynthetic photon flux density	$\text{mmol m}^{-2} \text{s}^{-1}$
q	specific humidity	g kg^{-1}
Q_E	latent heat flux density	W m^{-2}
Q_H	sensible heat flux density	W m^{-2}
Q_P	energy used by photosynthesis	W m^{-2}
Q_{10}	magnitude of change in respiration rate for a 10 K change in temperature	
\mathcal{R}	universal gas constant	$\text{J K}^{-1} \text{mol}^{-1}$
R_n	net radiation	W m^{-2}
R_{ld}	incoming long-wave radiation	W m^{-2}
R_{lu}	outgoing long-wave radiation	W m^{-2}

R_{sd}	incoming short-wave radiation	W m^{-2}
R_{su}	outgoing short-wave radiation	W m^{-2}
ΔS	storage of sensible and latent heat	W m^{-2}
S_B	physiological source/sink of CO_2	$\text{mmol m}^{-2} \text{s}^{-1}$, $\text{mg m}^{-2} \text{s}^{-1}$
S_c	storage of CO_2	$\text{mmol m}^{-2} \text{s}^{-1}$, $\text{mg m}^{-2} \text{s}^{-1}$
t	time	s
Δt	time period	s
T_a	air temperature	$^{\circ}\text{C}$, K
$T(f)$	product of all transfer functions	
T_b	transfer function for block-averaging over a finite time period	
T_p	transfer function for path-length averaging for a scalar	
T_s	soil temperature	$^{\circ}\text{C}$, K
T_w	transfer function for path-length averaging for vertical wind	
U	3d wind vector	m s^{-1}
u	longitudinal wind component	m s^{-1}
u_*	friction velocity	m s^{-1}
v	lateral wind component	m s^{-1}
VPD	vapour pressure deficit	Pa
w	vertical wind component	m s^{-1}
w_*	normalised vertical wind component	
WUE	water-use efficiency	kg kg^{-1}
x	distance in longitudinal wind direction	m
x	any property of interest	
y	distance in lateral wind direction	m
z	height above ground or depth	m
z_m	measurement height	m
z_0	roughness length	m
α	rotation angle for planar fit	$^{\circ}$
β	roll angle for planar fit	$^{\circ}$
β	Bowen ratio	
γ	yaw angle for planar fit	$^{\circ}$
γ	adiabatic index	
ζ	stability parameter	
θ	virtual acoustic temperature	K
θ_*	scaling temperature	K
λ	wave length	m
ρ	density of moist air	kg m^{-3}
ρ_a	density of dry air	kg m^{-3}
ρ_v	density of water vapour	kg m^{-3}
σ	standard deviation	
τ	shear stress	$\text{kg m}^{-1} \text{s}^{-2}$

List of Abbreviations

ANN	artificial neural network
aRSME	absolute root mean square error
BE	bias error
CET	Central European time (GMT+1)
CF	closure fraction
CO ₂	carbon dioxide
CSI	Campbell Scientific Inc., Logan, UT, USA
ETH	Eidgenössische Technische Hochschule Zürich, Switzerland
FACE	free-air concentration enrichment
FAO	Food and Agriculture Organization of the United Nations
GPP	gross primary production
H ₂ O	water
IPCC	Intergovernmental Panel on Climate Change
IRGA	infra-red gas analyser
LUE	light-use efficiency
MAE	mean absolute error
MOST	Monin-Obukhov similarity theory
N ₂	nitrogen
NEE	net ecosystem exchange
NEP	net ecosystem production
O ₂	oxygen
PAR	photosynthetic active radiation
PEP	phosphoenolpyruvate
rRSME	relative root mean square error
Rubisco	Ribulose-1,5-bisphosphate carboxylase/oxygenase
SDM	synchronous device for measurement
seco	Swiss State Secretariat for Economic Affairs
sonic	ultrasonic anemometer-thermometer
TER	total ecosystem respiration
UNFCCC	United Nations Framework Convention on Climate Change
WMO	World Meteorological Organization, Geneva, Switzerland
WRC	World Radiation Center, Davos, Switzerland
WUE	water use efficiency

1 Introduction

The Fourth Assessment Report of the Intergovernmental Panel on Climate Change (IPCC) concludes that global climate change is a given fact and that human activities since the industrialisation influence the global warming with very high confidence (IPCC, 2007). The most important anthropogenic greenhouse gas is carbon dioxide (CO₂). The atmospheric CO₂ concentration has increased substantially from a pre-industrial level of about 280 ppm to 381 ppm in 2006 (WMO, 2007). The main source of this increase is combustion of fossil fuel (75 %) and the remainder originates from land use changes (IPCC, 2007).

Land and ocean carbon cycles and their processes lead to a massive exchange of CO₂ between land and atmosphere ($\sim 120 \cdot 10^9$ t C yr⁻¹) as well as ocean and atmosphere ($\sim 90 \cdot 10^9$ t C yr⁻¹) and they mitigate CO₂ induced climate change. About 40 % of the anthropogenic CO₂ emissions in the 1990s remained in the atmosphere, about 30 % have been taken up by oceans, and another 25 % by terrestrial ecosystems. As estimates of CO₂ uptake by oceans show little change in the carbon sink, the processes in the terrestrial ecosystems dominate the variability in the growth rate of atmospheric CO₂ concentration. However, the related processes are sensitive to changes in climate, i.e. terrestrial ecosystem photosynthetic productivity changes in response to changes in temperature, precipitation, CO₂ concentration and nutrients (Denman et al., 2007).

Agriculture claims about one third of the global land area and is a main contributor to anthropogenic induced emission of greenhouse gases. It accounts for 25 % of the carbon dioxide, 50 % of the methane and 70 % of the nitrous oxide emissions (Hutchinson et al., 2007). The Kyoto protocol of the United Nations Framework Convention on Climate Change (UNFCCC) has risen the interest in the potential of agroecosystems to sequester carbon and thus, to attenuate the greenhouse effect (Vleeshouwers and Verhagen, 2002). On a global scale the major crop is maize with a yield of approximately $700 \cdot 10^6$ t in 2006 (data from the FAOSTAT data base of the FAO, www.fao.org). Therefore, the quantification of

carbon sequestration by this type of agroecosystem as well as the determination of the underlying processes and their interactions to environmental conditions and the management practice are important, but not yet fully understood.

State of current research

The scientific and political discussion about climate change and its impact on ecosystems has pushed the efforts to improve the knowledge about the carbon dioxide cycle and its dynamics (Houghton et al., 1990). For example to know in detail future demands on profitable crop varieties.

There are several methods to determine the carbon cycle and the related processes with specific strengths and weaknesses. For example, at large scales satellite data provide information derived from radiative measurements. Isotope analysis can be used to allocate different carbon sources. At smaller scales biomass survey or eddy covariance technique estimate carbon fluxes (Baldocchi et al., 2001).

Eddy covariance is a micrometeorological technique providing a direct measure of carbon, water and energy flux densities between the surface and the atmosphere. The idea of a direct measurement of turbulent flux densities was developed more than 50 years ago by Montgomery (1948), Obukhov (1951) and Swinbank (1951) (cited in Foken, 2006). First studies of CO₂ exchange were made in the 1960s applying the flux-gradient method. Technical difficulties arising from instrumentation and data collection delayed a routine use of the eddy covariance method to the 1980s (e.g. Desjardins, 1985; Verma et al., 1986, 1989). These studies were limited to short time periods, mainly carried out during the vegetation period. Further improvement, in instrumentation and in computer technology, made long-term, continuous measurements feasible in the early 1990s (e.g. Wofsy et al., 1993; Black et al., 1996; Goulden et al., 1996; Greco and Baldocchi, 1996).

Results of these observations showed the potential of the eddy covariance method to clarify the basic processes of terrestrial ecosystems and their role in the global carbon cycle. In the mid 1990s an initiative was started to establish a continuous, long-term measurement network (Baldocchi et al., 1996). The first systematic study, the EUROFLUX project, started in 1996 and focused on different types of forests under different climate regimes considering the important role of forests in the global carbon cycle. This project aimed at a standardisation of equipment (Grelle and Lindroth, 1996; Moncrieff et al., 1997) and methodology (Aubinet et al., 2000). As eddy covariance measurements became technically more feasible they emerged as the state-of-the-art technique to determine the net CO₂ flux density directly. During the following years several other regional networks (e.g. AmeriFlux, OzFlux, AsiaFlux) were established and consolidated in the global network FLUXNET. The number of sites increased rapidly to over 400 towers today covering a broad range of terrestrial ecosystems including e.g. grasslands and agricultural crops (Baldocchi et al., 2001). But still most of the studies particularly in Europe focus on forests. As mentioned above, agricultural ecosystems strongly influence the local CO₂ budget. The cultivated crop and the applied management practice cause a large diversity in the CO₂ flux densities of the agroecosystems (Schimel et al., 2000; Baldocchi et al., 2001).

Some of the first studies using the eddy covariance technique over maize were deployed by Desjardins et al. (1978) and Desjardins (1985). The aim of the research did not change since those days: on the one hand to quantify the net CO₂ flux density (net ecosystem exchange, NEE) and on the other hand to detect the key environmental and physiological factors controlling NEE. An advantage of the eddy covariance method is that the derived information about CO₂ flux densities is an integrated signal over a given area of a canopy. This is noteworthy because plant physiological studies are often technically restricted to leaf scale, and an extrapolation to canopy scale is not straightforward (Baldocchi, 1994). The first studies were limited to very short time periods (Desjardins et al., 1978) or were not continuous and values had to be interpolated (Desjardins, 1985). Further studies determined the CO₂ flux densities by the use of the Bowen-ratio method and/or chamber measurements (Held et al., 1990;

McGinn and King, 1990). Technical and instrumental progress enabled continuous measurements by the use of a sonic anemometer-thermometer (hereafter sonic) and an infra-red gas analyser (hereafter IRGA) (studies over maize e.g. by Baldocchi, 1994; Steduto and Hsiao, 1998*a,b*; Suyker et al., 2004, 2005; Verma et al., 2005).

With these continuous measurements the derivation of annual sums of NEE or the integration over a vegetation period became possible and the new challenge to fill missing or rejected data has risen. Standardised methods have been proposed e.g. by Aubinet et al. (2000) and Papale et al. (2006) for data treatment, by Mauder and Foken (2004) and Moncrieff et al. (1996) for quality control and by Falge et al. (2001*b*) and Moffat et al. (2007) for different gap-filling methods. This common strategy ensures the comparability between different sites and enables an up scaling on regional and global scale or provides an essential basis for modellers interested e.g. in crop development or biogeochemical cycles (Baldocchi et al., 2001; Suyker et al., 2005).

Particularly, gap-filling techniques are based on a broad range of approaches. Very common is the use of a regression analysis of NEE with key environmental factors like photosynthetic active radiation for daytime assimilation (e.g. a Michaelis-Menten function cited in Falge et al., 2001*b*) or soil temperature for night-time respiration (e.g. Lloyd and Taylor, 1994). Simple interpolation or look-up tables are applied (Falge et al., 2001*b*) and more recently, artificial neural networks (Papale et al., 2006) or process-based models (Gove and Hollinger, 2006; Stauch and Jarvis, 2006) are under consideration. Special attention is also given to night-time situations with low turbulence intensity because the eddy covariance method often fails under these conditions (Falge et al., 2001*b*; Gu et al., 2005; van Gorsel et al., 2007) as well as to advective transport processes, in particular in tall canopies (e.g. Aubinet et al., 2003; Finnigan et al., 2003; Feigenwinter et al., 2004; Heinesch et al., 2007; Feigenwinter et al., 2008).

Framework

The present thesis is embedded in the INTERREG IIIa Project Nr. 3c.10 "Impacts of climate change on vegetation in the Upper Rhine Valley", a collaboration of the universities of Freiburg i.Br. (Germany), Strasbourg (France) and Basel (Switzerland). The project was funded by the European Union and the Swiss State Secretariat for Economic Affairs (seco).

The climate of the Upper Rhine Valley is characterised by high temperatures and low precipitation. Thus, in-situ measurements of future climate conditions in other parts of Europe can be carried out. The project investigates the interactions between soil, vegetation and atmosphere in more detail, with focus on carbon and water balance. Different types of vegetation (maize, winter wheat and pine) with differences in the water demand and the type of photosynthesis were chosen. Besides long-term micrometeorological measurements, short-term studies on plant physiology (in particular isotope measurements) were carried out.

The present thesis covers the micrometeorological measurements in the maize canopy.

Objectives

The main objective of this study is the determination of the carbon balance. As mentioned above most of the studies about ecosystem carbon exchange derived from eddy covariance measurements focus on forests. Accordingly, the common methodology is developed and verified mostly for this type of land use. The assumptions, the methodology and their applicability are tested at a site under maize-fallow rotation and with limited fetch conditions.

A focus of this thesis is on general aspects of eddy flux calculations like quality control and flux corrections. By the goal of a long-term, e.g. yearly carbon budget the challenge of an appropriate gap filling technique arises as the eddy covariance method and the sensors used fail under some conditions. As maize with a different way of photosynthesis as well as bare field conditions differ significantly from a forest, the wide-spread approaches are investigated. An other topic is the determination of all terms of the mass conservation equation. In most studies, par-

ticularly in short canopies, the advective terms are neglected. To verify this assumption a short-term advection study was carried out. Besides, some considerations about the energy and water balance are made.

2 Theory

2.1 Net ecosystem exchange

This section gives a short overview about the biological behaviour relevant for processes involved in NEE. If not mentioned otherwise it is based on the textbooks by Larcher (1994), Barbour et al. (1999), Ehleringer and Cerling (2001) and Bonan (2002).

2.1.1 Definitions

Net CO₂ flux density of an ecosystem (net ecosystem exchange NEE) is the result of two processes: the sequestration of organic carbon by photosynthesis (gross primary production GPP) and the release of organic carbon by autotrophic and heterotrophic respiration (total ecosystem respiration TER). Any sinks and sources of inorganic CO₂ (e.g. precipitation or dissolution of carbonates) are included in eddy covariance measurements of NEE, but according to Lovett et al. (2006) they are important in oceans only. Therefore, NEE can be assumed to be the same as -NEP (net ecosystem production, the more common term in biology). The different sign is given by the widespread sign convention in micrometeorology: an uptake of CO₂ by the ecosystem is negative, a loss of CO₂ is positive. These definitions are summarised in Eq. 2.1 and Fig. 2.1.

$$-NEP = NEE = GPP - TER \quad (2.1)$$

2.1.2 C4 photosynthesis

Photosynthesis is the process of fixing carbon from atmospheric CO₂ into stable organic products. Three main processes are involved: (i) absorption of electromagnetic energy of the photosynthetic active radiation (PAR) by pigments (mainly chlorophyll and carotins), (ii) conversion of the electromagnetic energy to chemical energy by the light reactions, and (iii) fixation of carbon by the dark reactions. The diffusion of CO₂ into leaves is regulated by the stomata. Contrary to the C3 path-

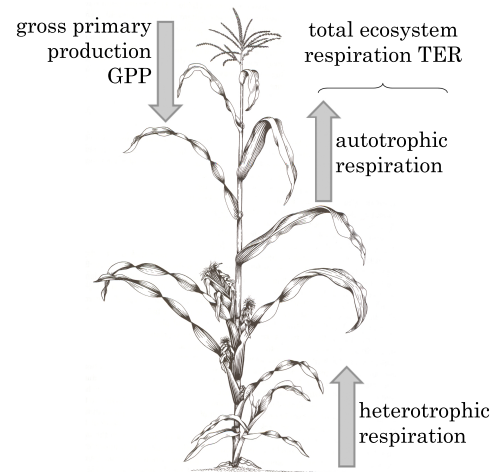


Figure 2.1: Overview of the CO₂ fluxes resulting in net ecosystem exchange NEE.

way, the light reactions and the dark reactions in the C₄ pathway of photosynthesis are spatially separated. The light reactions take place in the mesophyll cells, where a very efficient enzyme (phosphoenolpyruvate PEP) effects the fixation of CO₂ in a C₄ acid (oxaloacetate), thus electromagnetic energy is converted to chemical energy. This acid diffuses to the inner bundle-sheath cells, where it is decarboxylated and refixed in the C₃ pathway of photosynthesis (dark reactions). The CO₂ concentration within these cells is about 1000 ppm and thereby in the saturation range of the C₃ pathway. Hence, the C₄ pathway is a CO₂ concentration process within the cells. The nomenclature C₃ and C₄ originates from the first stable product formed in the photosynthesis pathway, an acid with a skeleton of three or four atoms of carbon.

Simultaneously to photosynthesis photorespiration occurs. Rubisco, an essential enzyme for the dark reactions, is oxidised by oxygen (O₂) resulting among others in CO₂. The intensity of this process is negatively correlated to the ratio of CO₂ to O₂ within the cells. Since C₄ plants show a high value for this ratio, photorespiration in C₄ plants is low or inhibited, whereas C₃ plants lose from 20 % up to 50 % of the CO₂ they fix. Additionally, the spatial separation of light reactions and dark reactions reduces the loss of water vapour via the stomata.

The energy used by photosynthesis is given by the energy used by the chemical processes. About 479 kJ are required per mole of CO₂ fixed by photosynthesis.

2.1.3 Respiration

Autotrophic respiration is the complementary process to photosynthesis, i.e. organic products are oxidised to gain energy needed to maintain living cells and for growth of new plant tissues. Hence, respiration is a different process than the above mentioned photorespiration which occurs simultaneously with photosynthesis within leaf cells. Heterotrophic respiration arises primarily from the decomposition of dead organic matter mainly by soil micro-organisms. This process is strongly related to soil temperature and soil moisture.

2.1.4 Controlling factors

Plants are optimising the ratio of CO₂ uptake and water loss by constantly adapting the stomatal resistance in response to changing environmental conditions such as sunlight, temperature or water availability. Biotic factors like growth form, photosynthetic pathway and growth stage modify the exchange of CO₂ between biosphere and atmosphere as well.

Sunlight — For photosynthesis not the radiative energy but the number of photons is important. Every photon, independent of its wavelength, has the same effect on photosynthesis. But only radiation with wavelengths between 400 nm and 700 nm (PAR) is used, the rest is reflected to prevent overheating. Compared to C3 plants, C4 plants show little light saturation, i.e. higher radiative input leads to a higher photosynthetic activity under conditions without any other limitation in water or nutrients. Consequently, the quantum yield or light-use efficiency (LUE), defined as the amount of fixed CO₂ per unit of absorbed PAR, of C4 plants is generally higher than of C3 plants.

The attenuation of sunlight by the canopy is defined by its architecture. For a maize canopy, particularly growth and orientation of the leaves, which

are strongly affected by plant density, are essential (Maddoni et al., 2001). Figure 2.2 shows the light attenuation within a maize canopy. The erectophile leaves enable sunlight to pass deep into the canopy. Generally, shaded leaves have lower photosynthetic capacity than sunlit leaves. Under cloudy conditions, notably high clouds, more diffuse radiation, which penetrates deeper into the canopy, is available for photosynthesis. Several studies show an increase of CO₂ uptake under these conditions (Hollinger et al., 1994; Fan et al., 1995; Goulden et al., 1997; Freedman et al., 2001; Suyker et al., 2004).

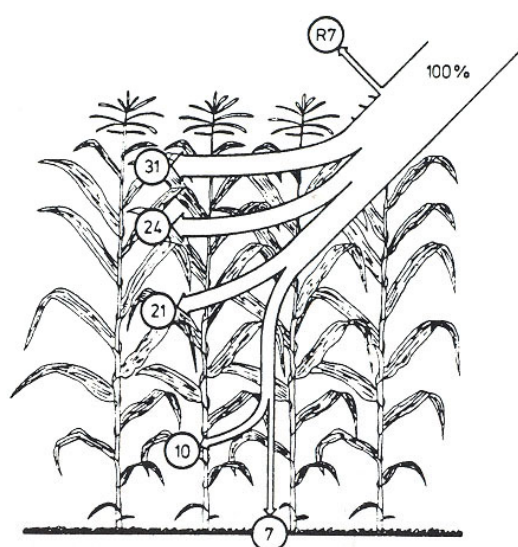


Figure 2.2: Light attenuation within a maize canopy (from Allen et al. 1964, cited in Larcher 1994).

Temperature — Temperature is an important driving factor both for assimilation and respiration. Optimum temperatures for photosynthesis of C4 plants are higher than for C3 plants, for maize they range from 22 °C to 28 °C. Crafts-Brandner and Salvucci (2002) show in their study that the inhibition of net photosynthesis by heat stress is not associated with stomatal closure but with inactivation of rubisco. By the higher CO₂ concentration in the bundle-sheath cells of C4 plants this inactivation is partially compensated. However, above 40 °C photosynthesis is stopped and above 50 °C fatal damage of leaf cells occurs. The lower limits are 10 °C and 0 °C, respectively (Schulze et al., 2002).

Temperature dominates auto- and heterotrophic respiration (Lloyd and Taylor, 1994; Goulden et al., 1996; Janssens et al., 2001; Law et al., 2001). The

temperature sensitivity of ecosystem respiration can be described by the Q_{10} coefficient describing the magnitude of change in respiration rate for a 10 K change in soil temperature:

$$Q_{10} = \left(\frac{\text{TER}_T}{\text{TER}_{ref}} \right)^{\left(\frac{10}{T - T_{ref}} \right)}, \quad (2.2)$$

where TER_T is the respiration rate at temperature T and TER_{ref} denotes the respiration at reference temperature T_{ref} .

Generally, Q_{10} declines with increasing temperature and decreasing soil moisture (e.g. Tjoelker et al., 2001; Janssens and Pilegaard, 2003; Xu and Baldocchi, 2004). A mean value of Q_{10} for ecosystems is ~ 2 . Besides, soil respiration depends on the amount of organic material (e.g. litter or the remainder of cultivated plants after harvest) available for decomposition (Larionova et al., 2007), on soil moisture, microbial activity and the amount of respiring biomass.

Water supply — Evapotranspiration rises with increasing temperature and is driven by the gradient in water vapour concentration between the atmosphere and the air within the leaves and the soil, respectively. With an ample water supply the influence of soil moisture and water vapour pressure on carbon assimilation is only of minor importance. Deficits have a negative impact on physiological processes as stomatal closure is induced to reduce evapotranspiration. At the same time the uptake of CO_2 is reduced. Because C4 plants have a much higher CO_2 concentration within the leaves and a more efficient enzyme fixing CO_2 in the mesophyll cells, some stomatal closure can occur without any effect on assimilation. Thus, the water-use efficiency (WUE), defined as the slope of the relationship of GPP and transpiration, is generally higher for C4 plants (Larcher, 1994; Young and Long, 2000). In water limited conditions maize is able to develop a ramified and deep root system to improve water uptake (Sharp and Davies, 1985; Larcher, 1994).

Atmospheric CO_2 concentration — Given the special pathway of C4 plants their photosynthesis saturates at atmospheric CO_2 concentrations of about 400 ppm. Consequently, current atmospheric

CO_2 concentrations are near this value and variations have little impact on photosynthetic capacity (Young and Long, 2000; Bonan, 2002). In accordance, a FACE (free-air concentration enrichment) experiment showed that an elevated CO_2 concentration (550 ppm) did not stimulate photosynthesis, biomass production or yield in the absence of drought (Leakey et al., 2004, 2006).

Growth stage — The NEE over a whole vegetation period changes with the amount of photosynthetic active biomass and with the development stage of the plants. The CO_2 assimilation capacity varies throughout the vegetation period, e.g. it is significantly reduced in senescent leaves (Smart, 1994).

Different growth stages can be distinguished. Emergence of the plants from the soil surface takes place about ten days after germination. The subsequent vegetative stages are defined according to the number of unfolded leaves. The last vegetative stage is the emergence of the tassel (cf. Fig. 2.3). With the appearance of silk at the ear and the pollen shedding the reproductive stages begin. They are divided by the development of the kernels, i.e. mainly the ratio of sugar to starch. Physiological maturity is attained when a black layer is visible at the base of the kernels. Afterwards the kernels dry out (from about 35 %) to reach biological maturity (senescence). For final storage grain moisture should be below ~ 15 % to avoid evolution of aflatoxins.

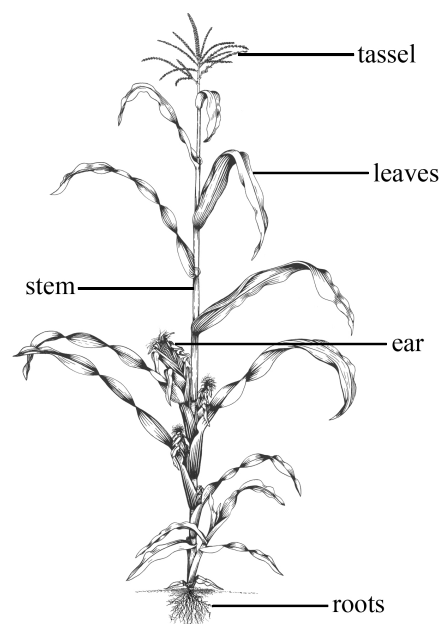


Figure 2.3: Mature maize plant.

2.2 Atmospheric boundary layer

The atmospheric boundary layer or planetary boundary layer is defined as the part of the atmosphere which reacts to and interacts with changes at the earth's surface within several hours (Stull, 1988). The state of the atmosphere depends on the following variables: the wind vector U with its longitudinal, lateral and vertical component (u, v, w) , air temperature T_a , specific humidity q , pressure p and density ρ . The manner how these variables depend on time (t) and space (x, y, z) can be described with the equation of state (ideal gas law) and the conservation equations for mass (continuity equation), momentum (Navier-Stokes' equations), moisture, and heat (first law of thermodynamics). However, the set of equations as a whole is so complex that no analytical solution can be found for boundary layer conditions. Depending on the scale of interest and on the order of magnitude, terms may be neglected or need to be parametrised.

The characteristics and the evolution of the atmospheric boundary layer show a daily pattern. In interaction to radiative gain or loss the surface warms or cools which forces changes in the boundary layer via transport processes. The transport of atmospheric properties like energy, mass and momentum within this layer is dominated in the horizontal by the mean wind and in the vertical by turbulent motions. The height of the atmospheric boundary layer grows as the air of the convective mixed layer entrains the free atmosphere above. During nighttime radiative cooling generates a shallow, statically stable layer with weak and sporadic turbulence, the nocturnal boundary layer. The flow aloft can be decoupled from the surface. Basically, the atmospheric boundary layer can be divided in an outer layer, an inner layer and a laminar boundary layer (Fig. 2.4). Their main properties are described below.

If not mentioned otherwise this and the following section are based on Oke (1987), Arya (1988), Stull (1988), Kaimal and Finnigan (1994), and Malhi et al. (2004).

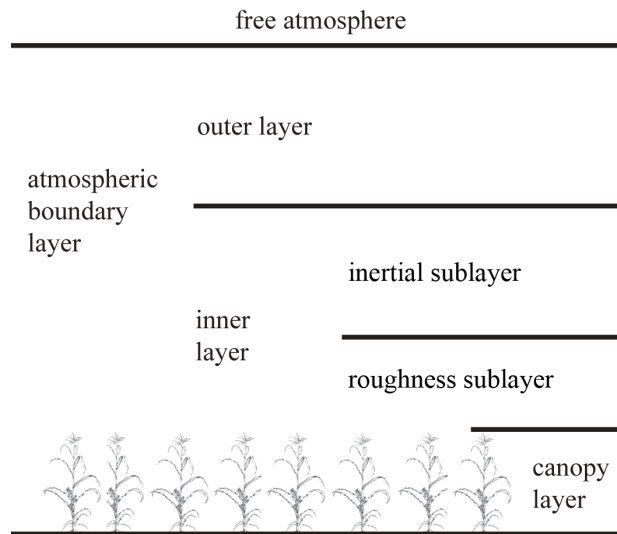


Figure 2.4: Scheme of the structure of the atmosphere without the lowest laminar boundary layer. The vertical extension of the individual layers is not scaled.

2.2.1 Outer layer

Within the outer layer the influence of friction increases with decreasing height, but turbulence is assumed to be independent of surface roughness. Besides the influence of earth's rotation diminishes and thus, the wind field gets more and more subgeostrophic. As these conditions change with height the vertical transport of momentum, heat and mass vary with height as well. Generally, they increase with decreasing height. During daytime a convective mixed layer driven by surface heating and characterised by strong convection is developed.

2.2.2 Inner layer

Within the lowest 10 % of the atmospheric boundary layer the influence of earth's rotation can be neglected and the flow is determined primarily by surface friction. In this inner layer (surface layer) strong gradients control the turbulent exchange of heat, mass and momentum at the surface and thereby the state of the whole boundary layer. Shear stress and vertical fluxes within this layer vary only little with height and are considered constant. The inner layer above a rough surface is further divided into an inertial sublayer and a roughness sublayer.

Inertial sublayer — Within the inertial sublayer (constant flux layer) the turbulence shows the above mentioned characteristics. Here the Monin-Obukhov similarity theory (MOST) is valid, i.e. the turbulence in the constant flux layer is taken to be driven by only four parameters:

- the height above the surface z (above rough surfaces the displacement height d has to be taken into account),
- the surface kinematic momentum flux $\overline{u'w'}$,
- the surface kinematic heat flux $\overline{w'\theta'}$ and
- the buoyancy parameter g/θ .

θ is the virtual acoustic temperature and g is the acceleration due to gravity. An overbar denotes a mean value, a prime denotes the fluctuation from the mean.

MOST states that a mean or turbulent property of the flow normalised by an appropriate variable is a universal function of the stability parameter ζ (e.g. Businger-Dyer functions in Panofsky and Dutton, 1984; Kaimal and Finnigan, 1994). The stability parameter ζ results from a non-dimensionalisation of the above mentioned parameters and is given by:

$$\zeta = \frac{z-d}{L}, \quad (2.3)$$

where L is the Monin-Obukhov length which is defined as:

$$L = -\frac{u_*^3}{k \frac{g}{\theta} \overline{w'\theta'}}, \quad (2.4)$$

where u_* is the friction velocity and k is the von Karman constant (taken as 0.4).

The scaling variables for wind velocity and for temperature are the friction velocity u_* (Eq. 2.5) and the scaling temperature θ_* (Eq. 2.6), respectively:

$$u_* = \left(\frac{\tau}{\rho}\right)^{(1/2)} = \left(-\overline{u'w'}\right)^{(1/2)}, \quad (2.5)$$

where τ is the shear stress and

$$\theta_* = \frac{-\overline{w'\theta'}}{u_*}. \quad (2.6)$$

Roughness sublayer — Within the roughness sublayer the flow is directly affected by individual roughness elements and the flow has to be treated as three dimensional. Thus, the flow is not in local equilibrium and local advection and horizontal turbulent transport processes are not negligible. The depth of the roughness sublayer is about twice the mean obstacle height depending on the size and the allocation of the roughness elements. The upper limit is given by the blending height where the influences from single roughness elements vanish.

The layer from the surface up to the mean obstacle height, h_c , is referred to as canopy layer. Most studies focusing on turbulence characteristics within and above plant canopies are carried out in forests, but a comparison by Kaimal and Finnigan (1994) shows a similar behaviour in maize (a study by Shaw et al. (1974)). Finnigan (2000) gives an overview of the turbulence within plant canopies which is characterised by intermittency and an extreme vertical inhomogeneity.

A feature in plant canopies is a strong inflection point in the mean velocity profile near canopy top. This inflection induces a turbulent shear flow which is characterised by intermittent coherent structures of the same scale as the canopy height (Högström and Bergström, 1996; Finnigan, 2000). The typical inflection-point profile, with a logarithmic profile above and an exponential profile within the canopy, develops because the canopy absorbs momentum not only at one surface but over the whole canopy height.

Momentum transport within and just above the canopy is dominated by sweeps, i.e. fast, downward moving gusts ($u' > 0$ and $w' < 0$), followed by ejections, i.e. relatively slow, upward moving air ($u' < 0$ and $w' > 0$). These structures can lead to counter-gradient transport. Jacobs et al. (2001) analysed two daily cycles of turbulence characteristics within and above a maize canopy. They concluded that during daytime the turbulence within and above the canopy is dominated by sweeps. During nighttime they found "plumes of relatively warm air occasionally rising from the warm canopy floor followed by relatively long periods of slow descending cold air". This illustrates that the exchange mechanism within and above the canopy in the roughness sublayer show a daily pattern mainly given by changing

atmospheric stability.

The characteristic properties of the roughness sub-layer are similar to the flow in a plane mixing layer (Raupach, 1989). Raupach et al. (1996) proposed that the strength of shear at $z = h_c$ can be described by canopy shear scale L_s :

$$L_s = \frac{\bar{u}(h_c)}{\left. \frac{\partial \bar{u}}{\partial z} \right|_{z=h_c}}. \quad (2.7)$$

They observed that L_s normalised by h_c is independent of wind velocity and thus, a function of canopy density and its aerodynamic drag only.

Eddies work against this aerodynamic drag. Thereby turbulent kinetic energy of large eddies is directly converted into fine-scale wake turbulence, where it is rapidly dissipated because of abounding intense shear layers of very fine scale in the foliage. Thus, the inertial eddy-cascade is bypassed and a spectral short cut results.

2.3 Eddy covariance method

Turbulent flows, induced by shear stress and buoyancy, consist of many different size turbulence elements, the eddies. They act as "means of conveyance" for physical properties such as momentum or CO₂. Thus, the vertical flux density at a given point in space can be determined as the product of the vertical wind component and the property of interest. As turbulence is highly variable and chaotic in space and time, it can be treated as a stochastic process. Hence, to get a reliable estimate of the vertical flux density an ensemble average should be calculated. In practice it is neither possible to make an average over many situations under identical conditions at one given point nor to carry out measurements at any point in a horizontal plane at a given height. Fortunately, the ergodic hypothesis can be made, i.e. spatial and time average converge over an appropriate time interval to the ensemble average. Taylor hypothesis of "frozen turbulence" allows time series measured at a single point to be interpreted as spatial variations, providing that the time series contains all information about the size distribution of the eddies.

Horizontal homogeneity simplifies the determination of vertical flux densities, because advective terms can be ignored. Hence, the statistical characteristics only vary in the vertical. Homogeneity is given if an adequate fetch is present and therefore the flow can be considered as adapted to the surface.

If the turbulent characteristics do not vary with time the time series are statistically stationary. Under this condition Reynolds decomposition can be applied to separate the instantaneous value of a variable x in its mean value (denoted by an overbar) and its fluctuation from the mean (denoted by a prime):

$$x(t) = \bar{x} + x'(t). \quad (2.8)$$

Applying the ergodic hypothesis and the assumption of homogeneity the vertical flux density can be calculated as the covariance between the vertical wind component w and a property of interest x :

$$\text{covariance}(w, x) = \frac{1}{N} \sum_{i=1}^N (w_i - \bar{w})(x_i - \bar{x}). \quad (2.9)$$

The Reynolds averaging conditions simplify the cal-

culaton of the vertical flux density. They can be summarised as: (i) all fluctuating quantities average to zero, (ii) correlations between fluctuating and average quantities vanish, and (iii) the average of an average equals the same average. Applying these assumptions and assuming that the average vertical wind component equals zero, the vertical flux density F becomes:

$$F = \text{covariance}(w, x) = \frac{1}{N} \sum_{i=1}^N w'_i x'_i = \overline{w'x'}. \quad (2.10)$$

Accordingly, the vertical turbulent flux densities of sensible heat Q_H , latent heat Q_E and carbon dioxide F_c are calculated as:

$$Q_H = \bar{\rho} c_p \overline{w'\theta'}, \quad (2.11)$$

$$Q_E = l_v \overline{w'q'}, \quad (2.12)$$

$$F_c = \overline{w'c'} \quad (2.13)$$

where c_p is specific heat of moist air at constant pressure, l_v is the latent heat of vaporisation and c denotes the CO₂ concentration.

Limitations — To meet all the required conditions for a strict application of the eddy covariance method the measurements have to be carried out in the inertial sublayer over flat terrain and over a canopy with a sufficient fetch. These requirements are often not fulfilled. Possible reasons are:

- Over tall canopies it is often not possible to install a tower reaching into the inertial sublayer.
- A limited fetch restricts the measurement height within which the source area is within the canopy under consideration.
- Given the roughness elements and the daily evolution of the atmospheric boundary layer the inertial sublayer probably shrinks or even vanishes.
- During stable night-time conditions turbulence is mostly weak and non-turbulent transport processes can become significant. Thus the vertical flux densities are often underestimated.

Therefore, to determine the NEE additional terms of the mass conservation equation have to be considered. Neglecting terms like storage, flux divergence

and advection can cause systematic error, which is particularly important when measurements are integrated over longer periods, e.g. if annual sums are calculated (Moncrieff et al., 1996; Massman and Lee, 2002).

2.4 Mass conservation equation

The conservation equation of mass is used to derive the exchange of CO₂ at the height of the eddy covariance measurements z_m . The instantaneous mass balance (Eq. 2.14) states that the CO₂ produced or absorbed by the physiological source/sink (term I) is either stored in the air (term II) or removed by flux divergence in all directions (term III).

$$\underbrace{S_B(t, x, y, z)}_I = \underbrace{\frac{\partial c}{\partial t}}_{II} + \underbrace{\frac{\partial uc}{\partial x} + \frac{\partial vc}{\partial y} + \frac{\partial wc}{\partial z}}_{III}. \quad (2.14)$$

The integration over a control volume and time of Eq. 2.14 has been discussed in detail by Finnigan (1999), Finnigan et al. (2003) and Feigenwinter et al. (2004). Applying Reynolds averaging, assuming continuity and a horizontally homogeneous concentration gradient and making the simplifications that horizontal turbulent flux divergence terms and horizontal variation of the vertical flux densities can be neglected the integration of Eq. 2.14 can be reduced to:

$$\begin{aligned} \underbrace{\int_0^{z_m} S_B(t, z) dz}_I &= \underbrace{\int_0^{z_m} \frac{\partial \bar{c}(z)}{\partial t} dz}_II + \\ &\underbrace{\int_0^{z_m} \frac{\partial \bar{w}'c'}{\partial z} dz}_III + \underbrace{\int_0^{z_m} \bar{w}(z) \frac{\partial \bar{c}(z)}{\partial z} dz}_IV + \\ &\underbrace{\int_0^{z_m} \left(\bar{u}(z) \frac{\partial \bar{c}(z)}{\partial x} + \bar{v}(z) \frac{\partial \bar{c}(z)}{\partial y} \right) dz}_V. \end{aligned} \quad (2.15)$$

Term I of Eq. 2.15 equals the NEE resulting from the change in storage of CO₂ (term II), the turbulent vertical flux density of CO₂ (term III) and the vertical and horizontal advection of CO₂ (term IV and V).

If the flow and the scalar fields are horizontally homogeneous the advective terms of Eq. 2.15 can be neglected. The storage term under steady conditions or over longer periods can be neglected as well (the

CO₂ stored during stable conditions at night is depleted in the morning with the onset of turbulence). In most studies sufficient homogeneity is assumed but the non-zero storage term under non-steady conditions is taken into account. NEE is then calculated as the sum of the turbulent vertical flux density of CO₂, F_c , and the storage term, S_c , and the determination of the NEE is reduced to a 1D-problem:

$$NEE = F_c + S_c. \quad (2.16)$$

This supposition is particularly critical during stable night-time conditions because in these situations most of the assumptions like stationarity for the eddy covariance method are not fulfilled (cf. section 2.3). Accordingly, numerous studies report an underestimation of night-time NEE by the use of Eq. 2.16 (e.g. Black et al., 1996; Goulden et al., 1996; Baldocchi et al., 1997; Aubinet et al., 2000). This inaccuracy is pronounced under low turbulence conditions as there are no ecological reasons to expect that respiration should be remarkably reduced compared to conditions at higher levels of turbulence. As this error is predominantly restricted to stable, nocturnal periods, it operates as a "selective systematic error" (Moncrieff et al., 1996) and leads to an overestimation of the carbon sequestration of an ecosystem. Several investigations about this problem and the potential reasons have given evidence that it is not primarily associated with measurement errors but with the neglected non-turbulent transport processes, i.e. the horizontal and vertical advection, which become significant under these conditions (Lee, 1998; Baldocchi et al., 2000; Paw U et al., 2000; Aubinet et al., 2002; Lee and Hu, 2002; Massman and Lee, 2002; Aubinet et al., 2003). The advective transport can be induced by an uneven topography, heterogeneity of the canopy or low turbulence conditions. A main limitation for the determination of the horizontal advective terms is that they can not be derived from single-tower measurements.

A common method to correct for the underestimation of night-time flux densities is the u_* -correction (Falge et al., 2001b). This correction is based on extrapolating the NEE during windy and turbulent to calm and low-turbulent night-time conditions because it is assumed that the advective transport processes are minor under windy conditions. For further details refer to section 3.4.2.

Storage term — The storage of CO₂ below the measurement height is often estimated from a time-averaged concentration profile (e.g. Finnigan et al., 2003, term II in Eq. 2.15). Finnigan (2006) points out that calculating S_c from single tower measurements results in an irreducible error of about 50 % because the use of instantaneous profiles contains a given random error and time-averaged vertical profiles imply a certain loss of high frequency information.

In the absence of profile measurements the storage term is often estimated from changes in the CO₂ concentration (Δc) measured above the canopy (Aubinet et al., 2000):

$$S_c = -\frac{\Delta c}{\Delta t} z_m. \quad (2.17)$$

Advection — The effect of a non-zero mean vertical velocity component \bar{w} and thus an estimation of the vertical advection term F_{VA} (term III in Eq. 2.15) was first suggested by Lee (1998):

$$F_{VA} = \bar{w}(\bar{c}_{zm} - \langle c \rangle), \quad (2.18)$$

where \bar{c}_{zm} is the mean CO₂ concentration at the measurement height and $\langle c \rangle$ is the mean CO₂ concentration in the layer below the measurement height.

The determination of the mean vertical velocity component \bar{w} is a crucial task. The measured value has to be cleansed of topographical and sensor misalignment effects, i.e. an appropriate tilt correction has to be carried out. In this study, the planar fit method according to Wilczak et al. (2001) is applied (cf. section 3.3.1). A comparison of \bar{w} derived from two adjacent instruments shows that the uncertainty in \bar{w} is of the same magnitude as the velocity itself (Heinesch et al., 2007). In a reply to Lee (1998) Finnigan (1999) points out that the horizontal advection terms can not be neglected as assumed by Lee (1998) and e.g. calculated by Baldocchi et al. (2000) and Paw U et al. (2000). In recent budget considerations both horizontal and vertical advective fluxes are taken into account (Aubinet et al., 2003; Feigenwinter et al., 2004; Aubinet et al., 2005; Feigenwinter et al., 2008).

3 Methods

3.1 Site description

The experimental site is located in the plains of the Southern Upper Rhine Valley on the northern edge of Eimeldingen (Germany, 47° 38' 21" N, 7° 35' 58" E, 277 m a.s.l., WGS-84), a village about 10 km North of the city of Basel, Switzerland (Fig. 3.1). The surrounding is a flat, small patched, agriculturally used area (mainly crops and some fruit orchards). The field measures about 320 m x 210 m. Maize was also cultivated on the adjacent fields in eastern direction, providing a fetch of uniform crop of ~100 m at minimum (Fig. 3.2). The prevailing winds from NNW, ESE, and WSW (Fig. 4.2) are in accordance with the regional flow pattern modified by the local topography, i.e. the orientation of the Southern Upper Rhine Valley and the High Rhine Valley as well as the "Burgunderpforte" in the West (Kaufmann and Weber, 1996).

Data analysed in this study were collected during almost continuous measurements from June 2004 until October 2006 at this site.

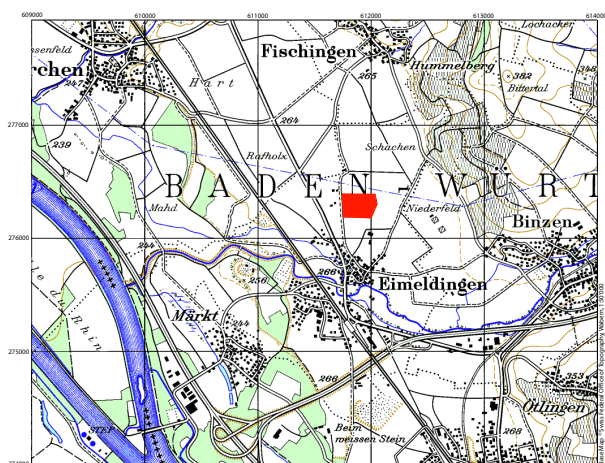


Figure 3.1: Map of the surrounding of the experimental site (red area) in Eimeldingen, Germany. (Base map data from swisstopo.)

Maize — Every year the field was seeded to maize (*zea mays* L.) in April at ~9 plants per square meter with a row spacing of ~0.7 m and an East-West row orientation. Growth of the plants was strongly de-



Figure 3.2: Aerial view of the site southbound (photograph by R. Vogt).

pendent on meteorological conditions, particularly temperature and precipitation (cf. section 2.1). Because the field is not irrigated both amount and temporal distribution of rain events are important. Final canopy height was reached in the beginning of August and differed from year to year: 2.5 m in 2004 and ~2.3 m in 2005 and 2006 (Fig. 3.3). Due to the growing maize and the increasing cover fraction albedo changed from 15 % to 20 % during vegetation period (Fig. 4.1e). The cobs were harvested beginning of October, respectively November in 2005. The remainder of the plants was chopped in small pieces, which lay on the ground for some weeks before being ploughed in. The yield in the three subsequent years was 107, 98, and 80 kg are⁻¹. The field lay fallow from harvest in autumn until emergence in May. Prior to the initiation of the study, the site had more than 30 years of history in maize cultivation.

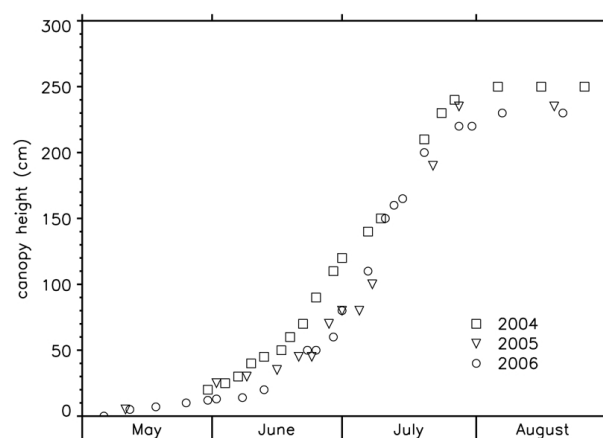


Figure 3.3: Development of canopy height from emergence in May until final canopy height is reached in August for vegetation periods 2004, 2005 and 2006.

Table 3.1: Soil carbon content.

depth (cm)	carbon content (%)	
	2004/06/30	2006/08/10
0 – 5	1.06	1.23
5 – 15	0.98	1.09
25 – 35	0.90	1.06

As a quality control of the calculated NEE by the eddy covariance method the above-ground biomass was determined. Destructive plant sampling was done approximately once a week during vegetation periods 2005 and 2006. A plant in a 50 m radius of the meteorological tower was selected randomly, dried at 105 °C and weighted afterwards. The carbon content of the dry matter is taken to be 50 %.

Soil — The soil is a silt loam (US-taxonomy). It contains 32 % sand, 55 % silt and 13 % clay. Soil sampling was conducted in three layers (0–5 cm, 5–15 cm, and 25–35 cm). Within each layer three samples were collected and the samples were combined into one composite sample per depth. Soil texture is rather homogeneous within this layer because of periodic ploughing. There is even a plough sole formed in a depth of ~30 cm. Particle size distribution was determined twice during the study (June 06, 2004 and August 10, 2006).

Carbon and nitrogen content were determined from the composite samples by a CHN-analysis (1000-CHN-Analysator, Leco Corporation, St. Joseph, MI, USA). Inorganic carbon content is below measurement limit (≤ 0.1 %). Carbon content is low (about 1 %) and decreases slightly with depth (Tab. 3.1). The difference in the absolute number between the two samples of ~15 % is primarily a consequence of a different state of decomposition of the biomass from the previous year and is not a clear indication for an increase of soil carbon stock. Nitrogen content did not change over time, is constant with depth and its value is 0.11 ± 0.01 %. The ratio of carbon and nitrogen, as an indicator for microbial decomposition, is about 10 ± 0.6 , a typical value for fertile agricultural soils (Scheffer et al., 1998).

3.2 Instrumentation

Long term measurements were carried out to get a reliable estimate of the natural variability of the NEE of a maize canopy. The measurements started in June 2004 and lasted until October 2006, thus including almost three vegetation periods. In 2006 an advection experiment was carried out, to verify the overall assumption that advective processes in short canopies are negligible. Table 3.2 gives an overview on the array of sensors, which is described in the subsequent sections.

3.2.1 Long-term measurements

A triangular lattice tower of six meter height and an edge length of 0.3 m was set up (Fig. 3.4). The tower had to be put down due to tillage in spring every year to ensure regrowth close to the tower and due to harvest. In autumn 2004 the tower was left in the field and the harvest was made manually but the tower was almost knocked over by the harvester.

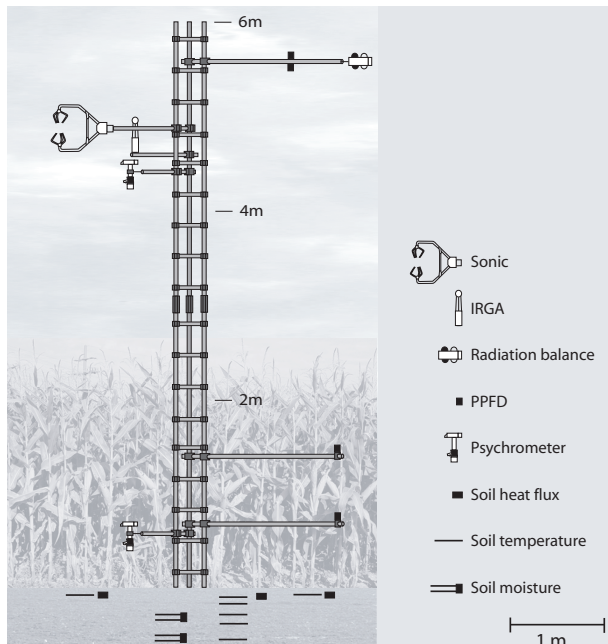


Figure 3.4: Schematic view of the main tower in Eimeldingen.

Turbulence — Carbon dioxide (CO_2) and water vapour (H_2O) concentration, the longitudinal u , lateral v and vertical w wind component as well as virtual acoustic temperature θ were continuously measured using the eddy covariance technique. The flux

system consisted of a sonic (CSAT3) and an open-path $\text{CO}_2/\text{H}_2\text{O}$ IRGA (Li7500). The instruments were aligned towards NNW to allow optimal measurements in the predominant wind directions. Due to the limited field size the height of the flux system had to be adjusted to canopy height ($z_m/h_c \sim 2$) to have sufficient fetch in all directions representative of the cropping system. Turbulence raw data (sampling frequency 20 Hz) were collected via SDM with a CR5000 data logger (CSI).

Radiation — The tower was equipped with quantum sensors (Li190SB) to measure photosynthetic photon flux density (PPFD). Two levels were within the canopy and a third at the top of the tower, where also the reflected PPF was measured. All components of the radiation balance, i.e. incoming short-wave radiation R_{sd} , outgoing short-wave radiation R_{su} , incoming long-wave radiation R_{ld} and outgoing long-wave radiation R_{lu} , were acquired at tower top by a net radiometer (CNR1). To prevent dew fall the sensor was ventilated from August 25, 2005 on.

Soil — Soil measurements included a five level temperature profile (-5, -10, -20, -30, -50 cm, CS107b), soil moisture measurements (-10, -30 cm, CS616) and three soil heat flux plates (Rimco HFP-CN3) at 5 cm depth, which were used to measure the average soil heat flux in the neighbourhood of the tower. The temperature profile, the upper soil moisture sensor as well as two heat flux plates were buried below the maize, the remaining sensors were placed in a furrow.

Others — In addition, air temperature and wet bulb temperature were collected via ventilated psychrometers (type Frankenberger). One instrument was mounted at 0.5 m, the other at the same height as the flux system. This sensor was not mounted during vegetation period 2006 because of presumable disturbance of the other measurements during the advection experiment. Precipitation was registered within the field above the canopy using a rain gauge.

Slow data were collected every five seconds and stored as 1 minute average values with a data logger (CR5000, CR10X, and CR10, CSI).

Table 3.2: Overview of the instrumentation at the Eimeldingen site.

variable	instrument type	measurement height (m)	sampling interval	storage interval
radiation balance	CNR1 ^a	6.0	5''	1'
photon flux density of PAR	Li190SB ^b	2x 6.0 (albedo) 2x within canopy	5''	1'
air temperature & wet bulb temperature	psychrometer type Frankenberger ^c	0.5 & variable	5''	1'
wind vector components & virtual acoustic temperature	CSAT3 ^d	variable	60 Hz	20 Hz
	USA-1 ^e	4x (0.75, 2.0)	40 Hz	20 Hz
	Gill R2 ^f	0.75	166.6 Hz	20 Hz
wind speed	A101M ^g	0.4, 0.6, 1.25, 1.95, 2.55, 3.25	5''	1'
H ₂ O, CO ₂	IRGA Li7500 ^b	variable	100 Hz	20 Hz
	IRGA Li6262 ^b	4x (0.5, 1.75)		5'
		1x (0.5, variable)		
precipitation	Hellmann rain gauge ^h	above canopy	5''	1'
soil temperature	CS107b ^d	-0.05, -0.1, -0.2, -0.3, -0.5	5''	1'
soil heat flux	Rimco HFP-CN3 ⁱ	3x -0.05	5''	1'
soil moisture	CS616 ^d	-0.1, -0.3	5''	1'

^a Kipp and Zonen, Delft, NL

^b LiCor Inc., Lincoln, NE, USA

^c Institute of Meteorology, Climatology and Remote Sensing, University of Basel, CH

^d Campbell Scientific Inc., Logan, UT, USA

^e Metek GmbH, Elmshorn, D

^f Gill Instruments Ltd., Lymington, UK

^g Vector Instruments, Rhyl, UK

^h Franz Ketterer Feinmechanik, Sölden, D

ⁱ McVan Instruments, Mulgrave, AUS

3.2.2 Advection experiment

During the vegetation period 2006 (from June 26 to October 9) an advection experiment was carried out. Four additional pylon towers of three meter height were erected in a distance of ~ 18.5 m from the main tower in a north-, east-, south- and westward direction, resulting in a square of an edge length of ~ 26 m (Fig. 3.5).

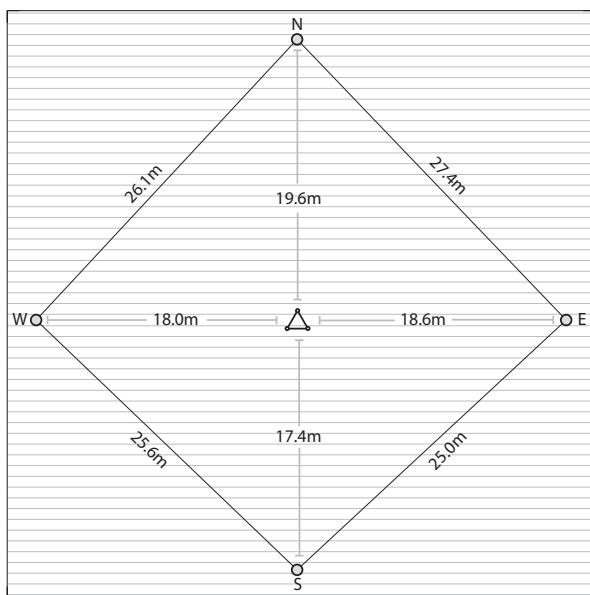


Figure 3.5: Schematic top view of the advection set-up. The triangle stands for the main tower, the grey circles denote the additional advection towers and the horizontal lines indicate the maize rows (from Lietzke, 2008).

On each tower two sonics (USA-1) were mounted, one at 0.75 m and one at 2 m (Fig. 3.6). The instruments were placed in the middle of two maize rows and were orientated towards North. The serial output data was continuously monitored and collected using an industrial PC (PIP 6, MPL, Dättwil, Switzerland) equipped with a LabView-based software (developed by A. Christen). As from 2006/09/22 1530 hours (CET) the lower sonic on the West tower had to be replaced by a Gill R2.

Air was sucked through 40 m long tubes to a closed path $\text{CO}_2/\text{H}_2\text{O}$ IRGA (Li6262). The ten inlets (Acro[®] 50 Vent Device with 1 μm PTFE membrane, PALL Gelman Laboratory, Ann Arbor, MI, USA) were mounted below the sensor head of the sonics at a height of 0.5 m and 1.75 m. The upper level at the main tower was at the same height as the open-path IRGA. The gas analyser was operated in dif-

ferential mode, i.e. measuring continuously a zero gas (N_2) in the reference cell. Each inlet/channel was sampled for 30 s. The first 10 s after switching were discarded and mean values computed over the remaining 20 s were stored. The mean CO_2 and H_2O concentrations were stored as five minute values with a CR21X data logger (CSI). The IRGA was calibrated every second/third day with a CO_2 gas of known concentration. The system was adapted from Vogt et al. (2006).

Additionally, a total of six cup anemometers (A101M) were mounted at the main tower at heights 0.4, 0.6, 1.25, 1.95, 2.55 and 3.25 m (Fig. 3.6).



Figure 3.6: Photo of the southern advection tower on the left and the main tower with the cup profile on the right.

3.3 Data processing

3.3.1 Turbulence measurements

Averaging time — The length of the integration period has to be chosen long enough to ensure that all significant flux-carrying wavelengths are included (e.g. Lenschow et al., 1994; Finnigan et al., 2003). A wrong averaging time would result in an underestimation of the fluxes. As a test, the cumulative F_c for the period July/August of all three years was calculated based on values with time intervals of 30, 60, and 120 minutes. The half hourly covariance values were determined by the eddy covariance method (cf. section 2.3) and afterwards aggregated to the other time intervals according to:

$$\overline{w'c'}_N = \frac{1}{N} \sum_{i=1}^N (\overline{w'c'})_i + \frac{1}{N} \sum_{i=1}^N (w_i - \bar{w})(c_i - \bar{c}). \quad (3.1)$$

A variation of less than 4 % in the cumulative flux was found. Thus, half hourly intervals were used for further calculations.

Sonic coordinate rotation — In practice the coordinate system of a sonic and the surface will not be perfectly aligned, such that fluctuations in the longitudinal components of the wind appear as vertical velocity fluctuations, and vice versa. Therefore, a tilt correction for these small deviations of the sonic coordinates is needed. If the normalised mean vertical wind component w_* , i.e. the ratio of the mean vertical wind component and the mean horizontal wind speed, above a plane surface shows a sinusoidal function of wind direction then the sonic is tilted (Fig. 3.7a).

There are mainly three methods to determine the orientation of a sonic relative to a Cartesian coordinate system aligned along the mean wind: double rotation ($\bar{v} = 0$ and $\bar{w} = 0$, according to Kaimal and Finnigan 1994), triple rotation (additionally $\overline{w'v'} = 0$, McMillen 1988) and planar fit ($\bar{v} = 0$ and normally $\bar{w} \neq 0$, Wilczak et al. 2001).

The third rotation can introduce additional uncertainty in the flux (Wilczak et al., 2001). Therefore, only double rotation and the planar fit method were compared. The main difference between the

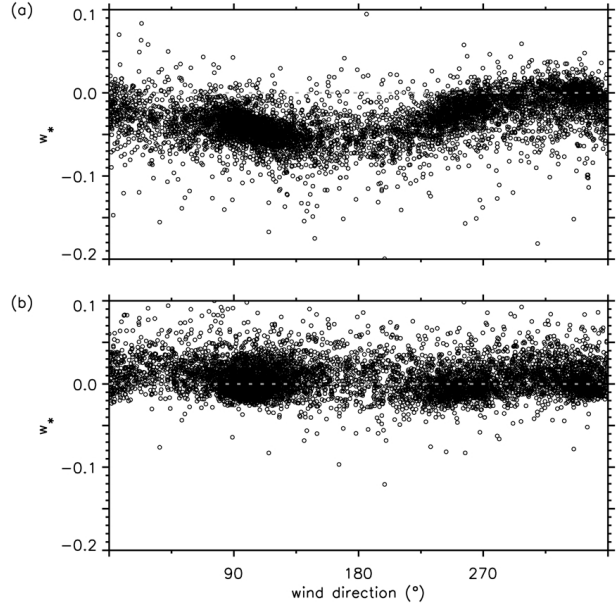


Figure 3.7: Wind direction vs normalised mean vertical wind component w_* for time period June to November 2005 (a) before and (b) after the coordinate rotation.

two methods is the time period to calculate the rotation angles. For double rotation these angles are calculated for each single run, which is equivalent to high-pass filtering, while for the planar fit method they are always the same (as long as the tilt of the sonic is constant). During periods of assimilation the carbon fluxes differ by only a few percent (fluxes determined by planar fit are 3 % smaller). During bare field conditions unrealistic high values result from double rotation whereas planar fit shows significantly smaller values (Fig. 3.8). Additionally, the planar fit method is less susceptible to sampling errors because many data runs are used to determine the rotation angles.

Thus, the planar fit method according to Wilczak et al. (2001) is applied for this study and is described briefly in the following. The plane of the new coordinate system is defined by the horizontal wind components placed parallel to the surface and the u -component aligned to streamlines of the flow. The orientation of the plane can be determined by a least-squares fit of the wind data to the equation:

$$\bar{w}_m = b_0 + b_1 \bar{u}_m + b_2 \bar{v}_m, \quad (3.2)$$

where b_0 , b_1 and b_2 are regression coefficients and \bar{u}_m , \bar{v}_m and \bar{w}_m are components of the mean wind vector in the instrument coordinate system. The regression coefficients are used to determine the rotation angle α about the v -axis, the roll angle β about the intermediate u -axis and the yaw angle γ about

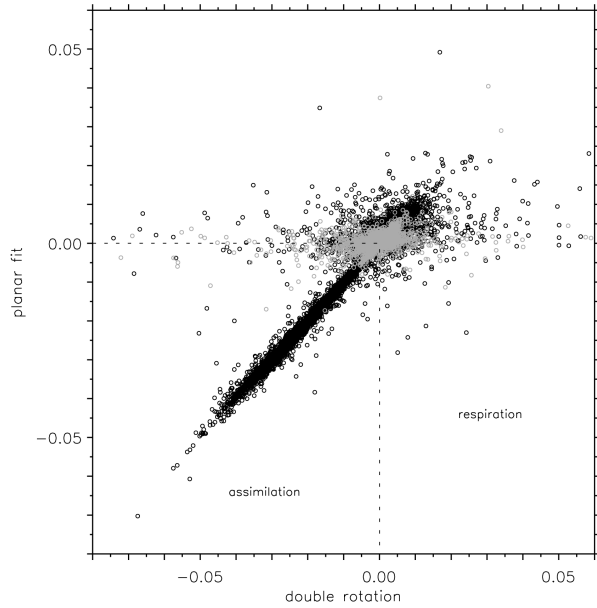


Figure 3.8: Comparison of $\overline{w'c'}$ ($\text{mmol m}^{-2} \text{s}^{-1}$) derived from double rotation and planar fit method for vegetation periods (from July to September) with black and for bare field conditions (from November to March) with grey circles.

the new z -axis (Fig. 3.9, Tab. 3.3). As the topography is almost flat no dependency of the rotation angles on wind direction is given and the angles are generally small.

By multiplying the measured data (subscript m) with the matrices given in Eq. 3.3, the data are rotated into the new coordinate system (subscript rot).

$$\begin{bmatrix} u_{rot} \\ v_{rot} \\ w_{rot} \end{bmatrix} = \mathbf{BCD} \begin{bmatrix} u_m \\ v_m \\ w_m \end{bmatrix},$$

where

$$\mathbf{B} = \begin{bmatrix} \cos \gamma & -\sin \gamma & 0 \\ \sin \gamma & \cos \gamma & 0 \\ 0 & 0 & 1 \end{bmatrix}, \quad (3.3)$$

$$\mathbf{C} = \begin{bmatrix} 1 & 0 & 0 \\ 0 & \cos \beta & -\sin \beta \\ 0 & \sin \beta & \cos \beta \end{bmatrix},$$

$$\mathbf{D} = \begin{bmatrix} \cos \alpha & 0 & \sin \alpha \\ 0 & 1 & 0 \\ -\sin \alpha & 0 & \cos \alpha \end{bmatrix}.$$

Figure 3.7b shows the data after applying the planar fit. The sinusoidal shape is removed and the mean

Table 3.3: Rotation angle α and roll angle β for planar fit with the number of values for their determination for different time periods. The yaw angle γ is always zero in this study.

time period	α ($^\circ$)	β ($^\circ$)	number
2004/06/01 – 2004/10/30	0.11	-1.19	6791
2004/11/01 – 2005/02/28	-0.75	-0.10	4869
2005/03/01 – 2005/05/31	-0.13	-0.30	2359
2005/06/01 – 2005/11/30	-0.63	-0.80	7028
2005/12/01 – 2006/02/28	-0.66	-0.06	3745
2006/03/01 – 2006/06/30	-0.64	-0.05	4670
2006/07/01 – 2006/10/09	0.14	-0.36	3704

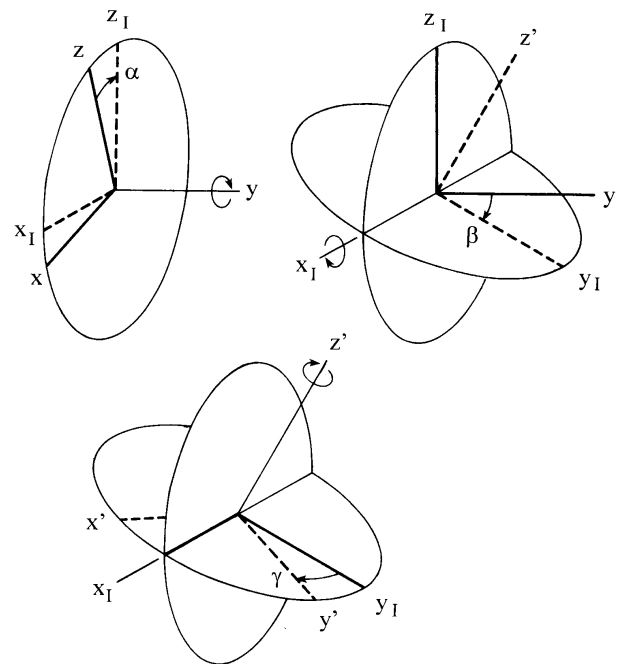


Figure 3.9: Definitions of the tilt angles α , β and γ for the xyz convention. The original axes are x , y and z , the intermediate axes are x_I , y_I and z_I , and the final axes are x' , y' and z' (from Wilczak et al., 2001).

value of w_* is shifted from -0.03 to +0.006.

3.3.2 Quality control of turbulence measurements

A first quality control is carried out on raw data. The diagnostic flags from the instruments as well as the automatic gain control of the open-path IRGA (valid range: 50–63 %) are checked. Additionally, values beyond a given range are rejected (Tab. 3.4) and spikes are removed. For spike removal windows of a length of ten minutes are used. The mean and the standard deviation are calculated and any data point that differs more than eight times the standard deviation from the mean is considered a spike.

Table 3.4: Applied limits to fast data.

variable	lower limit	upper limit	unit
u, v	-25	+25	m s^{-1}
w	-5	+5	m s^{-1}
θ	-20	+50	$^{\circ}\text{C}$
CO_2	0	50	mmol m^{-3}
H_2O	0	25	g m^{-3}

The process is repeated until no spikes are detected any more. The choice of the window length and the threshold value ($\pm 8 \sigma$) are based on visual inspection. This method is adapted from Vickers and Mahrt (1997). Flagged values are discarded, i.e. no interpolation is carried out. The statistics are calculated if 30000 out of 36000 values per half hour are given. The resulting data availability for sonic data is $\sim 80 \%$ and for the open-path IRGA 60.5 % and 54.8 % for H_2O and CO_2 concentration, respectively. Gaps are mainly caused by rain or dew on the sensors and the fact that the tower had to be put down for tillage.

Steady state and integral turbulence characteristic test — The stationarity of a data series can be tested by dividing a single record (e.g. $(\overline{w'\theta'})_{30}$ of a time interval of 30 minutes) into equal time intervals (e.g. $(\overline{w'\theta'})_i$ of a time interval of 5 minutes) and testing the subsequence for underlying trends or variations other than those due to expected sampling variations (Bendat and Piersol, 1986). Foken and Wichura (1996) proposed this test as follows:

$$RN_{cov} = \left| \frac{\frac{1}{N} \sum_{i=1}^N (\overline{w'x'})_i - (\overline{w'x'})_{30}}{(\overline{w'x'})_{30}} \right|. \quad (3.4)$$

For high quality data the difference between the two averaging intervals (RN_{cov}) has to be less than 30 %.

MOST states that the ratio of σ_w/u_* in the inertial sublayer is a function only of ζ . Empirical fits of this ratio are given e.g. by Panofsky and Dutton (1984) and Kaimal and Finnigan (1994):

$$\left(\frac{\sigma_w}{u_*} \right)_l = \begin{cases} 1.25 (1 + 3|\zeta|)^{\frac{1}{3}} & \text{if } \zeta < 0 \\ 1.25 (1 + 0.2\zeta) & \text{if } \zeta > 0. \end{cases} \quad (3.5)$$

The integral turbulence test by Foken and Wichura (1996) compares these parametrisations (subscript l)

with the measurements (subscript m):

$$ITC_{\sigma} = \left| \frac{\left(\frac{\sigma_w}{u_*} \right)_l - \left(\frac{\sigma_w}{u_*} \right)_m}{\left(\frac{\sigma_w}{u_*} \right)_l} \right|. \quad (3.6)$$

For high quality data the difference (ITC_{σ}) has to be less than 30 %.

The flag system according to the Spoleto agreement is chosen (Mauder and Foken, 2004). High quality data results in final flag 0. Final flag 1 denotes moderate quality data, i.e. they can be used for flux estimates without restriction. With final flag 2, i.e. $RN_{cov} > 1$ and $ITC_{\sigma} > 1$, data with low data quality are classified which have to be discarded. In the present study there is no need for rejecting any data, consequently all data is further used for calculation of vertical flux densities.

Spatial representativeness — One important aspect is the representativeness of the measurements at a single tower for the real ecosystem fluxes. The measurements are influenced by surface elements within a given area in upwind distance, the source area. This region can be estimated by different approaches (for an overview see e.g. Schmid, 2002). In this study a simple analytical model by Schuepp et al. (1990) for the cross-wind integrated flux footprint is used. This model assumes constant wind speed with height and atmospheric stability is taken into account by Businger-Dyer functions for Φ_m (Eq. 3.7 Panofsky and Dutton, 1984).

$$\Phi_m = \begin{cases} (1 + 16\zeta)^{-\frac{1}{4}} & \text{if } \zeta < 0 \\ 1 + 5\zeta & \text{if } \zeta > 0. \end{cases} \quad (3.7)$$

The position of the peak of the footprint x_{max} is calculated by:

$$x_{max} = \frac{U \Phi_m (z_m - d)}{u_* 2k}. \quad (3.8)$$

The extent of the footprint is estimated according to Wilson and Swaters (1991):

$$U \frac{(z_m - d)}{\sigma_w} < x < U \frac{(z_m - d) \Phi_m}{ku_*}, \quad (3.9)$$

where x is the upwind distance and U is the wind velocity.

Figure 3.10 displays the mean footprint during vegetation periods (2004 to 2006). During unstable

conditions the source area of the measurements lies within the maize field. For stable conditions the x_{max} estimates are located near the edge of the field. But fortunately maize was also cultivated on the adjacent fields in the main nocturnal wind direction (ESE).

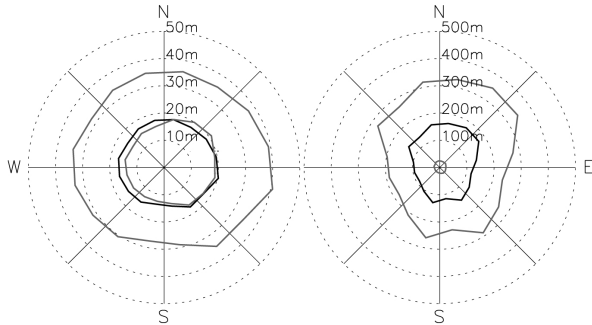


Figure 3.10: Mean of the footprint during vegetation periods for unstable (left) and stable (right) conditions. The black line indicates x_{max} according to Eq. 3.8 and the grey lines display the extent of the footprint according to Eq. 3.9.

This approach generally underestimates the extent of the footprint. This is also shown by a comparison with the method according to Kljun et al. (2004): for daytime values during vegetation periods x_{max} is located in a distance of ~ 50 m and 90 % of the source area are within ~ 140 m in along-wind distance. For night-time situations the number of values is too small for a general estimation as the criteria of a minimum u_* of 0.2 m s^{-1} has to be fulfilled.

Energy balance closure — According to the first law of thermodynamics the energy balance of a surface should be in balance, i.e. the available energy should be partitioned in the turbulent flux densities of sensible heat Q_H and latent heat Q_E (Eq. 3.10). Available energy includes net radiation R_n , soil heat flux density G , energy used by photosynthesis Q_P and storage of sensible and latent heat in the layer below the sensors ΔS :

$$R_n + G + Q_P + \Delta S = Q_H + Q_E. \quad (3.10)$$

The closure of the energy balance is often used as an indicator for data quality (e.g. Aubinet et al., 2000). The closure fraction (CF) is defined as:

$$CF = \frac{Q_H + Q_E}{R_n + G + Q_P + \Delta S}. \quad (3.11)$$

As shown in Fig. 3.11, the energy balance is not closed. During vegetation periods the closure fraction is 0.8, during bare field conditions the closure

is worse (52 %) mainly given by the very small turbulent fluxes during night-time. These results correspond to other studies (e.g. Wilson et al., 2002; Oncley et al., 2007; Barr et al., 2006). The energy balance is discussed in more detail in section 4.2.

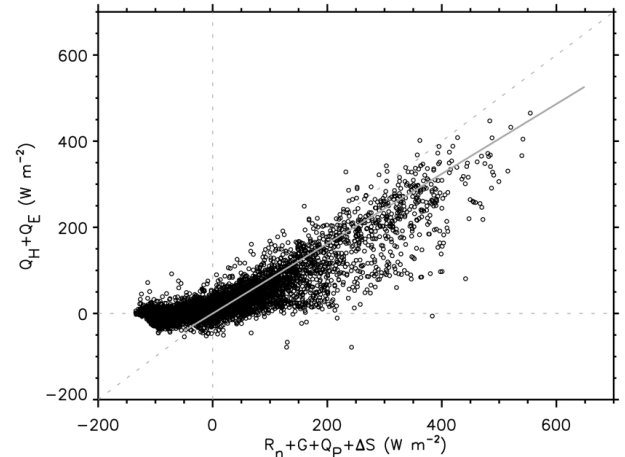


Figure 3.11: Available energy vs turbulent heat flux densities during vegetation periods. The linear regression forced through zero results in $y = 0.81x$.

3.3.3 Corrections of turbulent flux densities

Flow distortion correction — The wind vector measured by a sonic may be influenced by the sonic itself, its mounting devices, and the mast (Wieringa, 1980; Wyngaard, 1981, 1988). If the wind blows exactly along a sonic path, the wake behind the transducer induces an error, known as transducer shadow effect. The influence of the flow distortion can be determined experimentally by wind tunnel studies (Wyngaard, 1981). All sonics in the present study have inclined paths and therefore the transducer shadow is reduced. However, to minimize errors all sonics used have been checked in the wind tunnel at ETH Zurich, Switzerland by the Institute of Meteorology, Climatology and Remote Sensing, University of Basel in 2004. Correction matrices were determined for 4° classes according to Vogt (1995). Tower shadowing is minimal by the alignment of the sonic to NNW into a mean wind direction and the small number of winds from SSE (Fig. 4.2). Correspondingly, the ratio of σ_w to u_* is almost consistent as a function of wind direction.

Spectral loss correction — Measuring and analysing turbulence data leads to a spectral attenuation both at high and low frequencies. The bias

results from physical limitations of the sensors and the experimental set-up which act as a low-pass filter and the data analysis which acts as a high-pass filter (Massman, 2000). The resulting spectral attenuation is additionally dependent on measurement height, wind speed and atmospheric stability. There are two main approaches to correct this underestimation: the transfer function approach (e.g. Moore, 1986; Horst, 1997; Massman, 2000) and in-situ methods (e.g. Laubach and McNaughton, 1998). Here the transfer function approach is applied. Each effect causing a loss in flux density can be described by a frequency-dependent transfer function and the error of a turbulent flux density can be expressed as:

$$\frac{(\overline{w'x'})_m}{\overline{w'x'}} = \frac{\int_0^{\infty} T(f) Co_{wx}(f) df}{\int_0^{\infty} Co_{wx}(f) df}, \quad (3.12)$$

where subscript m stands for measured, f is the normalised frequency, $T(f)$ denotes the product of all appropriate transfer functions for high and low frequency spectral attenuation and $Co_{wx}(f)$ is the cospectrum.

For the present study a transfer function approach based on Moore (1986) is applied. The assumed cospectra Co_{wx} are simplifications of the Kansas spectra (Kaimal et al., 1972). For the existing instrumentation and data acquisition system the following transfer functions have to be considered: the transfer functions for block-averaging over a finite time period T_b (Kaimal et al., 1989):

$$T_b(f) = 1 - \frac{\sin^2(\pi f \Delta t)}{(\pi f \Delta t)^2}, \quad (3.13)$$

where Δt is the averaging time period and the transfer function for path length averaging for vertical wind T_w and a scalar T_p :

$$T_w(f) = \frac{2}{\pi f} \left(1 + \frac{e^{-2\pi f}}{2} - \frac{3(1 - e^{-2\pi f})}{4\pi f} \right), \quad (3.14)$$

$$T_p(f) = \frac{1}{2\pi f} \left(3 + e^{-2\pi f} - 4 \frac{(1 - e^{-2\pi f})}{2\pi f} \right). \quad (3.15)$$

Equations 3.14 and 3.15 are simplifications of more complex transfer functions (Moore, 1986).

The impact of spectral loss correction depends on the scalar flux and the corresponding necessary

Table 3.5: Average impact of spectral loss correction to Q_H , Q_E , and F_c for stable and unstable conditions. Statistics are calculated for situations with $|Q_H|$ or $|Q_E| > 10 \text{ W m}^{-2}$ and $|F_c| > 1 \mu\text{mol m}^{-2} \text{ s}^{-1}$.

flux	stability	
	$-2 < \zeta < 0$	$0 < \zeta < 2$
Q_H	+1.7 %	+2.5 %
Q_E	+0.9 %	+1.0 %
F_c	+0.7 %	+1.6 %

transfer functions. Path length averaging and block averaging cause just a minor correction. Generally, the correction factor is smaller under unstable conditions and during the vegetation period. Table 3.5 gives an overview of the impact on the scalar fluxes.

A transfer function for sensor separation was not applied because the covariance between vertical wind component w and the concentrations of H_2O and CO_2 was maximised in advance. For each half-hourly run, the measured time lag was determined by maximizing the covariance within a frame of ± 60 values. This increased the corresponding covariances on average by 4.0 % and 4.4 %.

Humidity correction — The temperature determined with a sonic is derived from the temperature dependent speed of sound c which is inversely proportional to the sum of the transit times between the transducers. Additionally, c depends on humidity:

$$c^2 = \frac{\gamma \mathfrak{R}}{m} T_a (1 + 0.51q), \quad (3.16)$$

where γ is the adiabatic index, \mathfrak{R} is the universal gas constant, and m is the molar mass of air. Due to its similarity to the virtual temperature the term $T_a(1 + 0.51q)$ is called acoustic virtual temperature θ , which is the temperature measured by a sonic. According to Schotanus et al. (1983) the covariance of θ and w have to be corrected for humidity influence as follows:

$$\overline{w'T'_a} = \overline{w'\theta'} - 0.51 \overline{T_a} \overline{w'q'}. \quad (3.17)$$

Schotanus et al. (1983) added an additional term for cross-wind error for which the sonics used correct internally.

Webb-Pearman-Leuning correction — Webb et al. (1980) pointed out that fluctuations in an air constituents density ρ'_s can result from fluctuations in water vapour density and temperature which are not associated with the net transport of s . Their key assumption is a zero mean vertical mass flow of air. But, turbulent motion consists of warmer, ascending and colder, descending air parcels which have different densities. In order to maintain the zero mean vertical mass flow the mean vertical velocity is unequal zero. By applying the eddy covariance method (cf. section 2.3) the mean vertical flux of an air constituent s ($\overline{w' \rho'_s}$) is neglected. Hence, the estimates of the turbulent flux densities by the eddy covariance method have to be corrected according to Webb et al. (1980):

$$\begin{aligned} \overline{w' \rho'_{s\text{corr}}} &= \overline{w' \rho'_{s\text{uncorr}}} + \frac{m_a}{m_v} \frac{\overline{\rho_s}}{\overline{\rho_a}} \overline{w' \rho'_v} \\ &+ \left(1 + \frac{m_a \overline{\rho_v}}{m_v \overline{\rho_a}} \right) \frac{\overline{\rho_s}}{T_a} \overline{w' T'_a}, \end{aligned} \quad (3.18)$$

where subscripts s , v and a of m and ρ denote water vapour or CO_2 , water vapour, and dry air, respectively.

This approach was supported e.g. by Leuning (2004) and Massman and Tuovinen (2006) and extended to three-dimensional flow (e.g. Paw U et al., 2000; Leuning, 2004). Recently, Leuning (2007) showed that with the key assumption of no source or sink of dry air within the layer below the measurement height the theory of Webb et al. (1980) to calculate the turbulent fluxes is correct for both steady and non-steady, horizontally homogeneous flows.

As can be seen from Eqs. 3.17 and 3.18 $\overline{w' T'_a}$ is an input for the density correction and $\overline{w' q'}$ is input for the humidity correction. Thus, the corrected covariances were calculated iteratively until the difference from one step to the next was less than 0.1 %. The resulting impact on the turbulent fluxes densities are given in Tab. 3.6.

Measurements in low ambient temperatures have shown that the measurements of the open-path IRGA Li7500 can result in a carbon uptake as the sensor is warmer than the surrounding air (given by the heating of the electronics). That induces a small internal boundary layer with less dense air as in the surrounding. According to Burba et al. (2006) an

Table 3.6: Average impact of humidity and density correction on Q_H , Q_E , and F_c for stable and unstable conditions. Statistics are calculated for situations with $|Q_H|$ or $|Q_E| > 10 \text{ W m}^{-2}$ and $|F_c| > 1 \mu\text{mol m}^{-2} \text{ s}^{-1}$.

flux	stability	
	$-2 < \zeta < 0$	$0 < \zeta < 2$
Q_H	-7.2 %	+1.2 %
Q_E	+4.7 %	-0.8 %
F_c	+12.5 %	-10.7 %

additional term in Eq. 3.18 can reduce this error, but their experiment was carried out with a vertically orientated instrument. In the present study the instrument was tilted inducing a wind direction dependency of the internal boundary layers and besides the impact of the can and the ball become also important. Therefore, this correction could not be applied and unrealistic carbon uptake values (e.g. during bare field conditions) were simply rejected from further analysis.

The applied spectral, humidity and density correction result for $\overline{w' T'_a}$ in a mean reduction of 5.2 %. $\overline{w' q'}$ and $\overline{w' c'}$ are increased by 6.5 % and 12.2 %, respectively.

3.3.4 CO_2 storage term

As described in section 2.4 there are two main methods to estimate the CO_2 storage term. For the present study profile measurements were available from the advection experiment only (from June 26 to October 9, 2006). Therefore, the CO_2 storage term had to be determined by the concentration changes above the canopy, from the measurements of the open-path IRGA.

A comparison of the two methods for the overlapping time period was carried out. Assuming that the profile measurements lead to a better estimate of the CO_2 storage term the comparison shows that the applied single-level method generally underestimates the storage term by a factor of 2 (Fig. 3.12) which is in accordance with findings from Finnigan (2006).

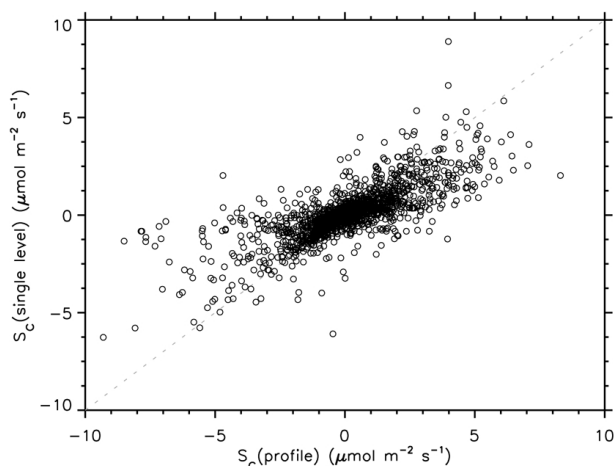


Figure 3.12: Comparison of estimates of the CO₂ storage term by the profile method and single-level method. The linear regression forced through zero results in $y = 0.50x$.

3.3.5 Radiation measurements

The net radiometer CNR1 was checked against reference instruments (Tab. 3.7, Fig. 3.13) during a field comparison from 2004 June 4 to June 8. Most of the reference instruments were calibrated by the World Radiation Centre (WRC) in Davos, Switzerland. The pygeometer PIR was further modified with three dome thermistors according to Philipona et al. (1995).



Figure 3.13: Set-up for the radiation comparison.

Figure 3.14 shows the analysis of the sensor comparison. R_{sd} is corrected by +2.5 %. The hysteresis indicates that one or the other sensor is not perfectly levelled. R_{su} values are multiplied by 1.2. R_{ld} shows a clear dependency on R_{sd} , supposing a leak in the filter or a temperature effect. This influence (2.5 %) as well as the temperature sensitivity are corrected, resulting in a remarkable reduction in the difference between the two sensors. Uncorrected R_n derived from measurements by the CNR1 has an offset of about -30 W m^{-2} to net radiation estimates from the sensor combination. By the described correc-

tions this offset reduces to 3 W m^{-2} .

The comparison was carried out before the CNR1 was ventilated which is assumed to reduce the temperature effect and therefore the difference in R_n . Based on this fact and the good correlation between uncorrected R_n of the CNR1 and the sensor combination no correction was carried out. The offset of 30 W m^{-2} is taken as a reliable estimate for the uncertainty in R_n .

Periods with dew fall on the CNR1 were detected visually using the difference between dew point temperature and case temperature. Resulting gaps shorter than two hours were linearly interpolated. For longer gaps a linear regression with data from a nearby meteorological station of the Institute of Meteorology, Climatology and Remote Sensing of the University of Basel (station Basel, Lange-Erlen) was applied. This problem no longer occurred after the sensor was ventilated from August 25, 2005 on.

For a reference measurement the PPFD sensors were operated parallel to a newly manufacturer calibrated sensor. Measurements took place on the roof of the institute for 12 days prior to the field measurements (Fig. 3.15).



Figure 3.15: Set-up for the comparison of the PPFD sensors.

3.3.6 Soil measurements

To calculate the soil heat flux density at the soil surface G the values of the heat flux plates G_z which were buried at a given depth z (here -0.05 m) have to be adjusted for the heat storage in the layer between

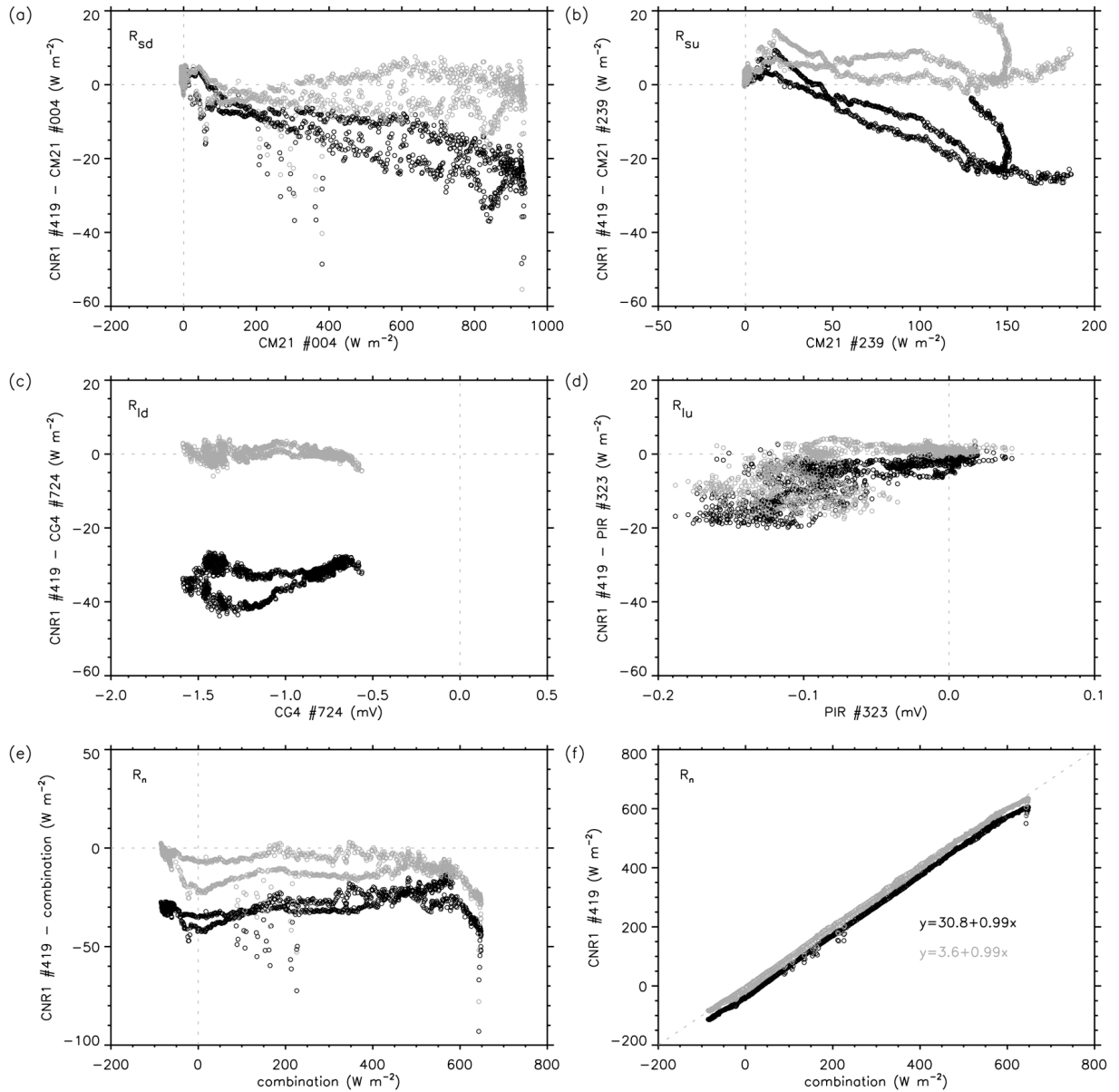


Figure 3.14: Signal of the reference sensor vs the difference between the CNR1 and the reference sensor for: (a) R_{sd} , (b) R_{su} , (c) R_{ld} , (d) R_{lu} and (e) R_n . In graph (f) R_n of the sensor combination vs R_n of the CNR1 are displayed. Black values are the measured values, grey values are the corrected values. The comparison is based on minute values from a clear sky day (June, 7 2004 1200 hours to June, 8 2004 1200 hours.)

Table 3.7: Instrumentation during radiation comparison.

variable	manufacturer	instrument	serial no.	calibration
$R_{sd}, R_{su}, R_{ld}, R_{lu}$	Kipp and Zonen, Delft, NL	CNR1	020419	manufacturer
R_{sd}	Kipp and Zonen, Delft, NL	CM21	910004	WRC
R_{su}	Kipp and Zonen, Delft, NL	CM21	950239	WRC
R_{ld}	Kipp and Zonen, Delft, NL	CG4	040724	manufacturer
R_{lu}	Eppley Laboratory Inc., Newport, USA	PIR	31207F3	WRC

the soil surface and the sensor Δz . This additional term depends on the temperature change $\overline{\Delta T_s}$ at the same depth z over time period Δt and the volumetric heat capacity of the soil c_v (Fuchs and Tanner, 1968):

$$G = G_z + c_v \left(\frac{\overline{\Delta T_s}}{\Delta t} \right) \Delta z. \quad (3.19)$$

The average heat capacity of the soil is given by its relative content of minerals x_{min} , organic matter x_{org} , water x_w and air x_p and their typical values of heat capacity, 2.1, 2.5, 4.2 and 0.0013 MJ m⁻³ K⁻¹, respectively (van Wijk and de Vries, 1963; Scheffer et al., 1998):

$$c_v = c_{min}x_{min} + c_{org}x_{org} + c_w x_w + c_p x_p. \quad (3.20)$$

The content of organic matter is assumed to be 2 % according to the soil analysis and the one of minerals to be 40 %. The volumetric content of water is measured and the remainder is assumed to be air.

The mean of the three adjusted measurements is further used as soil heat flux density G .

3.3.7 Temperature / humidity sensors

The psychrometers were constructed by the Institute of Meteorology, Climatology and Remote Sensing of the University of Basel using Pt100 resistors. The instruments were calibrated in the range from -3 °C to +40 °C in the laboratory after the field measurements in May 2007. Further details about instrumental design and the calibration procedure are given in Vogt and Reber (1992). In the field the psychrometers were ventilated to minimize radiation errors.

3.3.8 Closed-path gas analyser

Above a cell temperature of about 51 °C the closed-path IRGA Li6262 does not work properly, i.e. the values drop to ~200 ppm. These time periods as well as calibration periods are removed visually. Final data availability is 76 %.

A span (Eq. 3.21) and zero (Eq. 3.22) adjustment according to the application note 123 of LiCor Inc. (Lincoln, NE, USA) is applied to the raw data:

$$c = c' + (c_s - c'_s) \frac{c' Y_c(c')}{c'_s Y_c(c'_s)}, \quad (3.21)$$

$$c = c' - c_z R_c, \quad (3.22)$$

where c is the corrected CO₂ concentration, c' is the original measurement, c_s is the true span concentration, c'_s is the measured span concentration, and c_z is zero reading. c_s and c_z are acquired by manual calibration every second/third day.

The function $Y_c(c)$ is defined as:

$$Y_c(c) = \frac{\alpha + \beta c^{1.5}}{\alpha + c^{1.5} + \gamma c}, \quad (3.23)$$

where $\alpha = 6606.6$, $\beta = 1.4306$ and $\gamma = 2.2464 \cdot 10^{-4}$.

R_c is the ratio of the slope of the calibration curve where the measurement is to be corrected and the slope of the calibration curve at 0 ppm. It is determined by the data as $R_c = 1.0881 + 0.0016 c'$.

3.3.9 Advective terms

A brief overview of the methods to determine the horizontal and vertical advective terms is given in section 2.4. The applied method is described in detail in Feigenwinter et al. (2008). A crucial task is

the interpolation of the measured data to a three-dimensional grid of CO₂ gradients, wind speed and wind direction. In this study, the determination of the vertical wind profile bases on the work of Lietzke (2008).

Vertical wind profile — Basically, the six-level cup anemometer profile is used to derive a mean shape of the vertical wind profile and the generated mean shape is then adjusted to the sonic data (Fig. 3.16).

The canopy influenced wind profile can be split in an upper and a lower part (e.g. Kaimal and Finnigan, 1994). In the upper part a logarithmic wind profile is assumed, penetrating into the canopy down to the height $z_0 + d$, where z_0 is the roughness length. Lietzke (2008) showed that the rule-of-thumb values of $z_0 = 0.1h_c$ and $d = 0.6h_c$ are reliable estimates at this site. In the lower part, within the canopy, the wind is strongly retarded in the area of high leaf density and less in the "stem-space", where a local second maximum is expected (in analogy to the "trunk space" in forest canopies, Shaw (1977)). The vertical interpolation within the canopy is done by fitting a cubic spline to the mean cup-profile (wind speed at the surface is set to zero). As wind speed is generally low, particularly within the canopy, the mechanical threshold value of 0.14 m s^{-1} of the cup anemometers used becomes important. All lower values are set to this threshold value. The type of sensors used shows no over speeding. The data from the sonics is considered to be more reliable. Although, the sonics of type METEK show troubles in the measurement of low wind speeds (for details cf. Lietzke (2008)). Finally, the mean shape is linearly corrected to fit the averaged sonic wind speed. Due to different canopy heights at the advection towers the mean shape is derived for a normalised canopy height.

The resulting mean shape is adjusted to the half-hourly sonic data at each advection tower. The measurements above the canopy of the sonic at the main tower are assumed to be representative for all four sites. Given by the above mentioned problems of the sonics at low wind speeds data from the lowest level is not regarded to derive the instantaneous profiles. Wind direction is linearly interpolated between the above-canopy and the 2 m level and is then kept constant to the ground.

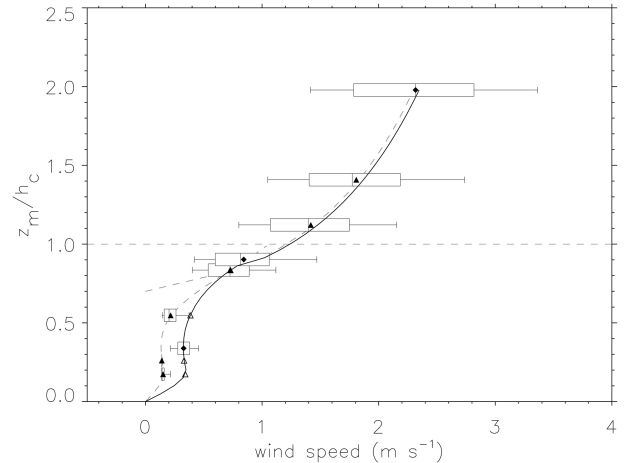


Figure 3.16: Final mean vertical wind profile (black line). The original shape (dashed line) is derived from cup anemometer measurements (\blacktriangle) and linearly adapted to mean sonic measurements (\blacklozenge). \triangle are the adapted cup values. Data is based on measurements from August 01 to October 09 during neutral conditions, its statistics are shown in boxplots. Adapted from Lietzke (2008).

Vertical CO₂ concentration profile — An artificial vertical CO₂ concentration profile with 40 layers is derived by linear interpolation between the three measurement heights. Again, the value from the uppermost level from the main tower is used for all four profiles. Given by the lack of information about the CO₂ concentration at ground level it is assumed that the concentration gradient from the lowest level to the ground is twice the concentration gradient between 0.5 m and 1.75 m (Feigenwinter et al., 2008).

Vertical advection — This term is determined as described in Eq. 2.18 (Lee, 1998). The mean CO₂ concentration below the sensor is derived from all interpolated concentration profiles within the control volume.

Horizontal advection — The horizontal grid is defined by 10×10 rectangular boxes with an edge length of $3.67 \text{ m} \times 3.70 \text{ m}$. For each level a minimum curvature surface function was used for interpolation. From this grid the local CO₂ gradient is calculated as described in Feigenwinter et al. (2008). For each rectangle the gradients between the four corners are averaged resulting in a mean gradient in x and y direction, assumed to be valid in the centre of the box. With these values a similar grid, shifted by half an edge, of the horizontal CO₂ gradient is derived. Afterwards the same method was applied for the u - and v -component of the wind. With the result-

ing values term V of Eq. 2.15 can be calculated by multiplying the CO_2 gradients with the corresponding wind components. The direction of the advective flow is bound to the direction of the wind flow and is positive if the gradient is positive in the same direction and negative if the gradient is negative.

3.4 Gap filling

Data coverage of the measured data for NEE is 54.8 %. On the one hand data are mainly missed due to sensor/logger malfunction or because the tower was put down for tillage. On the other hand data have to be rejected by quality control. For example under stable conditions the eddy covariance method often underestimates the flux densities and the respective measured values have to be rejected (Moncrieff et al., 1996) which has not been done yet. To end up with a carbon balance over a given time period a complete data series is needed. Thus, missing data has to be reconstructed. Therefore, the known relationship of NEE with environmental factors (cf. section 2.1) is used to derive parametrised equations which are afterwards used to fill missing NEE values. Recently, Moffat et al. (2007) presented a comparison of several gap-filling techniques like interpolation, probabilistic filling, look-up tables, non-linear regression (including artificial neural networks) and process-based models. In this study different non-linear regressions are applied which are described in the following subsections. Gap filling is based on NEE values calculated according to Eq. 2.16, i.e. the storage term is taken into account to avoid double counting (Aubinet et al., 2000).

3.4.1 Periods of assimilation

An often used method to fill gaps during daytime during vegetation periods is the application of a Michaelis-Menten function (1913, in Falge et al., 2001b). This approach uses a rectangular hyperbola to quantify the relationship between NEE and $PPFD_{net}$ (Eq. 3.24). Thus, at a given level of $PPFD_{net}$ the value of NEE gets saturated.

$$NEE = \frac{a' PPFD_{net} GPP_{sat}}{GPP_{sat} + a' PPFD_{net}} - TER_{day}, \quad (3.24)$$

where a' denotes the quantum yield, GPP_{sat} is the gross primary production under saturated light conditions and TER_{day} is the total ecosystem respiration during daytime.

In a first attempt, this relationship is used to model missing data. Considering the dependency of photosynthesis and respiration on temperature and on the different growth stages (assumed to be represented

by vegetation height) the data series is split in numerous categories. They are different for each vegetation period (Tab. 3.8). As in other studies (e.g. Suyker et al., 2004) no significant effect of soil water content on NEE is found, indicating that under the given soil moisture conditions the plants have never been under severe water stress. The partitioning is done visually, requiring a given number of data points and a threshold for correlation coefficient for each class. As mentioned in section 2.1 maize never reaches light saturation. Accordingly, GPP_{sat} reaches unrealistic high values. For some categories even the values of the quantum yield are high with $>0.05 \mu\text{mol} \mu\text{mol}^{-1}$. However, the modelled values are within 10 % of the measured values ($R^2 = 0.91$).

Nevertheless, a different approach is tested. As the relationship between NEE and $PPFD_{net}$ is linear for maize, the quantum yield during vegetation periods is determined by a linear regression at light levels above the light compensation point (i.e. $NEE \leq 0$, Baker et al., 1989; Baldocchi, 1994). To capture the current environmental conditions (air temperature, actual water supply) and the current stage of plant development an interval of one day is chosen. Figure 3.17 illustrates the changing quantum yield during vegetation period 2005. A comparison of the resulting artificial data series of NEE to the measured data shows a consistence within 10 % ($R^2 = 0.88$, Fig. 3.18).

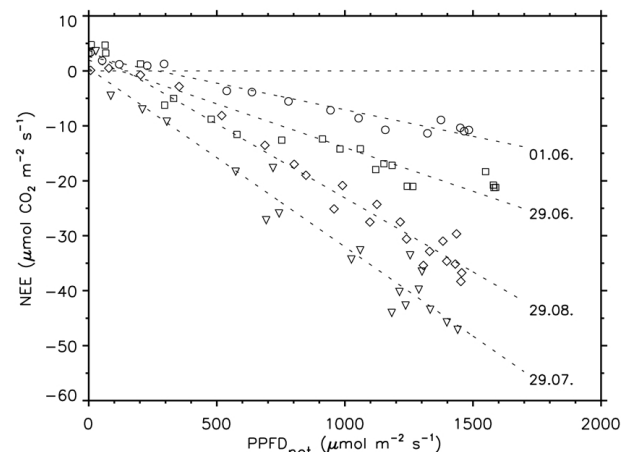


Figure 3.17: $PPFD_{net}$ vs NEE for some days representing different growth stages (from youngest to senescence) during vegetation period 2005.

To replace missing data of NEE a complete data series of $PPFD_{net}$ is necessary. Thereto a stepwise modelling is carried out using the relationship between global radiation R_{sd} and incoming PPFD as well as the PPFD albedo. First, a regression of R_{sd}

Table 3.8: Parameter for Michaelis-Menten equation (Eq. 3.24) to fill daytime data gaps during vegetation periods 2004–2006.

year	h_c (m)	T_a (°C)	a' ($\mu\text{mol } \mu\text{mol}^{-1}$)	GPP_{sat} ($\mu\text{mol m}^{-2} \text{s}^{-1}$)	R_{day} ($\mu\text{mol m}^{-2} \text{s}^{-1}$)	R^2
2004	0.0 – 0.4	0 – 22	0.010	40.5	0.6	0.95
		22 – 40	0.011	160.8	2.6	0.89
	0.4 – 0.8	0 – 40	0.023	182.8	1.7	0.79
	0.8 – 1.2	0 – 40	0.029	597.1	3.1	0.96
	1.2 – 1.6	0 – 40	0.058	108.7	7.1	0.92
	1.6 – 2.0	0 – 40	0.091	94.9	11.8	0.85
	2.0 – 2.4	0 – 22	0.052	186.4	5.6	0.94
		22 – 40	0.057	139.4	10.4	0.90
>2.4	0 – 40	0.035	221.1	3.0	0.86	
2005	0.0 – 0.4	0 – 22	0.016	41.2	2.7	0.70
		22 – 40	0.020	39.9	3.3	0.79
	0.4 – 0.8	0 – 40	0.036	35.7	3.9	0.75
	0.8 – 1.2	0 – 40	0.041	79.8	2.1	0.90
	1.2 – 1.6	0 – 40	0.042	132.3	7.9	0.77
	1.6 – 2.0	0 – 40	0.068	88.9	6.6	0.86
	2.0 – 2.3	0 – 40	0.061	107.1	5.9	0.87
		0 – 16	–	–	–	–
16 – 22	0.030	625.6	3.5	0.81		
22 – 40	0.037	204.0	6.6	0.87		
2006	0.0 – 0.6	0 – 22	0.010	194.2	2.2	0.63
		22 – 40	0.022	69.2	4.7	0.71
	0.6 – 1.0	0 – 40	0.042	47.1	2.7	0.81
	1.0 – 2.2	0 – 40	0.048	109.6	5.8	0.85
	>2.2	0 – 22	0.053	124.6	4.0	0.86
22 – 40		0.051	99.8	6.8	0.82	

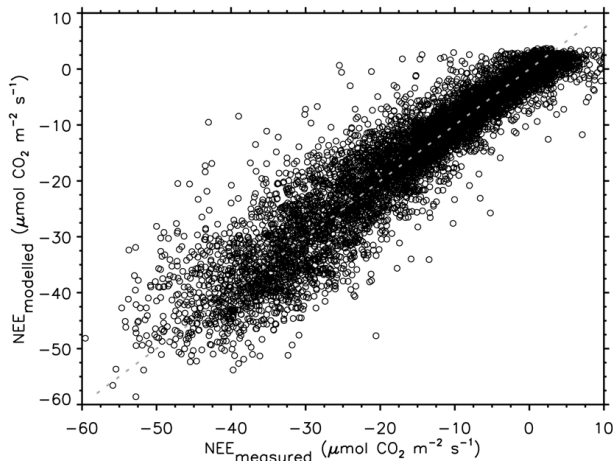


Figure 3.18: Measured vs modelled daytime NEE during vegetation periods. $y = -0.98 + 0.92x$, $R^2 = 0.88$.

and incoming PPFD is calculated for the existing data. Secondly, on a daily basis the PPFD albedo is calculated and missing values are linearly interpolated. Thirdly, R_{sd} data from the nearby rural meteorological station Basel, Lange-Erlen are used to determine a regression with the R_{sd} values at the site and to replace missing R_{sd} values. This data series is finally used to calculate a complete data series of $PPFD_{net}$ by the use of the previously determined relationship of R_{sd} and incoming PPFD as well as the PPFD albedo.

The difference between the hyperbolic and the linear approach is small (within 4 %). Still, the former method is susceptible to visual decisions and does not regard the special behaviour of C4 photosynthesis and therefore underestimates higher values of NEE. The latter method allows a better consideration of the current conditions for growth. Thus, the latter method is finally applied.

3.4.2 Periods of respiration

During night-time, turbulence intensity is often weak and therefore the eddy covariance method underestimates the NEE (Goulden et al., 1996; Moncrieff et al., 1996). A widespread way to overcome this problem is to replace rejected data by modelled NEE values which are estimated by a temperature function derived from measurements during well-mixed conditions.

A threshold value of u_* is used to distinguish between calm and well-mixed conditions (Aubinet et al., 2000; Falge et al., 2001a; Massman and Lee,

2002; Baldocchi, 2003). There are two principal methods to determine the threshold value of u_* : one is based on visual inspection of the data (Falge et al., 2001a) and the other uses a moving point test (for details of the latter method refer to Gu et al., 2005). For the former method the NEE values are normalised with a simulated flux (a first guess according to Eq. 3.25) to eliminate correlations between u_* and temperature and the values are grouped for u_* intervals of 0.01 m s^{-1} to reduce the scatter. Afterwards, for each u_* -class the median of this normalised respiration is calculated. This value increases as long as turbulence is insufficient. Both methods are tested with time windows of different size. The variation over time and different conditions (vegetation period/fallow and vegetation height) is small, but for many situations no threshold value can be defined by either method. Thus, all situations are handled in one run. The method according to Gu et al. (2005) results in a threshold value of 0.03 m s^{-1} , the visual inspection in a value of 0.05 m s^{-1} . But the scatter in the data is high, particularly under low u_* -conditions. To be on the safe side, the latter value is chosen. By this criteria, 24 % of the measured night-time data are rejected. Compared to other studies (e.g. the above mentioned) this threshold is rather low. But short canopies show generally lower u_* values than forested sites.

Soil temperature is the dominant environmental factor for respiration and most approaches to fill missing values are based on this relationship. In this study, a method according to van't Hoff (in Falge et al., 2001a) is applied, a non-linear least squares fit to the exponential function:

$$TER = a^{(b T_s)}, \quad (3.25)$$

where a and b are fitted coefficients and T_s is the mean soil temperature at a depth of -0.05 m . As shown e.g. by Xu and Baldocchi (2004) or Reichstein et al. (2005) this regression changes over time given by the changing phenology as well as by the amount of active biomass and litter in the upper layer of the soil. Thus, the data series is split in windows of 400 given night-time values. If no fit can be determined for one of these windows the temporal nearest fit is applied. Night-time situations and bare field conditions show the same relationship with soil temperature. However, there is large scatter in the data and the correlation between modelled and measured respiration values is low ($R^2 = 0.47$, Fig. 3.19). Par-

ticularly, high respiration values are underestimated by the parametrisation.

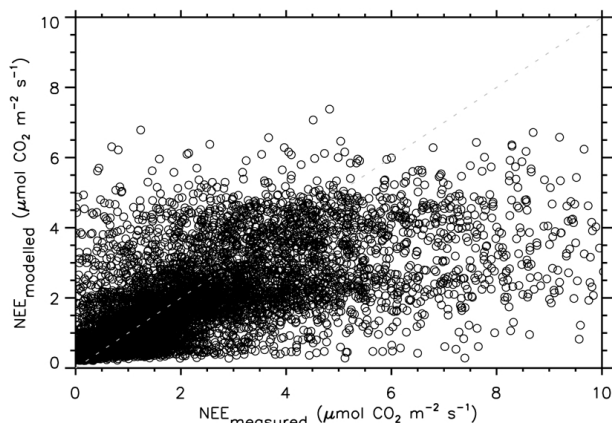


Figure 3.19: Measured vs modelled respiration during nighttime or bare field conditions. $y = 0.69 + 0.47x$, $R^2 = 0.47$.

3.4.3 Long gaps

Long gaps are mainly given because the tower had to be put down for tillage. A different approach is followed for these time periods as the conditions differ from the above derived relationships. For example after harvest of the kernels the remainder of the plants keep lying on the ground resulting in increased respiration rates. Therefore an artificial neural network (ANN, Neuralyst V1.4, Cheshire Engineering Corporation, Pasadena, USA) is used. The use of an ANN is also a standard method in the FLUXNET data base (Papale and Valentini, 2003).

An ANN is also an empirical non-linear regression model, but the dependencies of NEE on the input variables are not predefined. The architecture of an ANN is a model neuron with multiple inputs and a single output. Similar to the hitherto applied gap-filling methods air temperature, $PPFD_{net}$, absolute humidity, vegetation height and soil temperature are defined as dependent input variables. Each input is modified by a weight. The associated output is the measured NEE value. The ANN used applies a back-propagation algorithm for training. From the differences between the network output and the measured NEE, the error is determined and propagated backward through the network. By adjusting the weights of the input variables an optimal approximation of NEE is aimed. Afterwards the resulting ANN is used to estimate missing NEE values. As final ANN output the mean over ten runs is calculated.

The input data series have to be complete. Thereto, gaps are filled by the use of data from the same nearby meteorological station already used before. Air temperature and absolute humidity are gapfilled by a simple linear regression. For soil temperature the regression bases on the gapfilled air temperature data series. A daily time interval is chosen because variation between the two sites is smaller than on a shorter interval. Additionally, runs of the ANN with half hourly values show strong side effects and the series has to be split in smaller pieces of different length as results over longer time periods are unreasonable.

Daily values of NEE based on the measurements are almost limited to vegetation periods (i.e. to 105 out of a total of 861 days). Consequently, the output of the ANN matches the measured values during this time, but changing conditions in spring and autumn are badly represented. Particularly harvest induces a strong signal in the data series which should be represented by the ANN and carbon uptake should not begin before emergence of the plants. But temperature seems to be the main agent for the ANN resulting in a decrease of carbon uptake according to the temperature decrease in autumn and resulting in a carbon uptake as soon as temperature increases in March. Additionally, respiration during winter is almost constant with about $2 \text{ g C m}^{-2} \text{ d}^{-1}$. Therefore, the ANN is run with the gapfilled NEE data series, increasing the number of given data points to 709. Runs with the whole measurement period show a good reproduction of the values during vegetation periods and bare field conditions, but the output for changing conditions is still not reliable. Thus, the data series is split in three time periods: vegetation period, bare field conditions and changing conditions. Figure 3.20 shows the resulting relationship ($R^2 = 0.94$) between gapfilled daily sums of NEE and the output of the ANN.

3.4.4 Examples

In Fig. 3.21 to 3.23 three examples are given to illustrate the applied gapfilling methods.

The first two diagrams picture the applied parametrisations for assimilation and respiration periods based on a half hourly interval in comparison with the measured data. Figure 3.21 shows the begin-

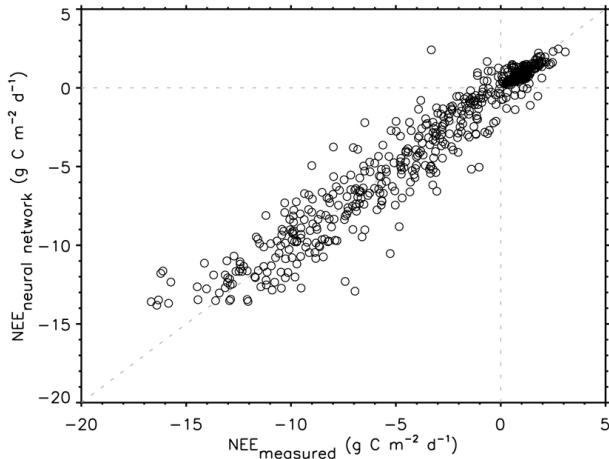


Figure 3.20: Daily sums of NEE: Measured or gapfilled by parametrisation vs modelled with an ANN for the whole measurement period. $y = -0.15 + 0.94x$, $R^2 = 0.94$.

ning of vegetation period 2005, the months of June and July. Figure 3.22 displays the comparison for bare field conditions, from December 2005 to January 2006. Generally, the parametrisations smooth the data series and extreme values are not reproduced which is pronounced during night-time and bare field conditions. The artificial data series capture the development during daytime situations with increasing assimilation values as well as the modifications by meteorological conditions.

In Fig. 3.23 the courses of both, the ANN and the measured/parametrised data series are illustrated for the whole measurement period, based on a daily interval. During vegetation periods the differences between the series is larger than during bare field conditions, but except the maximum values in summer 2004 the NEE is well represented by the ANN, capturing the growth stage of the plants as well as the variability given by the meteorological conditions. The ANN shows also reliable results for the strong decrease at harvest and for the time after emergence. This is of special interest because the data availability is rather low for this important time period of changing conditions, when the net sink of CO_2 changes to a net source of CO_2 or vice versa. Wrong estimates would have a strong negative impact on the reliability of the CO_2 budget. Values of the ANN during bare field conditions are slightly lower than the measurements.

3.4.5 Error estimation

The uncertainty associated with the gapfilling methods is estimated by evaluating the difference between the measured/observed data points and the modelled/predicted values by calculating the absolute and relative root mean square error (aRSME, Eq. 3.26; rRSME, Eq. 3.27) and the mean absolute error (MAE, Eq. 3.28):

$$\text{aRSME} = \sqrt{\frac{1}{N} \sum_{i=1}^N (p_i - o_i)^2}, \quad (3.26)$$

$$\text{rRSME} = \sqrt{\frac{\sum_{i=1}^N (p_i - o_i)^2}{\sum (o_i)^2}}, \quad (3.27)$$

$$\text{MAE} = \frac{1}{N} \sum_{i=1}^N |p_i - o_i|, \quad (3.28)$$

where o denotes observed values and p predicted values.

These parameters are listed in Tab. 3.9 and are determined from half hourly values for assimilation and respiration and from daily values for the ANN. For the calculation of the uncertainty of the ANN only the measured daily sums are considered. During periods of assimilation the rRSME for parametrisations and values by the ANN are 23.6 % and 18.4 %, respectively. The uncertainty for night-time and bare field conditions is more than twice as much.

The impact of the parametrisations on the sums over a given period (ΔSum) can be estimated from the bias error of the predicted NEE values (BE):

$$\Delta\text{Sum} = \text{BE } N_p \Delta t, \quad (3.29)$$

where N_p is the number of predicted values. For daily values Δt equals 1. The bias error is given by:

$$\text{BE} = \frac{1}{N} \sum_{i=1}^N (p_i - o_i). \quad (3.30)$$

The induced bias over the whole measurement period by the parametrisation for assimilation periods is 18.9 g C m^{-2} , for respiration periods ΔSum is -67.2 g C m^{-2} . About a third of the values are

Table 3.9: Error estimation for the different gap-filling methods by the absolute and relative root mean square error (aRSME, rRSME), the mean absolute error (MAE) and the bias error (BE). The unit of aRSME, MAE and BE for assimilation and respiration periods is ($\mu\text{mol CO}_2 \text{ m}^{-2} \text{ s}^{-1}$), for ANN the values are in ($\text{g C m}^{-2} \text{ d}^{-1}$), the unit for rRSME is (%).

	aRSME	rRSME	MAE	BE
assimilation	4.7	23.6	3.4	0.2
respiration	1.4	51.3	0.9	-0.4
ANN	1.6	18.4	1.2	0.5

parametrised resulting in a data coverage of $\sim 89\%$ and $\sim 61\%$ for assimilation and respiration periods, respectively. Regarding the whole measurement period 71.5% of the half hourly data are given.

Given by the large number of gaps (756) the induced bias by the ANN on the total sum is 353.0 g C m^{-2} . Repeating the same calculations with the measured/parametrised data series the induced bias by the ANN reduces to 1.8 g C m^{-2} for vegetation periods (52 gaps) and to -4.5 g C m^{-2} for bare field conditions (100 gaps). The corresponding rRSME is 21.0% and 35.4% , respectively. By the application of the ANN values the NEE data series becomes complete.

3.4.6 Gap filling of latent heat flux densities

To determine the total water need for maize growth the gaps in the data series of Q_E have to be substituted. Assuming that growth stage, vegetation coverage, soil moisture and air temperature are the principal agents for evapotranspiration, look-up tables for time windows of 10 days and temperature classes of 2 K are used. Figure 3.24 shows a comparison of measured and modelled values of latent heat flux densities during vegetation periods. About a quarter of the data is gapfilled. The induced bias over all three vegetation periods is 0.9 mm. The resulting rRSME for evapotranspiration during vegetation periods is 21.4% . For bare field conditions daily sums of evapotranspiration are correlated with daily sums of incoming PPFD ($R^2 = 0.81$). The resulting rRSME for bare field conditions is 26.5% . For the whole measurement period the total bias is 23.7% .

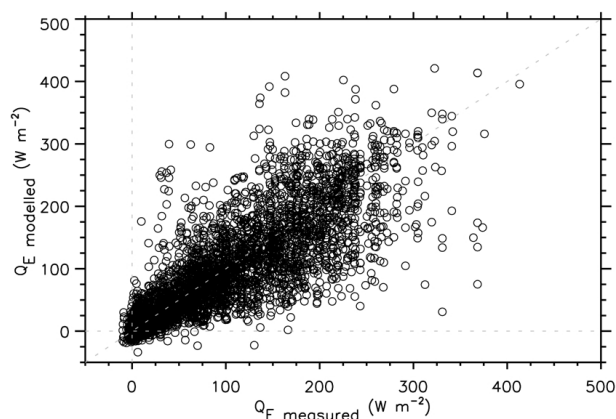


Figure 3.24: Measured vs modelled Q_E for vegetation periods. $y = 11.8 + 0.85x$, $R^2 = 0.75$.

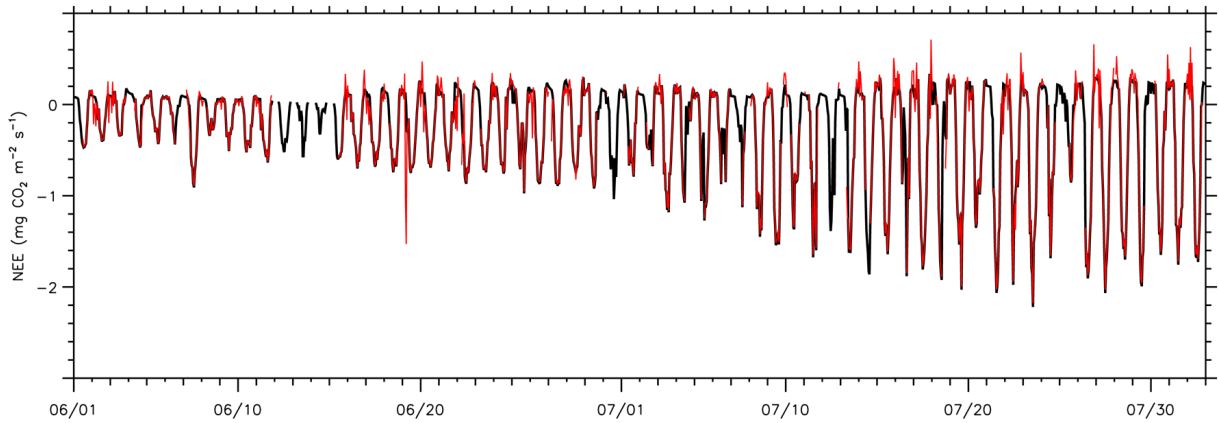


Figure 3.21: Course of NEE measured (red) and parametrised (black) from 2005/06/01 until 2005/08/02.

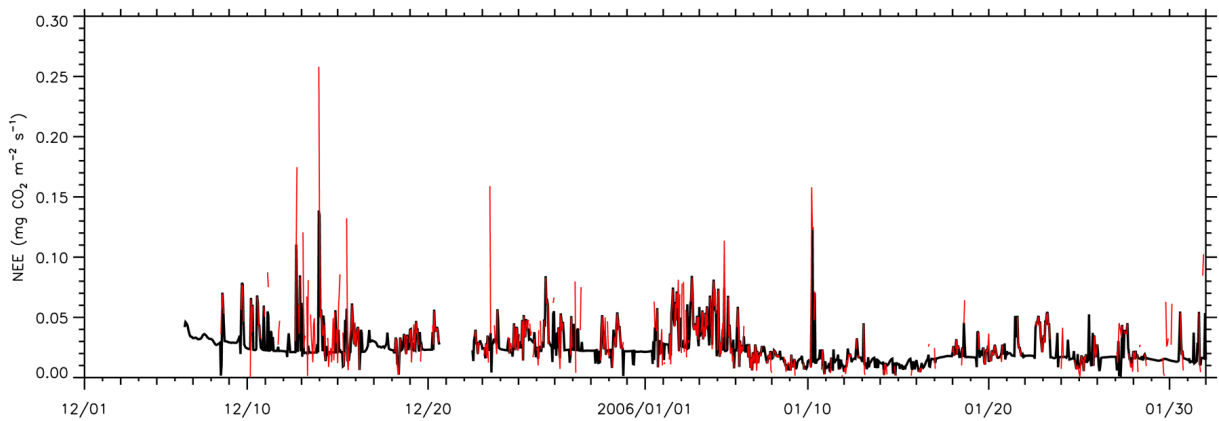


Figure 3.22: Course of NEE measured (red) and parametrised (black) from 2005/12/01 until 2006/02/01.

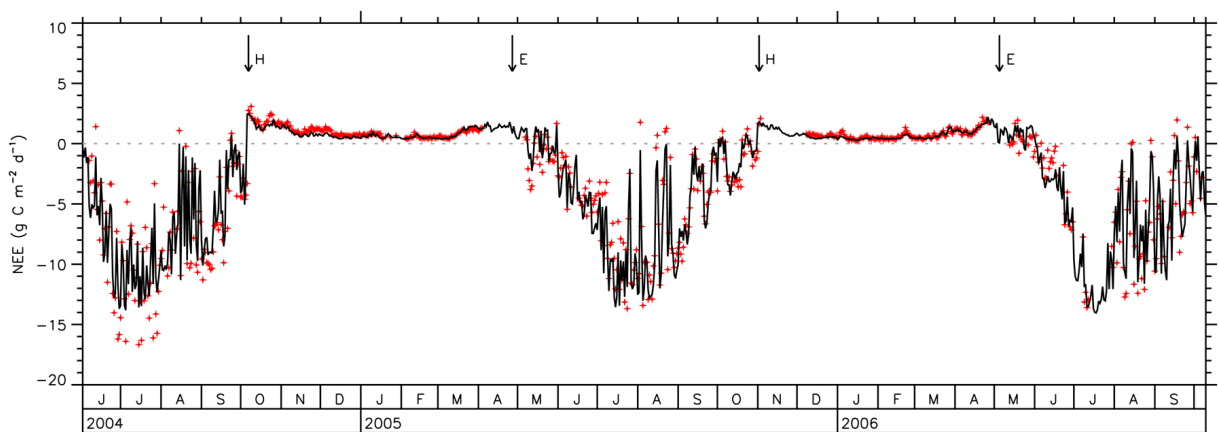


Figure 3.23: Course of daily totals of NEE for the whole measurement period: measured and parametrised values (red crosses) and output by an ANN (black line). Times of harvest (H) and emergence (E) are indicated by arrows.

4 Results and Discussion

4.1 Meteorological conditions

The processes of CO₂ exchange between soil, vegetation and atmosphere depend strongly on the meteorological conditions. Therefore, they are presented in more detail in this section.

Figure 4.1 gives an overview of the meteorological conditions on a daily interval for the whole measurement period from June 01, 2004 until October 10, 2006. In Tab. 4.1 the monthly values of mean air temperature, total precipitation and total PPF_{D_{net}} are summed up. The data series are filled with the use of data of the station Basel, Lange-Erlen. The completion of the meteorological parameters is achieved by regression analysis (cf. section 3.4) when a strong relationship between the two sites can be assumed (e.g. for R_{sd} , but not for vapour pressure deficit). For soil moisture, the impact of a given amount of precipitation is determined from the existing data and with this information and the completed precipitation data series the course of soil moisture during gaps shorter than seven days is estimated.

The annual pattern of air temperature exhibits similar courses for each year. However, some differences are noteworthy. January 2006 is so cold that the soil got frozen. August 2004, March 2005 and July 2006 are much warmer than the corresponding months in the other years. June and September are the most variable months. Based on half hourly data from the ventilated psychrometer the absolute minimum value of -13.3 °C is reached end of January 2005, the maximum value of 34.2 °C end of July 2006. The mean annual air temperature is 10.1 °C.

Precipitation shows great variability over the whole measurement period. Months with mean values alternate with wet months (e.g. October 2004 or August 2006) and dry months (e.g. July 2004 and July 2006). The year 2006 is wet compared to the two other years, except the month of July. Total precipitation from June until September, i.e. during the vegetation period, for all three years is 209, 223 and 432 mm, respectively.

The input of PPF_D is mainly given by the sun elevation and modified by the weather conditions. Accordingly, during months with high precipitation amounts PPF_{D_{net}} is reduced compared to the other years (e.g. in the month of August) and maximum values are reached in June/July. Maximum daily sums of 60 mol m⁻² d⁻¹ are reached in June.

The albedo of short-wave radiation and PPF_D during bare field conditions are approximately constant at 15 and 11 %, respectively (snow cover is excluded in these values). During vegetation periods the albedo values show an inverse behaviour due to phenological influences. The albedo of short-wave radiation drops continuously from ~20 % to a value of 15 %. With increasing plant coverage and biomass the PPF_D albedo drops below 5 % until July and increases with ongoing senescence to ~8 %.

Vapour pressure deficit (VPD) and soil moisture are strongly related to precipitation. Whereas VPD reacts almost immediately to a rain event, soil moisture has a given time delay. Small amounts of precipitation have no impact on soil moisture content in the measured depths of -0.1 m and -0.3 m.

The wind rose (Fig. 4.2) is tripartite in accordance with the dominant regional flow patterns from northern, eastern and western directions (cf. section 3.1). During night-time the predominant wind directions are from ESE throughout the year. The prevalence of this sector is given during daytime from November to February as well. But also the bough from northern directions gets more pronounced. From March to October the daytime wind rose shows all three dominant sectors with changing dominance of the northern and western boughs. Horizontal wind speed is generally low. During night-time the mean value is ~1 m s⁻¹, during the day it is about twice this value. Situations with wind speeds above 4 m s⁻¹ are rare (about 3 % of the measured data).

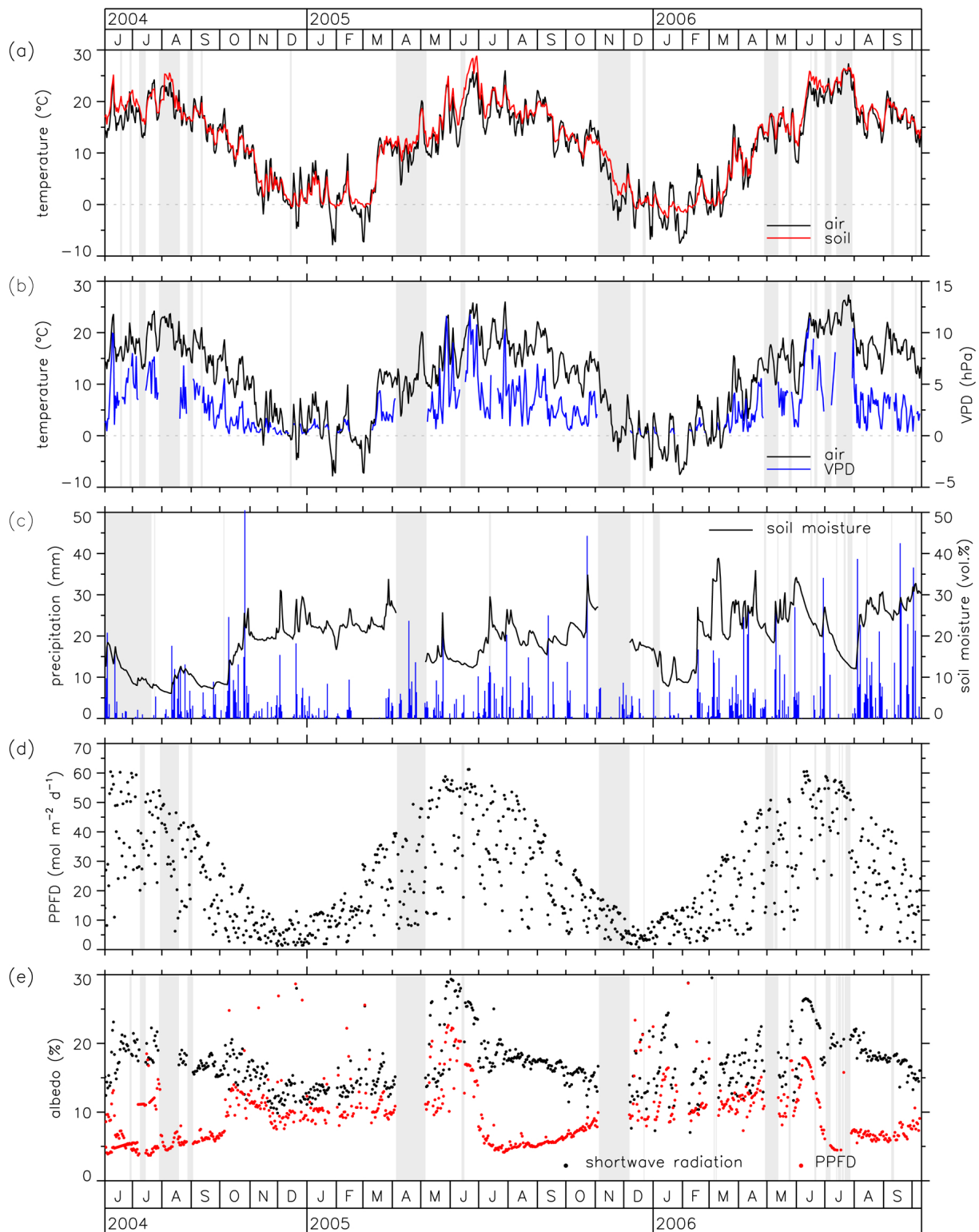
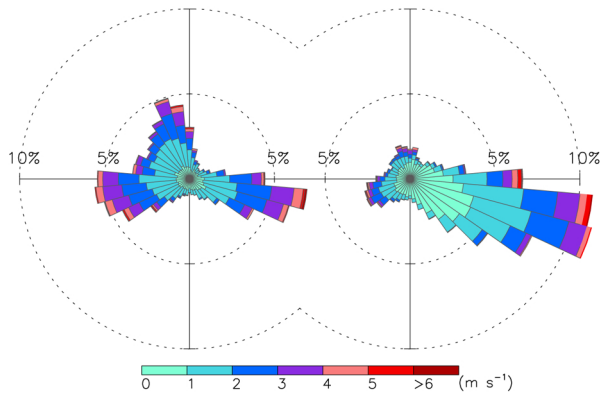


Figure 4.1: Daily averages of (a) air temperature and soil temperature in 5 cm depth, (b) air temperature and VPD, (c) soil moisture in 10 cm depth and daily total of precipitation, (d) daily total of net PPFD and (e) daily mean albedo (1200 – 1300 hours) of short-wave radiation ($\lambda = 305 - 2800$ nm) and PPFD ($\lambda = 400 - 700$ nm). Periods with snow cover are not shown in graph (e). Grey areas indicate time periods when no daily values could be calculated from data series at the Eimeldingen site. If values are displayed these are determined as described in the text mainly by regression analysis from data of a nearby meteorological station.

Table 4.1: Monthly values for mean air temperature, total precipitation and total PPF D_{net} . Values are based on gapfilled data.

	air temperature (°C)			precipitation (mm)			PPFD $_{net}$ (mol m $^{-2}$)		
	2004	2005	2006	2004	2005	2006	2004	2005	2006
January		1.8	-1.8		23	11		212	205
February		0.6	0.8		20	45		268	210
March		6.3	4.4		27	105		614	448
April		10.3	10.2		80	119		676	718
May		14.5	14.5		64	119		1001	854
June	17.1	19.1	18.7	65	30	79	1151	1179	1178
July	18.7	18.9	23.4	10	94	15	1177	1070	1410
August	19.2	16.9	16.2	101	60	197	910	994	720
September	15.7	16.0	17.7	33	39	141	720	700	630
October	12.1	12.5		177	80		370	470	
November	5.0	4.7		26	39		190	277	
December	1.4	0.5		68	32		130	118	

**Figure 4.2:** Wind rose with 10° sectors of daytime situations ($R_{sd} > 10 \text{ W m}^{-2}$) on the left and of night-time situations on the right based on half hourly data from the whole measurement period.

4.2 Energy balance

Most of the components of the energy balance (Eq. 3.10) have a direct impact on the NEE. Thus, a closer look on the general behaviour is of interest. Additionally, in section 3.3.2 it was already shown that the energy balance is not in equilibrium. The general pattern of the closure fraction and some possible causes are discussed in section 4.2.2.

4.2.1 Energy balance components

The mean diurnal course for vegetation periods and bare field conditions for each component are given in Fig. 4.3a-f. Figure 4.3g illustrates the diurnal pattern of available energy and turbulent flux densities and Fig. 4.3h displays the diurnal development of energy balance closure. The diagrams are discussed in the following subsections.

Net radiation — R_n (Fig. 4.3a) is particularly determined by R_{sd} and surface properties. The difference between vegetation periods and bare field conditions in the course of R_n is mainly given by the different sun's inclination. The mean daily maximum for vegetation periods and bare field conditions is reached around midday and the corresponding values are 360 and 175 W m^{-2} , respectively. Night-time values are about -50 W m^{-2} . R_n is partitioned into the other energy flux densities.

Soil heat flux density — G (Fig. 4.3b) depends strongly on vegetation coverage, thus on the amount of R_{sd} reaching the ground, and on soil properties, particularly on soil moisture. The mean diurnal course of G during vegetation periods is about a factor 1.8 greater than during bare field conditions, while R_n is more than doubled, thus illustrating the impact of the vegetation cover. For both periods the maximum value of -40 and -25 W m^{-2} , respectively, is reached around midday. Averaged over the whole day G becomes almost zero. During vegetation periods G consumes about 11 % of R_n during daytime and compensates 33 % of R_n during night-time. The corresponding values for bare field conditions are 14 % and 23 %. Temporarily in this section daytime and night-time values are defined as the means over

the time periods of 1000 to 1400 hours and 2200 to 0200 hours, respectively.

Storage term — ΔS (Fig. 4.3c) during vegetation periods is small with values of less than 2 W m^{-2} , i.e. less than 1 % of R_n . Under turbulent conditions in the afternoon ΔS becomes small. During bare field conditions ΔS becomes negligible. Summed up over 24 hours the storage term equals zero.

Energy used by photosynthesis — Q_P (Fig. 4.3d) is often neglected in energy balance considerations. Its pattern depends strongly on the course of R_n . The maximum value of 13 W m^{-2} , 3.5 % of R_n , is reached around midday. Figure 4.4 shows the daily sums during vegetation period 2005. Illustrating the steep increase in Q_P with growth of the plants up to daily sums of 350 J m^{-2} . With ongoing senescence Q_P decreases continuously.

Turbulent heat flux densities — The mean diurnal course of Q_H (Fig. 4.3e) is positive during daytime and negative at night. Q_E is positive throughout the day (Fig. 4.3f). Thus, the fluxes are of opposite direction during night-time. The daily maximums are reached around midday, a bit later during bare field conditions, with values of 97 and 29 W m^{-2} for Q_H and 172 and 70 W m^{-2} for Q_E , for vegetation periods and bare field conditions respectively. During daytime Q_H of vegetation periods is about four times the value of bare field conditions, for Q_E the factor is ~ 3 . Bowen ratio β , defined as the ratio of Q_H to Q_E , is 0.6 for daytime and -1.6 for night-time values during vegetation periods. During bare field conditions the relationship is similar with values of 0.4 and -1.3 . Considering the fraction of R_n used by Q_H and Q_E during daytime, values of 26 and 46 % for vegetation periods and 15 and 38 % for bare field conditions result, respectively.

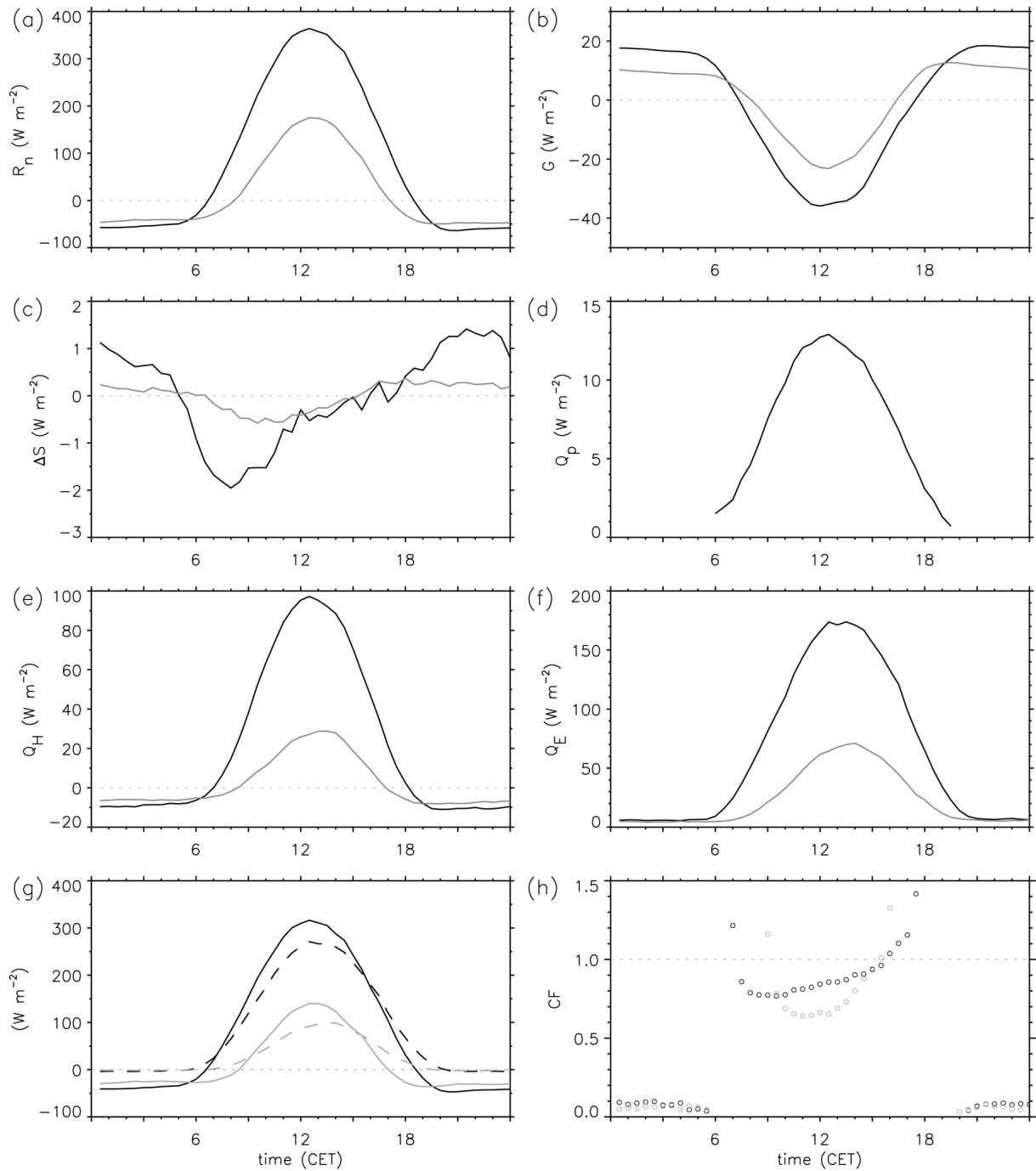


Figure 4.3: Mean diurnal course of the energy balance components for vegetation periods (black) and bare field conditions (grey) based on half hourly values: (a) net radiation R_n , (b) soil heat flux density G , (c) storage term ΔS , (d) energy used by photosynthesis Q_p , (e) sensible heat flux density Q_H , (f) latent heat flux density Q_E , (g) available energy (solid line) and turbulent heat flux densities (dashed line) and (h) mean diurnal course of closure fraction (CF) when the absolute value of both available energy and turbulent flux densities are $\geq 1 \text{ W m}^{-2}$. Values greater than 1.5 at sunrise and sunset are not displayed.

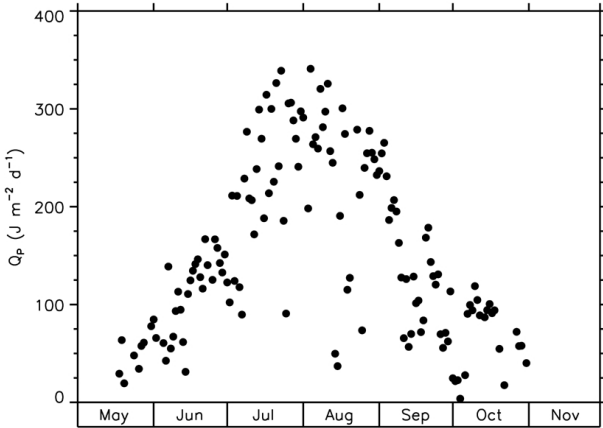


Figure 4.4: Daily sums of energy consumed by photosynthesis during vegetation period 2005.

4.2.2 Energy balance closure

The gap of energy balance closure shows a clear diurnal pattern which is similar for vegetation periods and bare field conditions (Fig. 4.3h). Daytime and night-time are again defined as common by sunrise and sunset. During night-time closure is poor with about 5–10%. Q_H and Q_E are small and of opposite direction. A steep change in closure fraction (CF, Eq. 3.11) is given when turbulence intensity changes significantly at sunrise and at sunset. During daytime energy balance closure starts with good values in the morning and drops during the subsequent hours before increasing again up to a complete closure in the afternoon. The turnaround during bare field conditions is around midday, during vegetation periods it is about two hours earlier. The zero-crossings of R_n , G and Q_H for vegetation periods as well as bare field conditions are within half an hour. The maximum value of Q_E is delayed compared to the other fluxes densities and Q_E decreases slower in the early evening resulting in a better closure. In Fig. 4.3g where the diurnal pattern of available energy and the total of Q_H and Q_E are displayed this delay is still visible and it is more pronounced during bare field conditions.

The partitioning of R_n into the other energy flux densities shows a diurnal pattern and is shown in Fig. 4.5 and described in the following for vegetation periods, but the pattern is similar for bare field conditions. During night-time the partitioning is almost constant: one third is consumed by G , about 15% by Q_H and Q_E is of opposite direction but the amount is about 10% of R_n . During daytime the patterns are

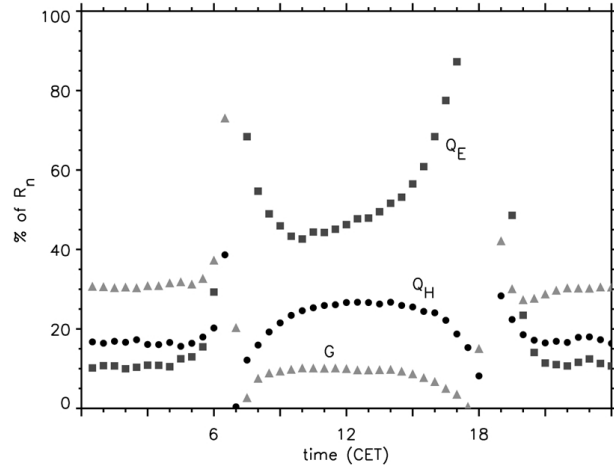


Figure 4.5: Mean diurnal pattern of the partitioning of R_n into Q_H (○), Q_E (□) and G (△) during vegetation periods. The direction of the fluxes is not taken into account.

different. G starts at ~10% and diminishes continuously to ~5% at sunset. Q_H consumes at sunrise about 10%, increases to about a fourth around 1000 hours and remains at this level until 1600 hours and decreases again to a level of 10% around sunset. Q_E starts at more than 100% around sunrise and drops to ~40% around 1000 hours. Afterwards the ratio of Q_E/R_n increases again to more than 100% around sunset. The slope gets stronger when Q_H/R_n starts to decrease. It is assumed that Q_E plays an important role in the disequilibrium between available energy and the turbulent heat flux densities.

In Fig. 4.6 the relationship between Bowen ratio and closure fraction is shown for different conditions. 75% of the values are $-1 < \beta < +1$. The smaller the absolute value of β the better the closure fraction is. The pattern during vegetation periods is more clear. Above $\beta = 1$ the closure fraction remains approximately constant, the variability is assumed to be given by the small number of cases. If β is of negative sign, i.e. Q_H and Q_E are of opposite direction, CF is poor but it increases with increasing $|Q_H|$. Both conditions are mainly given in October 2005 when the maize was left in the field for drying and most of the biomass was already inactive.

The dependence of the closure fraction on turbulence intensity reflected by friction velocity is displayed in Fig. 4.7. Unstable and stable conditions during vegetation periods and periods of bare field conditions show a similar pattern with a better closure of the energy balance with increasing u_* . The existence of vegetation causes a difference only dur-

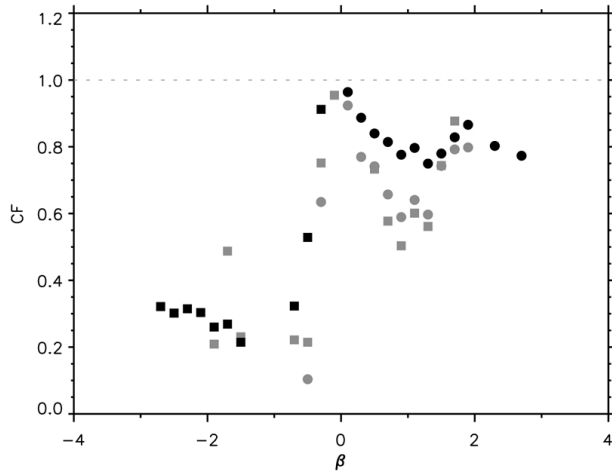


Figure 4.6: Bowen ratio (β) vs closure fraction (CF) for vegetation periods (black) and bare field conditions (grey), separated for unstable (\circ) and stable (\square) conditions. The values are the median for β -classes of 0.1 for conditions when the absolute values of the turbulent fluxes are $\geq 10 \text{ W m}^{-2}$.

ing unstable conditions. The pattern for unstable conditions during vegetation periods supports the determined threshold value for the u_* -correction of 0.05 m s^{-1} as described in section 3.4.2. The "perfect" threshold value would be $\sim 0.3 \text{ m s}^{-1}$, but only a small portion of the data (14 %) would remain and the largest improvement in CF is from the lowest to the next u_* -class.

The diurnal pattern of CF is found in different studies. In literature (e.g. Moncrieff et al., 1996; Mahrt, 1998; Wilson et al., 2002; Oncley et al., 2007) several reasons are discussed. One source of error is the inaccuracy of the sensors used and the given setup. The correspondingly applied corrections are described in section 3.3 and therefore these reasons for non-closure are assumed to be compensated. The imbalance can also originate from different source areas in the different terms of the energy balance equation or from a heterogeneity within the source areas, i.e. an insufficient fetch is given. As shown in section 3.3.2 a large portion of the source area of the turbulent flux densities, particularly under stable conditions, is located outside of the maize field and can therefore act as a source of error.

There is also an ongoing discussion about the implications of the energy balance non-closure on CO_2 flux densities as no equivalent quality test exists for these measurements (Twine et al., 2000; Barr et al., 2006). If the closure gap originates from inappropriate assumptions such as neglecting advective terms

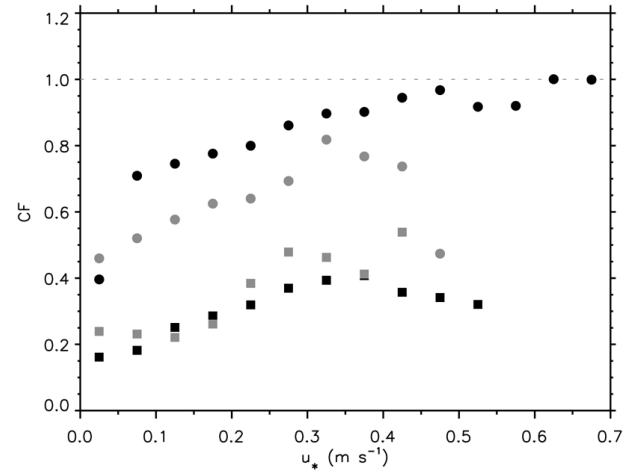


Figure 4.7: Friction velocity (u_*) vs closure fraction (CF) for vegetation periods (black) and bare field conditions (grey), separated for unstable (\circ) and stable (\square) conditions. The values are the median for u_* -classes of 0.05 m s^{-1} for conditions when the absolute values of the turbulent fluxes and the available energy are $\geq 10 \text{ W m}^{-2}$.

(cf. section 4.4.4) or an inappropriate averaging interval the determined CO_2 flux densities may contain similar errors, based on the basic assumption of similarity in the transport processes of the different properties.

4.3 Water balance

For agricultural considerations the water balance is of special interest, particularly the total water need for yield. Given by the definition of the water balance, precipitation equals the sum of evapotranspiration, surface and subsurface runoff and storage. In this study not all components are determined, runoff and storage are missing. The course of precipitation over the whole measurement period is already shown in Fig. 4.1. The pattern of evapotranspiration is depicted in Fig. 4.8. It is an important term for energy, water and carbon balance. The cumulative curves of both measured parameters for each vegetation period and period of bare field conditions, respectively, are displayed in Fig. 4.9 and the corresponding sums are listed in Tab. 4.2. For vegetation period 2004, the missing first weeks are compensated by an initial value, i.e. the mean sum of evapotranspiration of the other vegetation periods up to a vegetation height of 0.2 m. The bias in the numbers is $\sim 24\%$.

Evapotranspiration shows a clear seasonal pattern, mainly modified by radiation. Soil moisture content, given by the amount and the temporal distribution of precipitation and the active biomass influence the evapotranspiration as well. During bare field conditions evapotranspiration shows a strong correlation with radiation and accordingly with air temperature. For example, the second half of March 2005 and March 2006 are characterised by relative high air temperatures, compared to the precedent time period (cf. Fig. 4.1), and evapotranspiration shows relative high values as well. After emergence evapotranspiration increases. With beginning of June air temperature increases strongly and evapotranspiration shows a slight break-in, independent of the precipitation pattern, before reaching the maximum daily values of ~ 3.5 mm in mid-July. From August, when final canopy height is reached, evapotranspiration starts to decrease continuously until harvest. This behaviour is mainly given by the decrease of active biomass and is most pronounced in October 2005.

Regarding mean daily values of precipitation for vegetation periods and periods of bare field conditions the variability is low and the value is ~ 2 mm d^{-1} . An exception is vegetation period 2006 when the value is almost doubled. Mean daily evapotranspiration values show a clear difference given

by radiation and the existence of biomass. During vegetation periods the value is about four times greater than during bare field conditions (2.3 compared to 0.6 mm d^{-1}).

The ratio of the sum of evapotranspiration over the whole vegetation period to the yield determines the total water need. The values for the three subsequent years are 321, 397 and 422 mm kg^{-1} . Thus, for 1 g of kernels 3.1, 2.5 and 2.4 mm precipitation is needed, respectively. For vegetation periods 2004 and 2005 total evapotranspiration is greater than total precipitation. Thus, a change in soil water storage must take place which is qualitatively supported by the measurements (cf. Fig. 4.1c).

Water use efficiency WUE is generally defined by the relationship of GPP and transpiration. As neither GPP nor transpiration is measured directly by the given set-up, WUE is defined in a slightly different way. Instead of GPP the values of NEE as a measure for assimilation and instead of transpiration the water vapour flux density, i.e. evapotranspiration as a measure for transpiration are taken into relation. As NEE underestimates and Q_E overestimates the terms the resulting values for WUE are lower than by the common definition. The course of WUE for every vegetation period is shown in Fig. 4.10. A general increase of WUE with time after emergence is given. Regarding half hourly values of WUE, its maximum values decrease with increasing air temperature and water vapour deficit. But below that threshold WUE is relatively insensitive to both parameters as was also found by Baldocchi (1994) in a short-term study. As transpiration is strongly correlated with photosynthesis, WUE shows also a strong relationship with PPFD and the amount of biomass.

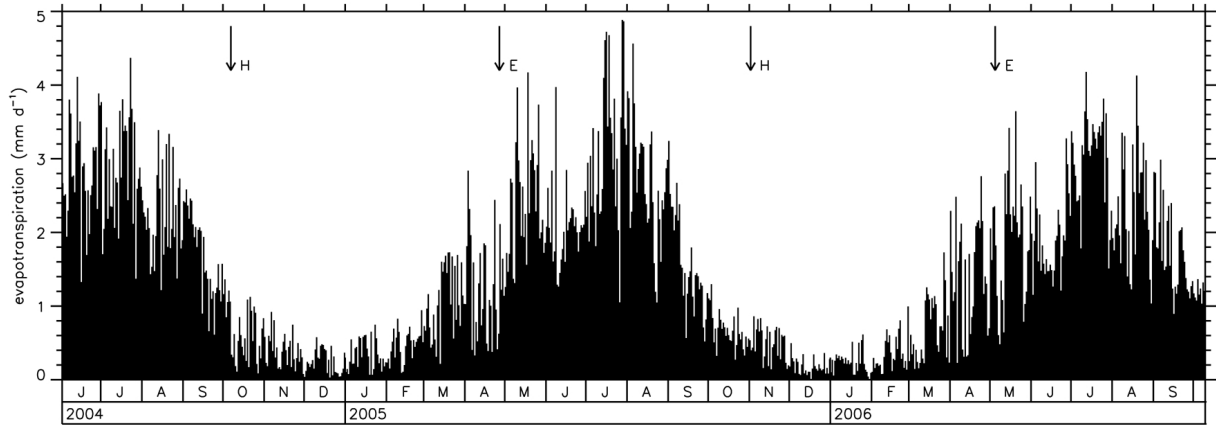


Figure 4.8: Daily sums of evapotranspiration for the whole measurement period. The arrows indicate harvest (H) and emergence (E) of the plants.

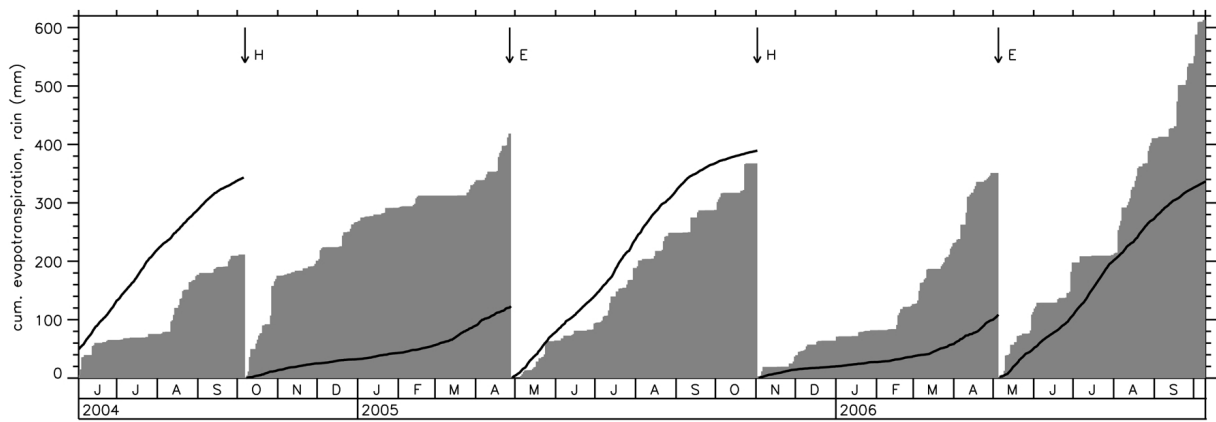


Figure 4.9: Cumulative curves of evapotranspiration (black) and precipitation (grey) for each vegetation period and period of bare field conditions, respectively. The arrows indicate harvest (H) and emergence (E) of the plants.

Table 4.2: Sums of the terms of the water balance for each vegetation period and period of bare field conditions, respectively.

	precipitation (mm)	evapotranspiration (mm)	runoff+storage (mm)
vegetation period 2004	211	343	-132
fallow 2004/05	418	123	+295
vegetation period 2005	368	389	-21
fallow 2005/06	351	108	+243
vegetation period 2006	613	338	+275

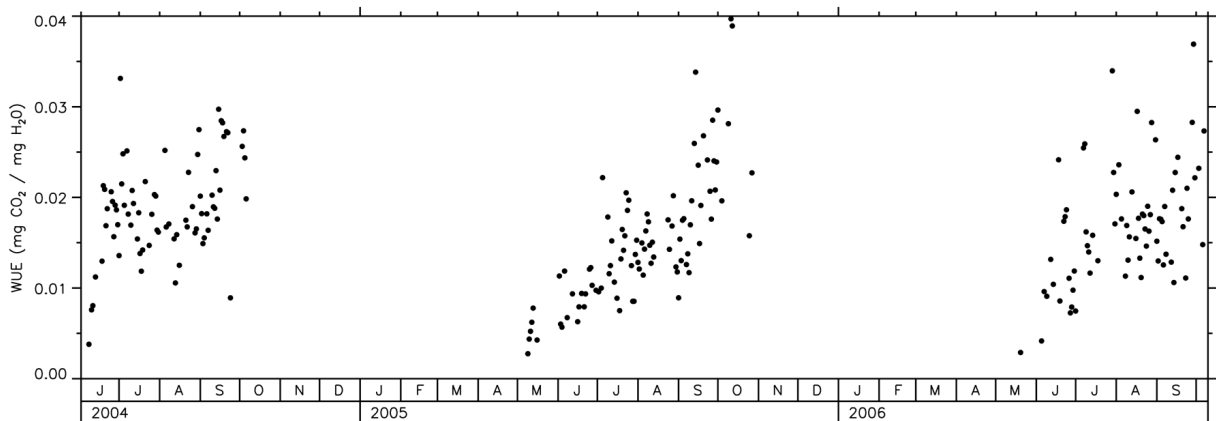


Figure 4.10: Pattern of the water use efficiency WUE over the whole measurement period.

4.4 Carbon balance

In this section the results for the carbon balance are presented. The balance is based on the NEE measurements and information about the harvest. The analysis is restricted to considerations of NEE according to Eq. 2.16 ($F_c + S_c$) as GPP and TER are not estimated although they would provide more detailed information about the ongoing processes in carbon assimilation and respiration of the ecosystem. The estimate of TER is usually done by extrapolating night-time NEE values, which are assumed to equal TER, to daytime respiration values by the application of a derived temperature response function (Reichstein et al., 2005). It is the same method as used for gap filling of night-time data (section 3.4.2). This method is not applied because the reliability of the derived relationship is low and a rather high error is induced in the data. Additionally, there is a given uncertainty from biological considerations in the correctness of this approach, because the behaviour of the agents of evapotranspiration is probably different for daytime and night-time situations (Davidson et al., 2006).

In the first subsection the overall picture with its seasonal patterns and inter-annual variability is given. Afterwards, the results are discussed in response to the driving forces for NEE and in more detail for some given time periods. Finally, some considerations are made about the advective terms.

4.4.1 Seasonal pattern and inter-annual variability

Daily values of NEE for the whole measurement period are shown in Fig. 4.11. Generally, the pattern in all three years is similar. During the first month after emergence the daily NEE values fluctuate around zero. The absolute values are small and in the range of daily values during bare field conditions. As the proportion of bare soil is still large, soil efflux is rather high and counter-balances the assimilation. Afterwards, the ecosystem becomes a net sink of carbon until harvest. During the vegetative stages in June and July, characterised by a strong increase of photosynthetic active biomass, the daily NEE values increase strongly. With the onset of the reproductive stages the daily totals begin to

decrease. This trend continues with ongoing senescence as the portion of the photosynthetic non-active organs becomes higher. After harvest intense respiration is given by the decomposition of the plant residues. During fallow the field is a constant source of carbon, even at low temperatures.

This pattern is strongly modified by the meteorological conditions (cf. Fig. 4.1) which cause also positive daily sums during vegetation periods when photosynthetic assimilation breaks down and is balanced by soil efflux. Additionally, the physical health of the plants limits the potential NEE. Several examples are described in section 4.4.3.

For a first instance the year 2005 is described in more detail because of some extraordinary circumstances. The second half of April was very rainy and the soil became silty. At this growth stage around emergence the plants are very sensitive to flooding and a large part of the young plants died off. Therefore, the sowing had to be carried out a second time. After the emergence of the seeds of the second sowing there was more photosynthetic active biomass than in the two other years, as nevertheless partially both seeds germinated, ending up in higher NEE values in the first part of June. With ongoing growth the "twin"-plants compete for water, nutrients and PAR, resulting in less robust stalks and in a potential reduction of yield (Hashemi et al., 2005). A fair weather period with high temperatures in the second half of June with mean daily temperatures of 20–25 °C led to a stagnation of the daily NEE values. At the beginning of July a hail event occurred and damaged the leaves with a significant long-term effect on photosynthetic capacity and therefore on growth. Some plants were even bent. The increase of the daily NEE values in June and July is less steep and the maximum values are lower than in the two other vegetation periods. Because of rainy weather conditions at the beginning of October the kernels were too wet for harvest and the plants remained on the field until begin of November. Particularly, in the second part of October only a small fraction of the biomass was still photosynthetically active and the soil efflux balances the assimilation.

In Fig. 4.12 the cumulative curves of NEE for the different vegetation and fallow periods are displayed. For a better comparability of the different "years" the cumulative curves of NEE are also dis-

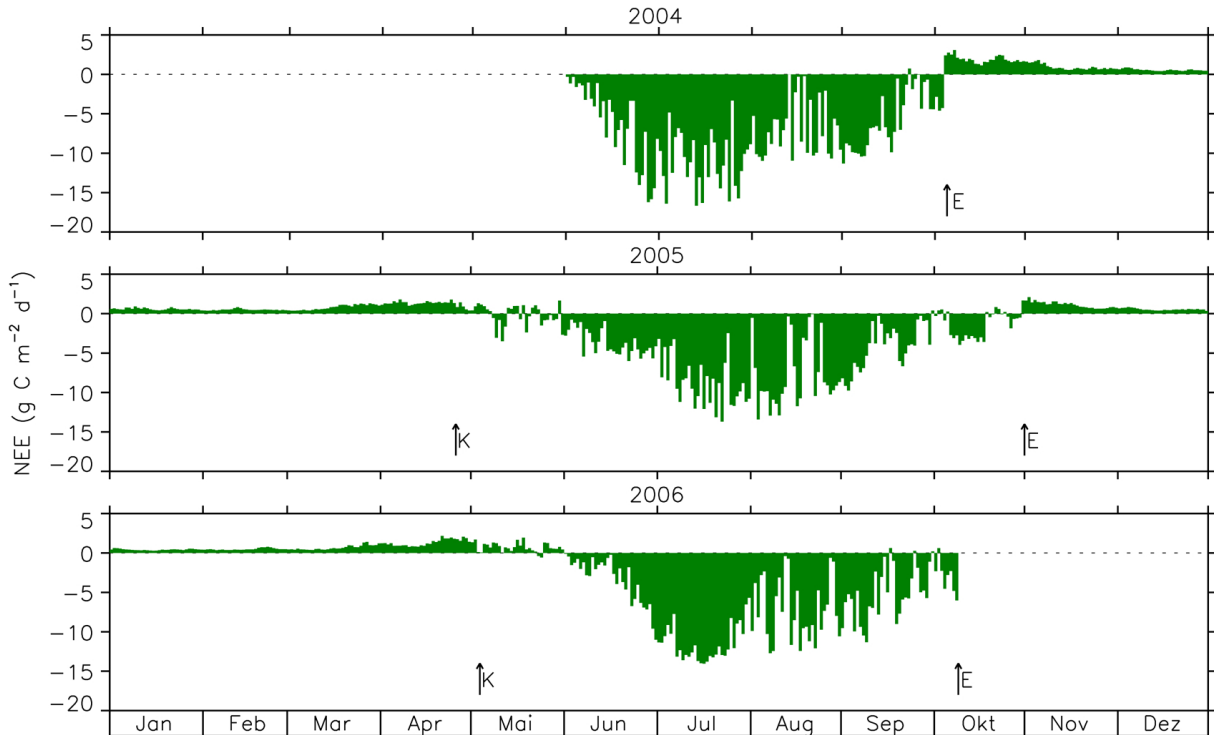


Figure 4.11: Daily sums of NEE for the three subsequent years (from top down). The arrows indicate harvest (H) and emergence (E) of the plants.

Table 4.3: Carbon balance. Grain yield is adjusted to 15 % moisture content and 50 % carbon content of the dry matter.

year	vegetation period		grain yield		fallow	"year"
	emergence	(g C m ⁻²)	harvest	(g C m ⁻²)	(g C m ⁻²)	(g C m ⁻²)
2004	June 1	-930	October 5	455	186	-289
2005	April 25	-785	October 31	417	142	-226
2006	May 3	-841	October 9	340		

played in Fig. 4.14. Here, a "year" is defined as the time period between two subsequent points in time of emergence (for 2006 it lasts only until harvest). In 2004 no measurements exist for the first few weeks after emergence. They started when canopy height was already 0.2 m. A comparison with 2005 and 2006 shows that this period does not affect the final carbon balance significantly as the corresponding totals of NEE are -1 and +1 g C m⁻², respectively. Thus, up to a canopy height of ~0.2 m (reached at June, 01 2004, May, 28 2005 and June, 13 2006) carbon assimilation is balanced out by soil respiration. Afterwards, the assimilation increases strongly. For 2004 and 2006 the course is rather similar. The greatest difference arises in the last month before harvest given by much more precipitation and correspondingly less PPF_{D_{net}} in 2006. The reasons for the special behaviour in 2005 are described in detail above. The regime during fallow is also very similar for both periods. However, the cumulative NEE

for bare field conditions in 2004/05 is higher than in 2005/06. Particularly the respiration rates just after harvest are higher as temperatures are higher and more biomass is available for decomposition. Besides, the period of bare field conditions is ~20 days longer in 2004/05.

Additionally to the cumulative curve, the values determined by biomass sampling (cf. section 3.1) are shown in Fig. 4.12. To determine the carbon content a density of 9 plants per square meter and a carbon content of the dry matter of 50 % are assumed. The agreement of these values with the estimates by the eddy covariance method is good. The values derived from biomass sampling are expected to be larger because heterotrophic respiration is not captured by this method. Uncertainty in the values is given by the circumstance that only the above-ground biomass of one single plant is measured. Suyker et al. (2004) report a final root-shoot ratio of

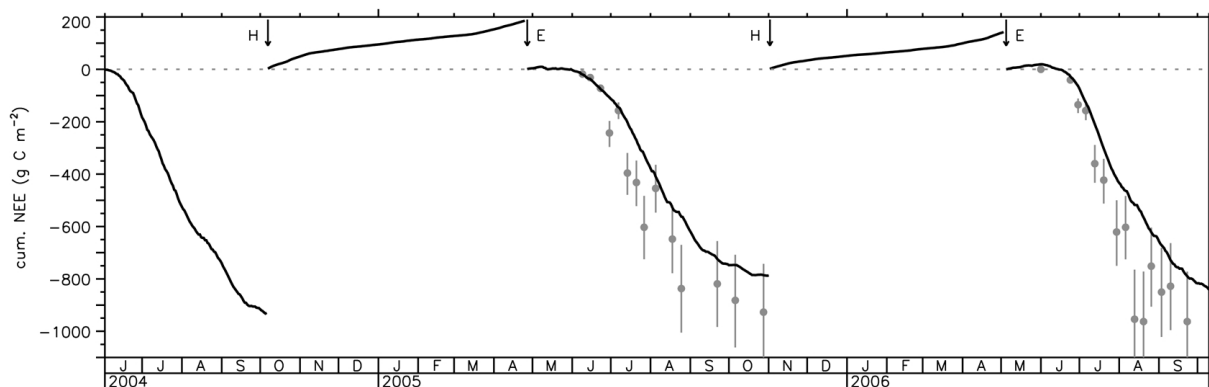


Figure 4.12: Cumulative curve of NEE, separating vegetation periods and bare field conditions. The dots mark the biomass determined by destructive sampling, assuming a density of 9 plants per square meter and a carbon content of the dry matter of 50 %. The lines mark a deviation of $\pm 20\%$ of this value. The arrows indicate harvest (H) and emergence (E) of the plants.

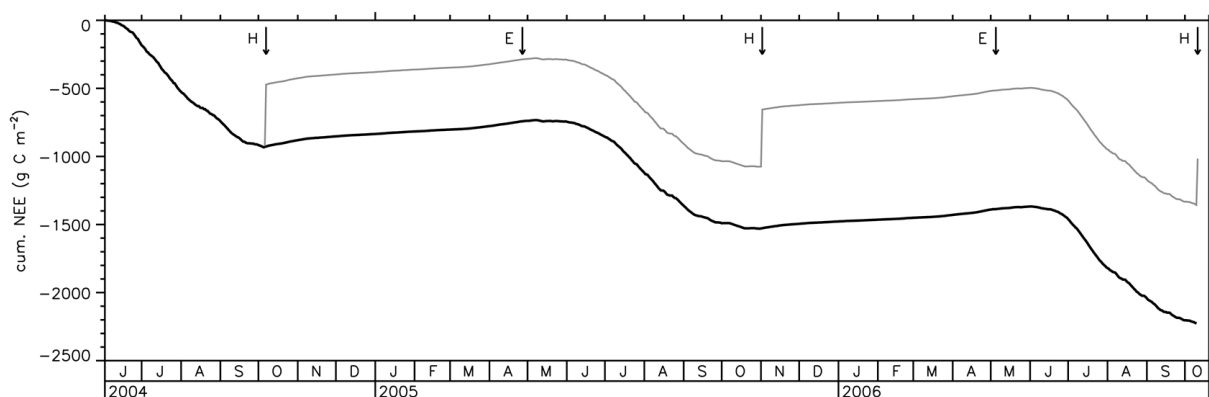


Figure 4.13: Cumulative curve of NEE in black. The grey curve takes the harvest into account. The arrows indicate harvest (H) and emergence (E) of the plants.

0.15 for rain-fed maize. But this ratio changes over time (Han et al., 2007) and is suspect to the actual conditions, e.g. under dry conditions maize intensifies the growth of fine roots.

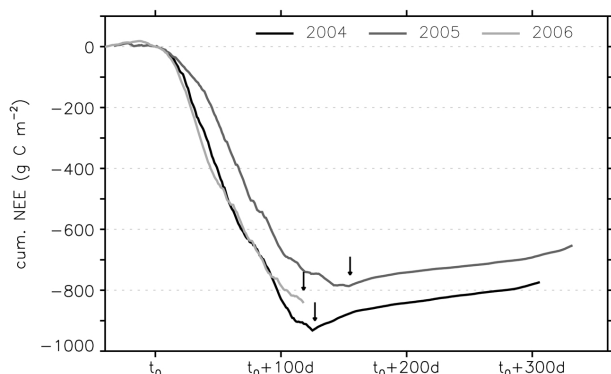


Figure 4.14: Cumulative curve of NEE for the three "years". t_0 is defined as the point in time when $h_c = 0.2$ m (at June, 01 2004, May, 28 2005 and June, 13 2006). The arrows indicate the time of harvest.

The cumulative NEE over the whole measurement period is shown in Fig. 4.13. Neglecting the outgoing yield a final carbon sink of 2.2 ± 0.4 kg C m⁻² results. If harvest is taken into account the sink

diminishes to 1.0 ± 0.2 kg C m⁻². The uncertainty estimates are based on the rRSME values for the different calculation approaches (measurement, parametrisation, ANN) according to their relative portion (cf. section 3.4.5). Table 4.3 summarises the totals of the carbon balance for vegetation period, harvest, bare field conditions and the "year". The variability in carbon assimilation during vegetation period is $\sim 10\%$, for bare field conditions it is $\sim 15\%$. For the three years 49, 53, and 40 % of the assimilated carbon at the end of the vegetation period are reaped and another 20 % are respired during bare field conditions in the winter half year. For the determination of the values for yield a humidity content of 15 % and a carbon content of the dry matter of 50 % are assumed. The remainder of 30 %, about 260 g C m⁻² are stored in the soil. This storage is not a final increase in carbon stock of the soil. It is more likely temporarily not yet decomposed biomass (cf. soil analysis in section 3).

4.4.2 Driving forces

In section 2.1 an overview about the controlling factors of NEE is given. In this section two physiologically integrating parameters - quantum yield for periods of assimilation and Q_{10} for periods of respiration - are discussed to illustrate these relationships.

Quantum yield — The course of the quantum yield (Fig. 4.15) shows a strong seasonal pattern mainly depending on growth stage and meteorological conditions. The general pattern indicates the different growth stages. As long as the plants are rather small (h_c below about 0.5 m) the quantum yield remains below $\sim 0.01 \mu\text{mol CO}_2 \mu\text{mol}^{-1} \text{PPFD}_{net}$. During this stage, i.e. the first 50-60 days after emergence, the amount of photosynthetic active biomass and the vegetation coverage are rather small. Therefore, the NEE is strongly influenced by soil respiration. Within about the next four weeks, the quantum yield increases strongly to about $0.03 \mu\text{mol CO}_2 \mu\text{mol}^{-1} \text{PPFD}_{net}$. During this period the plants grow almost to their final height. With starting tasseling the quantum yield flattens out. With ongoing senescence the quantum yield starts to decrease ~ 160 days after emergence, approximately in September.

The course of the quantum yield is predominantly modified by temperature as well as by the amount and temporal distribution of precipitation (cf. Fig. 4.1, Tab. 4.1). In 2004, from mid-July until mid-August a pronounced break-in in quantum yield is given by high mean daily temperatures (25°C) and a low soil moisture level. The plants recovered after a rainy period in August. The special conditions in 2005 are already described above (section 4.4.1). Given by the delay of the plants of the second sowing the quantum yield in June is lower than in 2006. However, the plants made up leeway until mid-July. The impact of the hail event on July, 29 lasted until harvest and is also visible in lower maximum values for quantum yield. Vegetation period 2006 started almost ideal. But in July, there was only one significant rain event in the beginning. Soil moisture dropped significantly and air temperatures (with a mean value of 23.4°C) were high. This slight drought led to a break-in in the quantum yield. The plants recovered in the rainy month of August. During vegetative growth and tasseling maize is sen-

sitive to moisture stress, finally resulting in a reduction of yield. In 2006 the dry conditions existed in this sensitive period. In 2004 the small drought took place in a later growth stage. Accordingly, the impact on yield in 2004 is negligible whereas in 2006 the yield is reduced (Tab. 4.3). In 2006 only 40 % of the assimilated carbon can be reaped, compared to $\sim 50\%$ in the two other years.

Quantum yield is in addition often linked to atmospheric humidity and CO_2 concentration. As a C4 plant, maize shows no relationship with these parameters (cf. section 2.1). This fact is illustrated for water vapour pressure deficit in Fig. 4.16. Under the given soil moisture conditions the impact on quantum yield is of minor importance and restricted to extreme situations (e.g. in July 2006 as described above and in more detail in section 4.4.3).

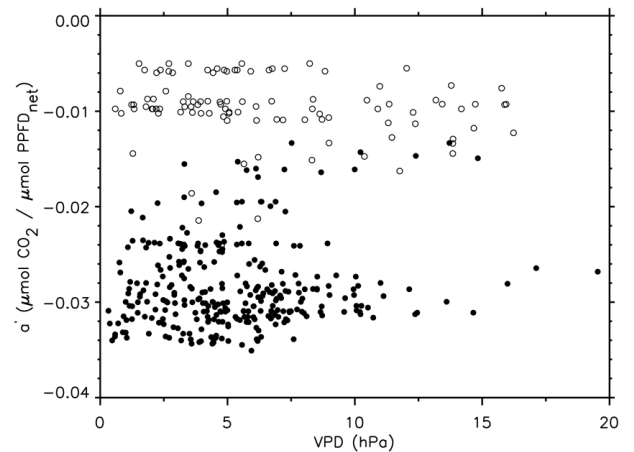


Figure 4.16: Daily quantum yield as a function of vapour pressure deficit VPD of all three vegetation periods. The VPD values are means of daytime values. The open circles are situations when $h_c \leq 0.5$, the full circles are situations when $h_c > 0.5$.

Temperature sensitivity of respiration — For the present study a mean Q_{10} of 2.3 ± 0.4 results. The resulting mean values for different soil temperature classes, T_{ref} in Eq. 2.2, and different soil moisture conditions are displayed in Fig. 4.17. During vegetation periods only night-time, during bare field conditions all values are taken into account. Considering the whole measurement period the Q_{10} value increases from about 2.1 to 2.8 at T_{ref} of 10°C . At higher temperatures it shows a strong decline to about 1.6. Dry conditions are rare at low temperatures and the pattern of Q_{10} values is almost the same as for the mean. Wet conditions show lower values with the same pattern except for low temperatures when Q_{10} is significantly higher.

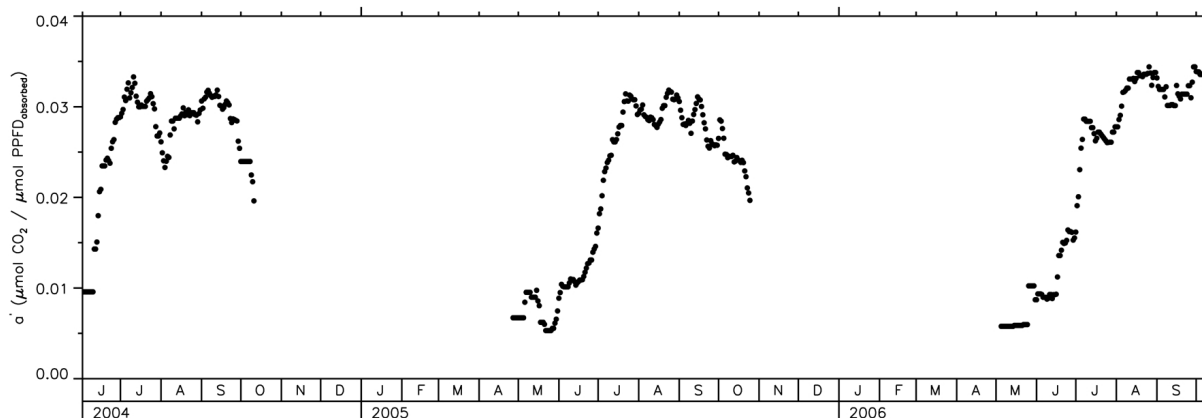


Figure 4.15: Pattern of the quantum yield over the whole measurement period.

Q_{10} shows a similar behaviour for vegetation periods and bare field conditions, i.e. an increase of Q_{10} with increasing T_{ref} up to a maximum value, followed by a strong decline, only the temperature range is shifted. The influence of soil moisture is different for both periods. Whereas during vegetation periods Q_{10} is reduced under dry conditions, it shows lower values under wet conditions during bare field conditions (not shown).

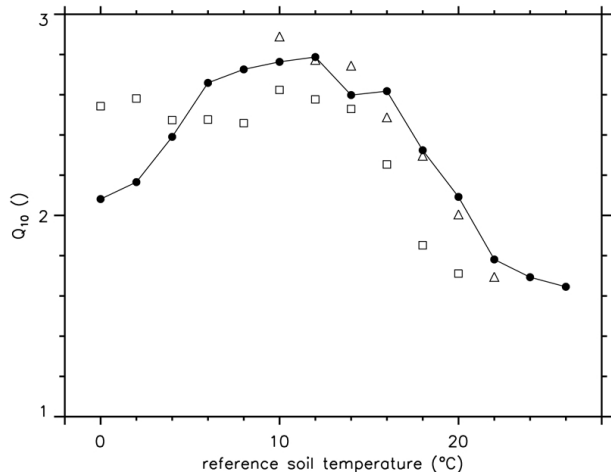


Figure 4.17: Mean Q_{10} values as a function of reference soil temperature. Values for the whole measurement period for all conditions (\bullet), for dry conditions (soil moisture below 15 vol.%, Δ), and wet conditions (soil moisture above 25 vol.%, \square) are shown.

4.4.3 Examples

In this section four different time periods are discussed in more detail to illustrate the relationships between NEE and the main agents.

In Fig. 4.18 ten days during July 2005 are displayed. This period is taken to be an example of intense plant growth. Within these ten days the vegetation height increases from 1.2 to 1.8 m. The meteorological conditions are as follows: Mean air temperature is 19.8 °C, total precipitation is 46 mm and total $PPFD_{net}$ is 380 mol m⁻². The interaction of $PPFD_{net}$ and NEE is pronounced. For example, on July 16 the rain event around midday and the preceding clouds reduce $PPFD_{net}$ and result in a break-down of CO₂ assimilation and NEE becomes almost zero. Soil moisture is above a critical value during these days and has no impact on NEE. The biomass increases remarkably and at the same time the quantum yield increases from 0.025 to 0.030 μmol C m⁻² s⁻¹ per μmol PPFD_{net} m⁻² s⁻¹. This higher capacity to fix carbon can be seen by comparing two similar, almost clear sky days, July 13 and July 17: the daily sums of NEE are 9.5 and 12.1 g C m⁻², respectively.

The next example is the month of October 2005 (Fig. 4.19). The meteorological conditions are as follows: mean air temperature is 12.5 °C, with a lower solar inclination total $PPFD_{net}$ reaches 470 mol m⁻². Precipitation occurs at the beginning of the month and around the 23, with a total of 80 mm. The plants are senescent and in the two other years harvest takes place at the beginning of October, but due to the rainy period the kernels became too wet for harvest and the subsequent storage. Thus, the plants were dried on the field until the beginning of November. The photosynthetic active biomass decreases as more and more leaves wither. Accordingly, the quantum yield decreases from 0.029 to 0.020 μmol C m⁻² s⁻¹ per μmol PPFD_{net} m⁻² s⁻¹. The development of decreasing potential $PPFD_{net}$

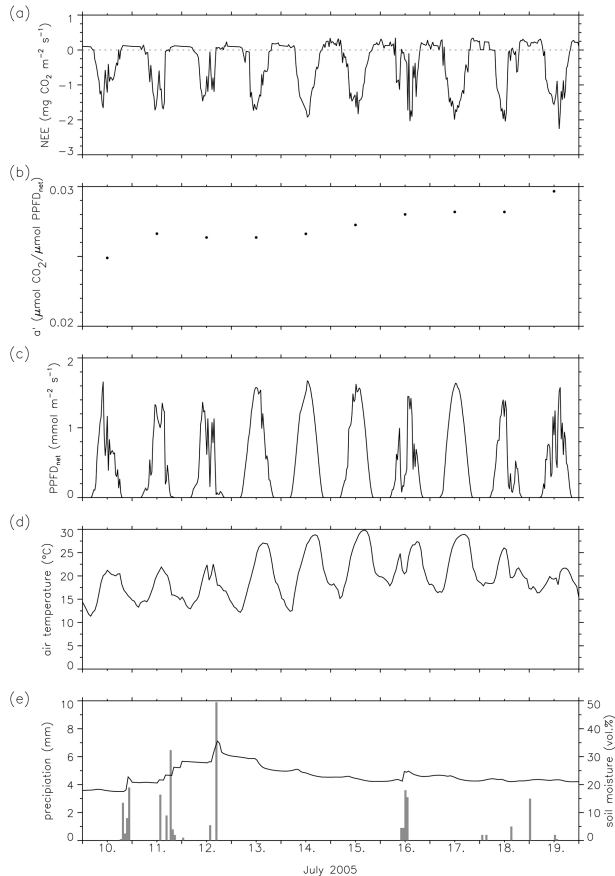


Figure 4.18: Course of (a) NEE, (b) quantum yield, (c) $PPFD_{net}$, (d) air temperature and (e) precipitation and soil moisture from July 10 to July 20 2005. Data are based on half hourly values.

and decreasing quantum yield is reflected in the daily sums of NEE. As an example, during the first period of fair weather conditions from October 8 to 16 the NEE is about $3 \text{ g C m}^{-2} \text{ d}^{-1}$, for the second period from October 27 to 30 it is only about $1 \text{ g C m}^{-2} \text{ d}^{-1}$.

The third example (Fig. 4.20) shows a period over two months with contrasting meteorological conditions, from July to August 2006. The month of July is warm (mean air temperature: $23.4 \text{ }^\circ\text{C}$), the amount of $PPFD_{net}$ is high (1410 mol m^{-2}) and precipitation is extremely low (total of 15 mm). The month of August was colder (mean air temperature: 16.2 °), $PPFD_{net}$ is about half as in July and precipitation occurred on most of the days (total precipitation: 197 mm). Canopy height increases from 0.85 m at the beginning of July to its mature value of 2.3 m at the beginning of August. The daily sums of NEE are a direct consequence of available PPFD: for example the strong decrease from July 21 until August 6 or the tiny daily sums on August 13

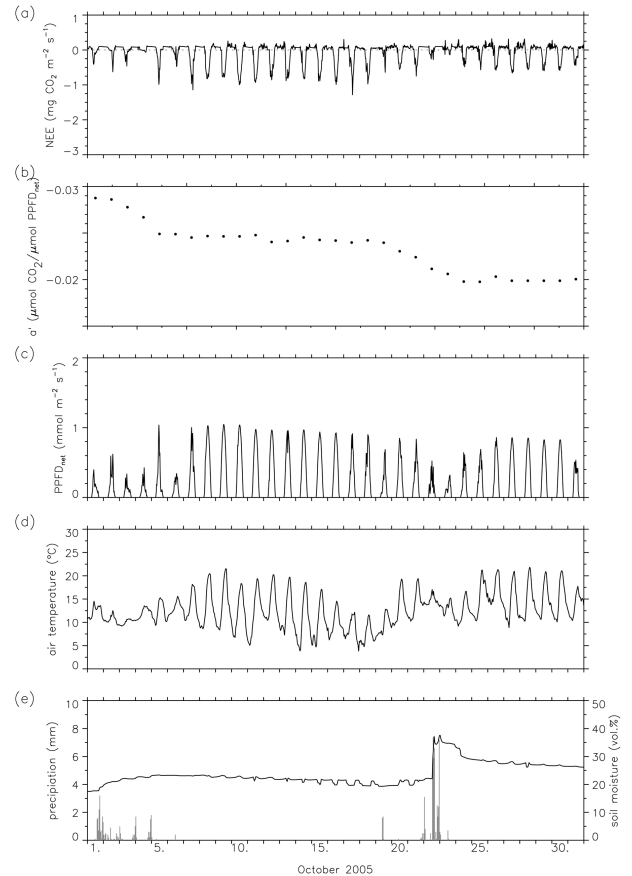


Figure 4.19: Course of (a) NEE, (b) quantum yield, (c) $PPFD_{net}$, (d) air temperature and (e) precipitation and soil moisture during October 2005. Data are based on half hourly values.

and 14. In July soil moisture decreases continuously from 25 to 12 vol.%. At a first sight the dry conditions have no impact on NEE, but from July 8 to 26 the daily sums are about constant. Generally, they should increase as the quantum yield increases simultaneously with the increasing biomass at this growth stage (cf. Fig. 4.18). In contradiction the quantum yield is slightly reduced from 0.029 to $0.026 \text{ mol C m}^{-2} \text{ s}^{-1} \text{ per mol PPFD}_{net} \text{ m}^{-2} \text{ s}^{-1}$. There is also a steep increase in PPFD albedo (cf. Fig. 4.1e). During the two other vegetation periods the PPFD albedo increases slightly during vegetation period. Under these conditions of water stress the daily maximum of NEE is slightly shifted into the morning. Already with the first light rain events end of July the quantum yield increases again and it is suggested that the plants adapted to the dry conditions and improved water uptake by developing a ramified and deep root system.

The last example illustrates bare field conditions, from November 2004 to March 2005 (Fig. 4.21). Air temperature is relatively high at the beginning and at

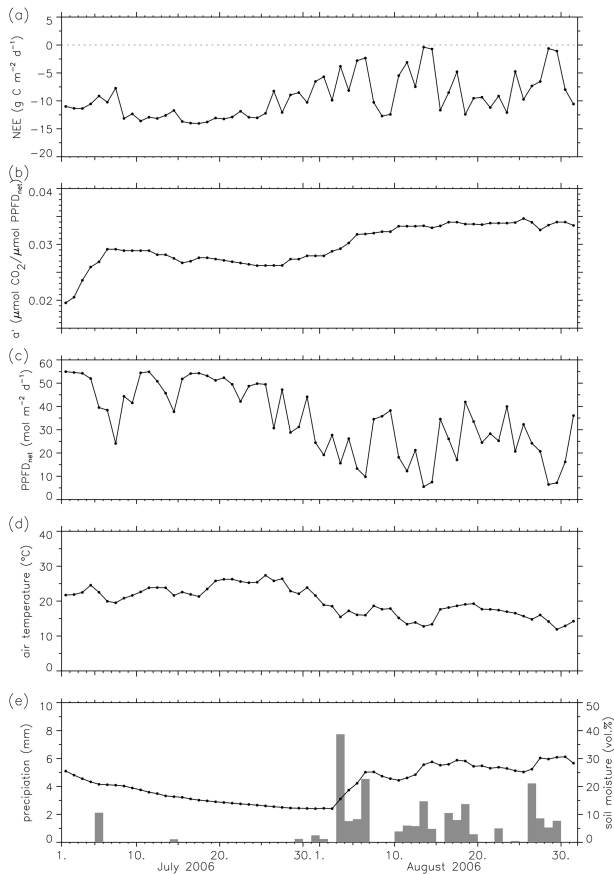


Figure 4.20: Course of (a) NEE, (b) quantum yield, (c) $PPFD_{net}$, (d) air temperature and (e) precipitation and soil moisture from July to August 2006 based on daily values.

the end of the displayed time period. Meanwhile, air temperatures are much lower with a mean value of $1.5\text{ }^{\circ}\text{C}$, but periods with temperatures below $0\text{ }^{\circ}\text{C}$ alternate with periods above $5\text{ }^{\circ}\text{C}$. Precipitation adds up to 164 mm . Soil moisture content is at about the same level for the whole period. $PPFD_{net}$ is irrelevant for the resulting NEE as there is no vegetation present. But air and accordingly soil temperature induce respiration even at low temperatures. Microbial activity is restricted but however, it is assumed that the CO_2 concentration gradient between the soil air and the atmosphere is still large and diffusion takes place.

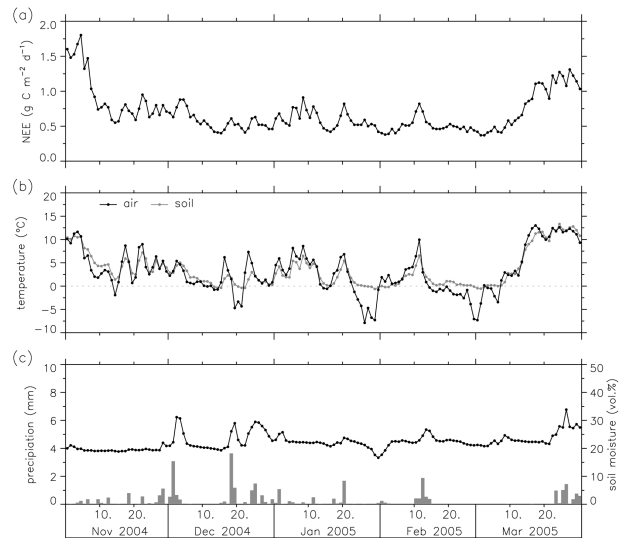


Figure 4.21: Course of (a) NEE, (b) air and soil temperature and (c) precipitation and soil moisture from November 2004 to March 2005 based on daily values.

4.4.4 Advection

In this section results from the advection experiment are shown. Although measurements started end of June, data analysis is restricted to the time period August and September 2006 when final canopy height is reached. From meteorological considerations the month of July, characterised by hot and dry conditions, would have been preferred. But, the maize is strongly growing from 0.85 m up to the final height of 2.30 m . Thus, the conditions change probably too fast to be able to detect some general patterns. And particularly, the given instrumentation with only three fixed measurements levels is not able to capture advective fluxes under these conditions. The meteorological conditions of the two subsequent months differ significantly. August and September are rainy with a total precipitation amount of 338 mm and a mean temperature of $\sim 17\text{ }^{\circ}\text{C}$ (cf. Fig. 4.1 and Tab. 4.1).

Figure 4.22 gives an overview of the diurnal pattern of all terms of the mass conservation equation (Eq. 2.15), which are discussed below, as well as for some agents. The sign convention is maintained. Thus, a positive term refers to a transport of CO_2 out of the control volume and a negative term corresponds to an enrichment of CO_2 within the control volume.

Eddy flux and storage term — The sum of $F_c + S_c$ results in a total of -383 g C m^{-2} over the whole time period. In accordance with the reduced quantum yield and the ongoing senescence, maximum daily sums reduce from -10 to -5 g C m^{-2} . During rainy conditions assimilation is almost balanced by respiration. These two factors result in a great variability in the half hourly values of F_c (Fig. 4.22a), particularly during daytime. At night the variability is much smaller.

As a measure for turbulence intensity u_* is displayed in Fig. 4.22d. As expected a clear diurnal course with a maximum in the afternoon is given. The variability throughout the day is large and particularly during night-time the values of u_* are low.

The storage term is small, but shows a pronounced diurnal pattern (Fig. 4.22b), even if the variability is large. During well mixed conditions in the afternoon the term is around zero. Shortly after sunset, turbulence intensity decreases and photosynthesis is stopped but the soil is still warm and respiration is significant. Thus, the enrichment of the control volume is largest. As the soil cools down, respiration decreases and the CO_2 enrichment slows down. In the morning with the onset of turbulence, the stored CO_2 is depleted.

Vertical advection — $|\bar{w}|$ is mainly $< 0.02 \text{ m s}^{-1}$ (Fig. 4.22c). The mean vertical velocity shows a stability dependent diurnal pattern (cf. Fig. 4.23). Regarding median values \bar{w} is negative, i.e. directed to the canopy during stable and slightly unstable conditions and the velocity decreases with increasing stability. During unstable conditions \bar{w} becomes positive and the values and their variability are slightly higher.

The difference in CO_2 concentration between the top measurement level and the mean concentration below is shown in Fig. 4.22e. During daytime the CO_2 concentration within the canopy is lower, given by the carbon assimilation of the plants. Thus, the differences are positive. They are low and the variability is small, an indication for well mixed conditions. During night-time the difference changes sign, becomes much more pronounced and the variability is enormous. Situations with almost no gradient occur as well as situations with a gradient of $1000 \mu\text{mol m}^{-3}$. Thus, a decoupling of the canopy

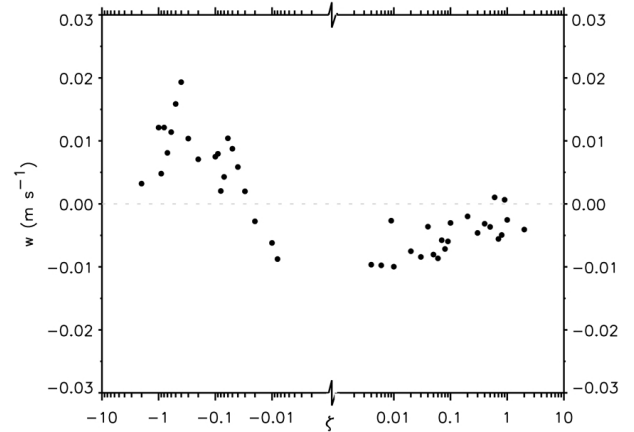


Figure 4.23: Median vertical velocity \bar{w} for different classes of stability parameter ζ . Data are based on half hourly values from August 1st to October 1st 2006 measured above the canopy at the main tower.

sublayer from the exchange processes above can occur or not. The development of the CO_2 gradient at sunset is faster than the reduction after sunrise. In Fig. 4.24 the mean daily course of the mean CO_2 concentration profile within the control volume is depicted. During daytime the concentration differences are negligible. With sunset photosynthesis stops and the CO_2 concentration increases generally over the whole regarded layer. The vegetation and particularly the soil release CO_2 by respiration. Due to the break-down of turbulence and thus due to reduced mixing the enrichment of the layer starts from the surface. With sunrise (R_{sd} becomes positive between 0600 and 0700 hours) and accordingly with the onset of photosynthesis and turbulence the depletion starts at the upper boundary of the canopy sublayer. From about 0700 hours on the vertical differences become again very small. Compared to advection studies at forest sites the mean concentration gradient is high, but these studies show also a high variability between the sites (Feigenwinter et al., 2004; Aubinet et al., 2005; Feigenwinter et al., 2008) and additionally, soil respiration is supposed to be stronger in the maize canopy.

The resulting vertical advection F_{VA} is shown in Fig. 4.22g. During daytime and thus, under well mixed conditions F_{VA} is small and mainly positive. During night-time the variability is much higher and the pattern much less clear. F_{VA} can result in a gain or a loss of CO_2 for the control volume which is determined by the direction of \bar{w} .

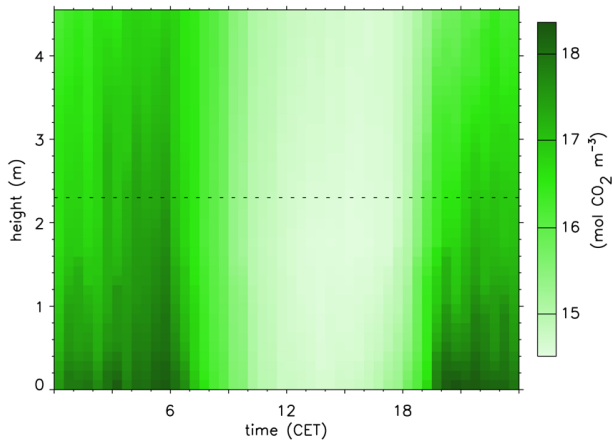


Figure 4.24: Mean daily course of mean CO₂ concentration profile within the control volume from August 1st to October 1st 2006. The dashed line represents mean h_c . Data are interpolated according to section 3.3.9.

Horizontal advection — Horizontal advection F_{HA} is small, shows no clear diurnal course and a large variability (Fig. 4.22f). F_{HA} can be either positive or negative. Figure 4.25 depicts a mean diurnal course of the mean horizontal advection within the control volume. The picture is very patchy and illustrates the uncertainty of the derived values.

Influence of advection on carbon balance — The sum of $F_{VA} + F_{HA}$ is displayed in Fig. 4.22h. The value tends to be positive. Horizontal and vertical advection are either of the same or of opposite direction. Compared with the eddy flux the amount is negligible during daytime (<1 % of F_c). During night-time the range of the sum of the advective terms compared to F_c is very variable, almost from 0 % to 100 %.

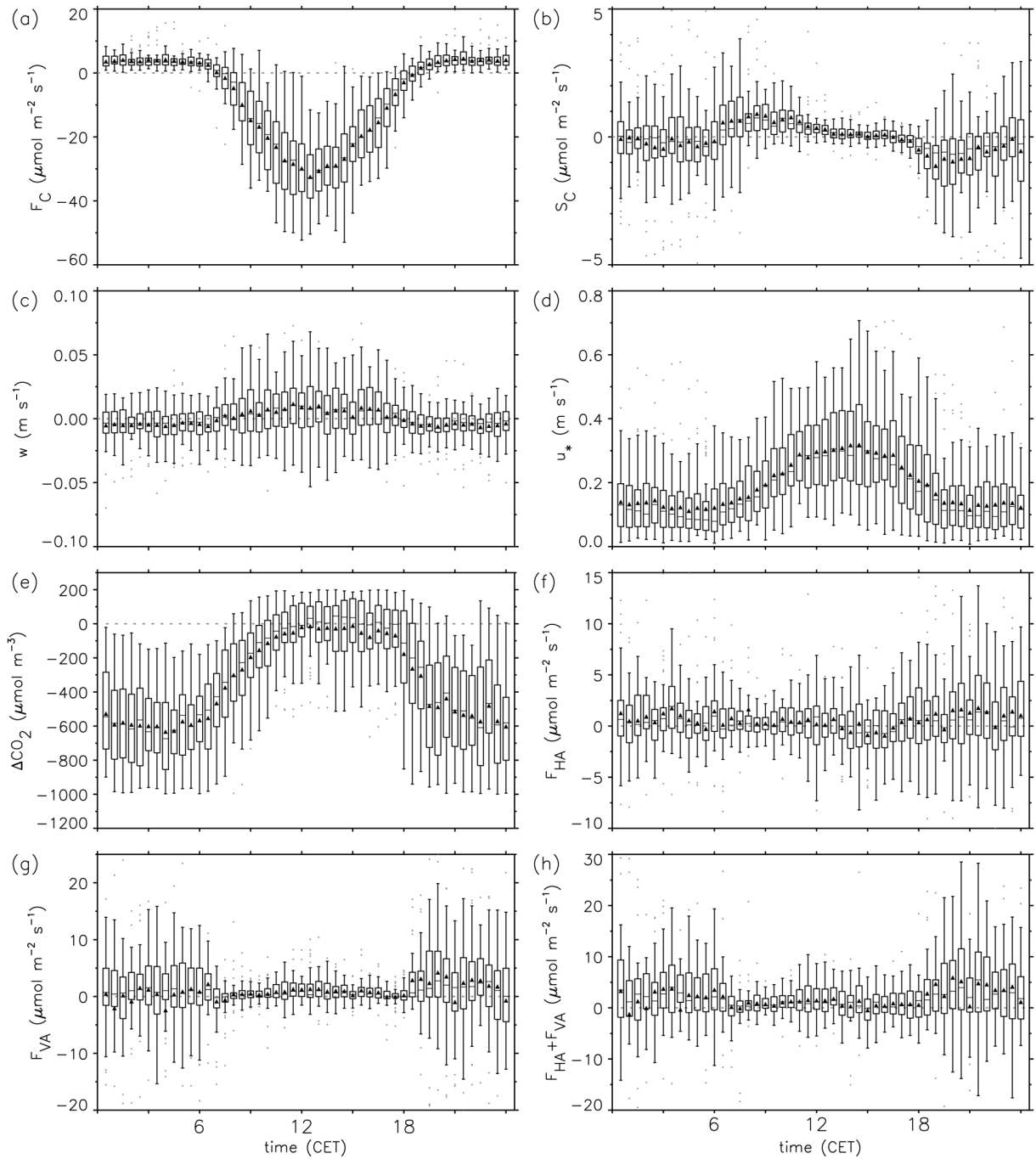


Figure 4.22: Mean diurnal course of different parameters concerning the CO_2 fluxes according to the mass conservation equation (Eq. 2.15): (a) eddy flux F_c , (b) storage term S_c , (c) mean vertical wind velocity \bar{w} , (d) friction velocity u_* , (e) difference in CO_2 concentration between the top measurement level at 4.55 m and the mean concentration below ΔCO_2 (term $\langle \bar{c}_m \rangle - \langle c \rangle$) in Eq. 2.18), (f) horizontal advection F_{HA} and (g) vertical advection F_{VA} . Graph (h) shows the difference of total NEE according to term I in Eq. 2.15 ($F_c + S_c + F_{HA} + F_{VA}$) and NEE according to Eq. 2.16 ($F_c + S_c$). Not all outliers are shown in the boxplots. Data are, if necessary, aggregated to half hourly values and are based on measurements from August 1st to October 1st 2006.

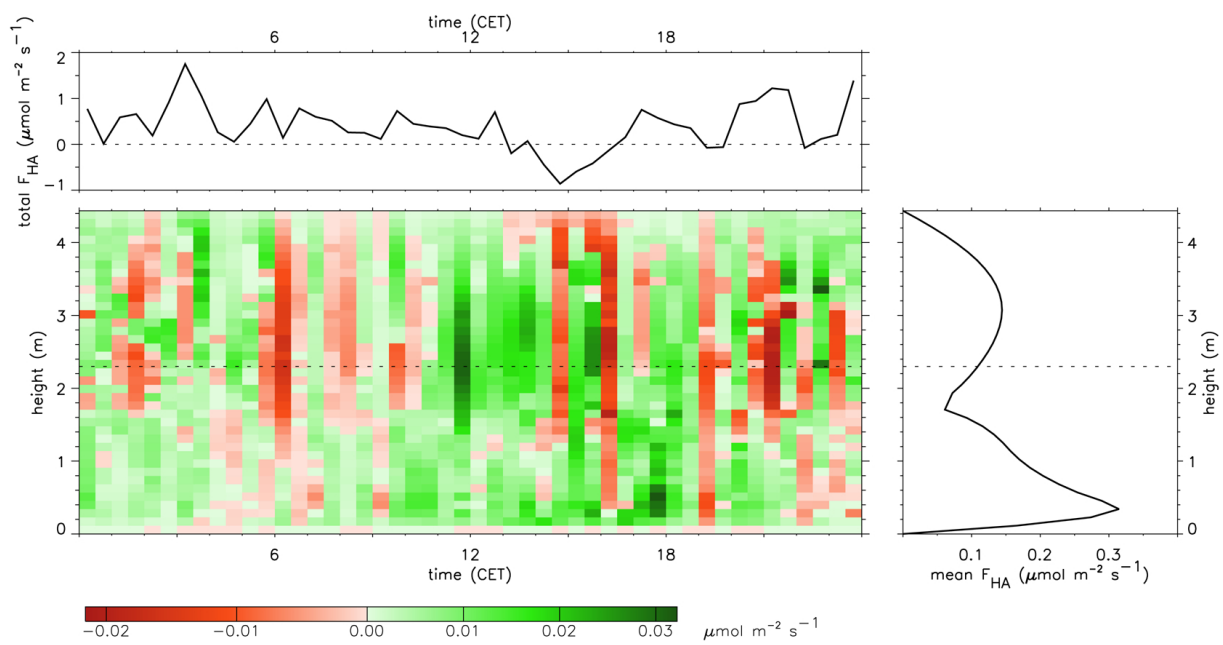


Figure 4.25: Mean diurnal course of F_{HA} depending on height. Top: total F_{HA} in the control volume. Right: mean daily profile.

5 Summary and Conclusions

Reliable estimates of net ecosystem exchange of an agroecosystem under maize-fallow rotation are provided by the use of micrometeorological state-of-the-art instrumentation, even at this site with non-ideal fetch. The fast changing conditions, at harvest or during the three-month growing period from bare field to fully grown maize, are captured as well. The measurement of the main driving forces for assimilation and respiration allowed a reliable parametrisation and gap filling of the NEE.

5.1 Methodology

The applied methodology is mainly developed from measurements in forests (Aubinet et al., 2000). It is shown to be valid in this type of land use, although slight modifications are made. In the following some considerations about the strengths and the weaknesses of the instrumentation and the flux determination are made.

Instrumentation — For the long-term measurements state-of-the-art instruments for eddy covariance measurements have been used in this study without any serious problem. Dewfall on the radiation sensor was inhibited by ventilation of the sensor. A weakness of the open-path IRGA is its sensitivity to water on the lens. In a humid climate it would be worth to measure the CO₂ flux densities for a given time period also with a closed-path IRGA. Thus, it could be tested if the assumption of a similar behaviour of NEE during rainy conditions is correct and the relationships for gap-filling derived from dry conditions can be applied or if e.g. some flushing occurs. An other problem with the open-path IRGA originates from a temperature difference between the sensor and the surrounding air, which can lead to a significant overestimation of carbon uptake under cold temperatures. An advantage of the sensor is that it needs almost no maintenance and calibration for CO₂ showed its long-term stability.

To put down the tower during tillage is necessary to

ensure most undisturbed conditions as the tillage by machines can not be replaced by handwork. But it would have been very useful to install a basic station nearby measuring the main driving forces for respiration. Particularly at harvest the conditions differ significantly from all other periods and this data is needed for a reliable parametrisation of NEE.

Particularly the decomposition of the organic matter in the soil is not a linear process as it depends on microbial activity, temperature and soil moisture and the decomposition of the organic material from the former year takes longer than to the next vegetation period. Periodic analysis of the soil would allow a qualitative measure for the status of decomposition and would give information about soil carbon stock development.

One parameter missed is the leaf area index which is an input in models and the information of the stratification of the canopy would also give additional useful information for the parametrisation of the incanopy wind profile, e.g. needed for considerations about advective fluxes.

Information about the nitrogen cycle would be a further benefit as the carbon cycle is strongly related to it.

For the advection experiment a similar set-up to the experiments in forests was used which is assumed to be a good approach also in a maize canopy. But, it became obvious that the spatial resolution of the wind and CO₂ profile was too small. For the wind the two levels have been given by the physical dimension of the instruments used. Thus, it is suggested to use smaller 2D sonics for future experiments. As wind speed is generally low within the canopy the ability of the instruments to resolve them is essential. Unfortunately, the instruments used in this study showed severe problems. As the soil is the main source for respired CO₂ one measurement should be carried out as close to the ground as possible. As the expected differences in CO₂ concentration are small a good calibration and a sensor comparison is recommended.

Quality control — An important task is the quality control of the measurements, i.e. the definition of the criteria and threshold values for an acceptance or rejection of the data. Particularly under low turbulence conditions the eddy covariance method often fails and leads to an underestimation of the fluxes, for CO₂ to an underestimation of the respiration term. To overcome this problem the u_* correction was applied in this study. The determination of the threshold value turned out to be difficult as the friction velocity at night is generally small and the scatter is high.

The applied corrections compensate for deficits of the sensors and the set-up. The chosen approach for spectral correction bases on the universality of the Kansas spectra. An assumption which would be worth to check, particularly for CO₂ flux density.

In a small-patched agricultural area as present the limited fetch under periods of transition and stable conditions becomes a source of error. For further studies an integration of the source area in the quality control, as e.g. recently proposed by Göckede et al. (2008), can improve the data quality, but contains also the risk of discarding a large portion of the values, which strengthens the task of an appropriate gap filling approach.

Gap filling — For this study different gap filling methods are applied, depending on the time of day, the length of the gap and the availability of data of the driving forces. For daytime situations during vegetation periods a simple linear regression with available photosynthetic active radiation results in reliable values. The approach takes the different type of photosynthesis of maize as a C4 plant into account.

For night-time or bare field conditions the applied parametrisation with soil temperature, independent of the specific mathematical function, leads to values containing a large error as the scatter in the measurements is high. Including the biomass and/or net primary production as applied by Han et al. (2007) could improve the accuracy of the parametrisation. A reliable parametrisation would also allow the estimation of TER and GPP.

The use of an artificial neural network enabled to fill up the long gaps during tillage. It is suggested

that including actual biomass for vegetation periods and the biomass remaining for decomposition during bare field conditions as input parameters would improve the results.

Another approach for gap filling could be the use of growth simulation models (e.g. CERES-Maize, Jones (1986)) or of physically driven soil-vegetation-atmosphere-transfer models (e.g. Haverd et al., 2007).

Advection — The instrumental deficits are already discussed above. It is suggested that an increase of spatial density in the vertical and the horizontal plane would improve the reliability of the results as the small scale heterogeneity would be captured. For vertical advection the determination of an accurate mean vertical velocity turned out to be a crucial task as an error can even change the sign of the advective term. For night-time situations, when advection is assumed to be more pronounced, a different approach proposed by van Gorsel et al. (2007) could give additional information.

5.2 Synthesis

Besides unlimited PAR the combination of the optimal temperature range with the needed precipitation amount corresponding to the needs of the actual growth stage are essential for optimal maize growth.

There are only a few studies determining the carbon balance of a maize canopy with the eddy covariance technique (Desjardins et al., 1978; Desjardins, 1985; Baldocchi, 1994; Steduto and Hsiao, 1998*a,b*; Suyker et al., 2004, 2005; Verma et al., 2005). The resulting patterns of the present study for different time scales, from half hourly up to seasonal, are comparable to them. The peak in the daily sums of NEE is -17, -14 and -14 g C m⁻² for the three subsequent years. Desjardins (1985) reports a value of ~14 g C m⁻² and Suyker et al. (2005) one of 17 g C m⁻² for irrigated maize. A study in rain-fed maize shows lower values for yearly NEE, yield and the resulting "year", but a similar variability (Suyker et al., 2004, 2005; Verma et al., 2005). For the present study the resulting numbers have been summarised in Tab. 4.3.

The mentioned studies are restricted to the vegetation period as often another type of crop is cultivated afterwards. With the type of harvest conducted at the study site, the time period of respiration becomes important for a "yearly" balance approach. About 40 % of the biomass remaining on the field at harvest is decomposed during the dormant season. The finally resulting numbers for the carbon balance show a "yearly" sink of this agroecosystem of $\sim 250 \text{ g C m}^{-2}$. It is supposed that this sink does not increase the soil carbon content but indicates that the decomposition of the old biomass takes longer than to the next vegetation period.

The assumption of a negligible advective terms in short canopies could neither proofed nor declined. There have been to many instrumental uncertainties and additionally, the meteorological conditions, rainy and cold for the season, have not been ideal for this type of experiment.

5.3 Outlook and future research

Possible exploration of the present data set —

The present study is part of a larger project. At two additional sites measurements with the same type of sensors have been carried out, one in a pine forest and the other above winter wheat. The comparison of the results could enlighten the differences between the three types of vegetation under similar meteorological conditions with respect to the driving forces for NEE or the water need. This data set could be the basis for a regional up scaling or for model validation.

Future experimental areas —

The variability between the different years illustrates the need for long-term studies not only in forests but also in agroecosystems. The eddy covariance technique provides reliable and direct measurements of energy, water and carbon exchange of this agroecosystem. However, there are still many details not yet fully understood in the exchange and transport processes between soil, vegetation and atmosphere. A strong collaboration of soil scientists, hydrologists, biologists and meteorologists in terms of theoretical knowledge, measurement techniques and modelling approaches could improve the knowledge significantly.

Bibliography

- Arya, S. (1988), *An introduction to micrometeorology*, Academic Press, San Diego.
- Aubinet, M., Berbigier, P., Bernhofer, C., Cescatti, A., Feigenwinter, C., Granier, A., Grünwald, T., Havrankova, K., Heinesch, B., Longdoz, B., Marcolla, B., Montagnani, L. and Sedlak, P. (2005), 'Comparing CO₂ storage and advection conditions at night at different CARBOEUROPE sites', *Boundary-Layer Meteorology* **116**, 63–94.
- Aubinet, M., Grelle, A., Ibrom, A., Rannik, U., Moncrieff, J., Foken, T., Kowalski, A., Martin, P., Berbigier, P., Bernhofer, C., Clement, R., Elbers, J., Granier, A., Grünwald, T., Morgenstern, K., Pilegaard, K., Rebmann, C., Snijders, W., Valentini, R. and Vesala, T. (2000), 'Estimates of the annual net carbon and water exchange of forests: The EUROFLUX methodology', *Advances in Ecological Research* **30**, 113–175.
- Aubinet, M., Heinesch, B. and Longdoz, B. (2002), 'Estimation of the carbon sequestration by a heterogeneous forest: night flux corrections, heterogeneity of the site and inter-annual variability', *Global Change Biology* **8**, 1053–1071.
- Aubinet, M., Heinesch, B. and Yernaux, M. (2003), 'Horizontal and vertical CO₂ advection in a sloping forest', *Boundary-Layer Meteorology* **108**, 397–417.
- Baker, N., Bradbury, M., Farage, P., Ireland, C. and Long, S. (1989), 'Measurements of the quantum yield of carbon assimilation and chlorophyll fluorescence for assessment of photosynthetic performance of crops in the field', *Philosophical Transactions of the Royal Society of London. Series B, Biological Sciences* **323**, 295–308.
- Baldocchi, D. (1994), 'A comparative-study of mass and energy-exchange rates over a closed C3 (wheat) and an open C4 (corn) crop. II. CO₂ exchange and water-use efficiency', *Agricultural and Forest Meteorology* **67**, 291–321.
- Baldocchi, D. (2003), 'Assessing the eddy covariance technique for evaluating carbon dioxide exchange rates of ecosystems: past, present and future', *Global Change Biology* **9**, 479–492.
- Baldocchi, D., Falge, E., Gu, L., Olson, R., Hollinger, D., Running, S., Anthoni, P., Bernhofer, C., Davis, K., Evans, R., Fuentes, J., Goldstein, A., Katul, G., Law, B., Lee, X., Malhi, Y., Meyers, T., Munger, W., Oechel, W., Paw U, K., Pilegaard, K., Schmid, H., Valentini, R., Verma, S., Vesala, T., Wilson, K. and Wofsy, S. (2001), 'FLUXNET: A new tool to study the temporal and spatial variability of ecosystem-scale carbon dioxide, water vapor, and energy flux densities', *Bulletin of the American Meteorological Society* **82**, 2415–2434.
- Baldocchi, D., Finnigan, J., Wilson, K., Paw U, K. and Falge, E. (2000), 'On measuring net ecosystem carbon exchange over tall vegetation on complex terrain', *Boundary-Layer Meteorology* **96**, 257–291.
- Baldocchi, D., Valentini, R., Running, S., Oechel, W. and Dahlman, R. (1996), 'Strategies for measuring and modelling carbon dioxide and water vapour fluxes over terrestrial ecosystems', *Global Change Biology* **2**, 159–168.
- Baldocchi, D., Vogel, C. and Hall, B. (1997), 'Seasonal variation of carbon dioxide exchange rates above and below a boreal jack pine forest', *Agricultural and Forest Meteorology* **83**, 147–170.
- Barbour, M., Burk, J., Pitts, W., Gilliam, F. and Schwartz, M. (1999), *Terrestrial Plant Ecology*, Benjamin/Cummings, Menolo Park, California.
- Barr, A., Morgenstern, K., Black, T., McCaughey, J. and Nesic, Z. (2006), 'Surface energy balance closure by the eddy-covariance method above three boreal forest stands and implications for the measurement of the CO₂', *Agricultural and Forest Meteorology* **140**, 322–337.
- Bendat, J. and Piersol, A. (1986), *Random data - Analysis and measurement procedures*, John Wiley & Sons, New York.

- Black, T., den Hartog, G., Neumann, H., Blanken, P., Yang, P., Russell, C., Nesic, Z., Lee, X., Chen, S., Staebler, R. and Novak, M. (1996), 'Annual cycles of water vapour and carbon dioxide fluxes in and above a boreal aspen forest', *Global Change Biology* **2**, 219–229.
- Bonan, G. (2002), *Ecological Climatology - Concepts and Applications*, University Press, Cambridge.
- Burba, G., Anderson, D., Xu, L. and McDermitt, D. (2006), Correcting apparent off-season CO₂ uptake due to surface heating of an open path gas analyzer: progress report of an ongoing study, in '27th Conference on Agricultural and Forest Meteorology, San Diego, May 22–25'.
- Crafts-Brandner, S. and Salvucci, M. (2002), 'Sensitivity of photosynthesis in a C4 plant, maize, to heat stress', *Plant Physiology* **129**, 1773–1780.
- Davidson, E., Janssens, I. and Luo, Y. (2006), 'On the variability of respiration in terrestrial ecosystems: moving beyond Q₁₀', *Global Change Biology* **12**, 154–164.
- Denman, K., Brasseur, G., Chidthaisong, A., Ciais, P., Cox, P., Dickinson, R., Hauglustaine, D., Heinze, C., Holland, E., Jacob, D., Lohmann, U., Ramachandran, S., da Silva Dias, P., Wofsy, S. and Zhang, X. (2007), *Couplings Between Changes in the Climate System and Biogeochemistry*, in S. Solomon, D. Qin, M. Manning, Z. Chen, M. Marquis, K. Averyt, M. Tignor and H. Miller, eds, 'Climate Change 2007: The Physical Science Basis. Contribution of Working Group I to the Fourth Assessment Report of the Intergovernmental Panel on Climate Change', Cambridge University Press, Cambridge, pp. 499–587.
- Desjardins, R. (1985), 'Carbon-dioxide budget of maize', *Agricultural and Forest Meteorology* **36**, 29–41.
- Desjardins, R., Allen, L. and Lemon, E. (1978), 'Variations of carbon dioxide, air temperature, and horizontal wind within and above a maize crop', *Boundary-Layer Meteorology* **14**, 369–380.
- Ehleringer, J. and Cerling, T. (2001), Photosynthetic pathways and climate, in E.-D. Schulze, M. Heimann, S. Harrison, E. Holland, J. Lloyd, I. Prentice and D. Schimel, eds, '*Global Biogeochemical Cycles in the Climate System*', Academic Press, San Diego, pp. 267–278.
- Falge, E., Baldocchi, D., Olson, R., Anthoni, P., Aubinet, M., Bernhofer, C., Burba, G., Ceulemans, G., Clement, R., Dolman, H., Granier, A., Gross, P., Grünwald, T., Hollinger, D., Jensen, N., Katul, G., Keronen, P., Kowalski, A., Lai, C., Law, B., Meyers, T., Moncrieff, J., Moors, E., Munger, J., Pilegaard, K., Rannik, U., Rebmann, C., Suyker, A., Tenhunen, J., Tu, K., Verma, S., Vesala, T., Wilson, K. and Wofsy, S. (2001a), 'Gap filling strategies for long term energy flux data sets', *Agricultural and Forest Meteorology* **107**, 71–77.
- Falge, E., Baldocchi, D., Olson, R., Anthoni, P., Aubinet, M., Bernhofer, C., Burba, G., Ceulemans, R., Clement, R., Dolman, H., Granier, A., Gross, P., Grünwald, T., Hollinger, D., Jensen, N., Katul, G., Keronen, P., Kowalski, A., Lai, C., Law, B., Meyers, T., Moncrieff, H., Moors, E., Munger, J., Pilegaard, K., Rannik, U., Rebmann, C., Suyker, A., Tenhunen, J., Tu, K., Verma, S., Vesala, T., Wilson, K. and Wofsy, S. (2001b), 'Gap filling strategies for defensible annual sums of net ecosystem exchange', *Agricultural and Forest Meteorology* **107**, 43–69.
- Fan, S.-M., Goulden, M., Munger, J., Daube, B., Bakwin, P., Wofsy, S., Amthor, J., Fitzjarrald, D., Moore, K. and Moore, T. (1995), 'Environmental controls on the photosynthesis and respiration of a boreal lichen woodland: a growing season of whole-ecosystem exchange measurements by eddy correlation', *Oecologia* **102**, 443–452.
- Feigenwinter, C., Bernhofer, C., Eichelmann, U., Heinesch, B., Hertel, M., Janous, D., Kolle, O., Lagergren, F., Lindroth, A., Minerby, S., Moderow, U., Mölder, M., Montagnani, L., Queck, R., Rebmann, C., Vestin, P., Yernaux, M., Zeri, M., Ziegler, W. and Aubinet, M. (2008), 'The ADVEX advection field campaigns: Comparison of mean horizontal and vertical non turbulent advective fluxes at three CarboEurope forest sites', *Agricultural and Forest Meteorology* **148**, 12–24.
- Feigenwinter, C., Bernhofer, C. and Vogt, R. (2004), 'The influence of advection on the short

- term CO₂-budget in and above a forest canopy', *Boundary-Layer Meteorology* **113**, 201–224.
- Finnigan, J. (1999), 'A comment on the paper by Lee (1998): "On micrometeorological observations of surface-air exchange over tall vegetation"', *Agricultural and Forest Meteorology* **97**, 55–64.
- Finnigan, J. (2000), 'Turbulence in plant canopies', *Annual Review of Fluid Mechanics* **32**, 519–571.
- Finnigan, J. (2006), 'The storage term in eddy flux calculations', *Agricultural and Forest Meteorology* **136**, 108–113.
- Finnigan, J., Clement, R., Malhi, Y., Leuning, R. and Cleugh, H. (2003), 'A re-evaluation of long-term flux measurement techniques - Part I: Averaging and coordinate rotation', *Boundary-Layer Meteorology* **107**, 1–48.
- Foken, T. (2006), '50 years of the Monin-Obukhov similarity theory', *Boundary-Layer Meteorology* **119**, 431–447.
- Foken, T. and Wichura, B. (1996), 'Tools for quality assessment of surface-based flux measurements', *Agricultural and Forest Meteorology* **78**, 83–105.
- Freedman, J., Fitzjarrald, D., Moore, K. and Sakai, R. (2001), 'Boundary layer clouds and vegetation-atmosphere feedbacks', *Journal of Climate* **14**, 180–197.
- Fuchs, M. and Tanner, C. (1968), 'Calibration and field test of soil heat flux plates', *Soil Science Society of America Proceedings* **32**, 326–328.
- Göckede, M., Foken, T., Aubinet, M., Aurela, M., Banza, J., Bernhofer, C., Bonnefond, J., Brunet, Y., Carrara, A., Clement, R., Dellwik, E., Elbers, J., Eugster, W., Fuhrer, J., Granier, A., Grünwald, T., Heinesch, B., Janssens, I., Knohl, A., Koble, R., Laurila, T., Longdoz, B., Manca, G., Marek, M., Markkanen, T., Mateus, J., Matteucci, G., Mauder, M., Migliavacca, M., Minerbi, S., Moncrieff, J., Montagnani, L., Moors, E., Ourcival, J.-M., Papale, D., Pereira, J., Pilegaard, K., Pita, G., Rambal, S., Rebmann, C., Rodrigues, A., Rotenberg, E., Sanz, M., Sedlak, P., Seufert, G., Siebicke, L., Soussana, J., Valentini, R., Vesala, T., Verbeeck, H. and Yakir, D. (2008), 'Quality control of CarboEurope flux data - PART 1: Coupling footprint analyses with flux data quality assessment to evaluate sites in forest ecosystems', *Biogeosciences* **5**, 433–450.
- Goulden, M., Daube, B., Fan, S., Sutton, D., Bazzaz, A., Munger, J. and Wofsy, S. (1997), 'Physiological responses of a black spruce forest to weather', *Journal of Geophysical Research-Atmospheres* **102**(D24), 28987–28996.
- Goulden, M., Munger, J., Fan, S., Daube, B. and Wofsy, S. (1996), 'Measurements of carbon sequestration by long-term eddy covariance: Methods and a critical evaluation of accuracy', *Global Change Biology* **2**, 169–182.
- Gove, J. and Hollinger, D. (2006), 'Application of a dual unscented Kalman filter for simultaneous state and parameter estimation in problems of surface-atmosphere exchange', *Journal of Geophysical Research* **111**, D08S07, doi:10.1029/2005JD006021.
- Greco, S. and Baldocchi, D. (1996), 'Seasonal variations of CO₂ and water vapour exchange rates over a temperate deciduous forest', *Global Change Biology* **2**, 183–197.
- Grelle, A. and Lindroth, A. (1996), 'Eddy-correlation system for long term monitoring of fluxes of heat, water vapour, and CO₂', *Global Change Biology* **2**, 297–307.
- Gu, L., Falge, E., Boden, T., Baldocchi, D., Black, T., Saleska, S., Suni, T., Verma, S., Vesala, T., Wofsy, S. and Xu, L. (2005), 'Objective threshold determination for nighttime eddy flux filtering', *Agricultural and Forest Meteorology* **128**, 179–197.
- Han, G., Zhou, G., Xu, Z., Yang, Y., Liu, J. and Shi, K. (2007), 'Soil temperature and biotic factors drive the seasonal variation of soil respiration in a maize (*Zea mays* L.) agricultural ecosystem', *Plant Soil* **291**, 15–26.
- Hashemi, A., Herbert, S. and Putnam, D. (2005), 'Yield response of corn to crowding stress', *Agronomy Journal* **97**, 839–846.
- Haverd, V., Cuntz, M., Leuning, R. and Keith, H. (2007), 'Air and biomass heat storage fluxes in a

- forest canopy: Calculation within a soil vegetation atmosphere transfer model', *Agricultural and Forest Meteorology* **147**, 125–139.
- Heinesch, B., Yernaux, M. and Aubinet, M. (2007), 'Some methodological questions concerning advection measurements: a case study', *Boundary-Layer Meteorology* **122**, 457–478.
- Held, A., Steduto, P., Orgaz, F., Matista, A. and Hsiao, T. (1990), 'Bowen ratio/energy balance technique for estimating crop net CO₂ assimilation, and comparison with a canopy chamber', *Theoretical and Applied Climatology* **42**, 203–213.
- Högström, U. and Bergström, H. (1996), 'Organized turbulence structures in the near-neutral atmospheric surface layer', *Journal of Atmospheric Sciences* **53**, 2452–2464.
- Hollinger, D., Kelliher, F., Byers, J., Hunt, J., McSeveny, T. and Weir, P. (1994), 'Carbon dioxide exchange between an undisturbed old-growth temperate forest and the atmosphere', *Ecology* **75**, 134–150.
- Horst, T. (1997), 'A simple formula for attenuation of eddy fluxes measured with first-order-response scalar sensors', *Boundary-Layer Meteorology* **82**, 219–233.
- Houghton, J., Jenkins, J. and Ephraums, J. (1990), *Climate Change: The IPCC Scientific Assessment*, Cambridge University Press, Cambridge.
- Hutchinson, J., Campbell, C. and Desjardins, R. (2007), 'Some perspectives on carbon sequestration in agriculture', *Agricultural and Forest Meteorology* **142**, 288–302.
- IPCC (2007), *Climate Change 2007: The Physical Basis. Contribution of Working Group I to the Fourth Assessment Report of the Intergovernmental Panel on Climate Change.*, Cambridge University Press, Cambridge, chapter Summary for Policymakers, pp. 1–18.
- Jacobs, A., van de Wiel, B. and Holtslag, A. (2001), 'Daily course of skewness and kurtosis within and above a crop canopy', *Agricultural and Forest Meteorology* **110**, 71–84.
- Janssens, I., Lankreijer, H., Matteucci, G., Kowalski, A., Buchmann, N., Epron, D., Pilegaard, K., Kutsch, W., Longdoz, B., Grünwald, T., Montagnani, L., Dore, S., Rebmann, C., Moors, E., Grelle, A., Rannik, U., Morgenstern, K., Oltchev, S., Clement, R., Gudmundsson, J., Minerbi, S., Berbigier, P., Ibrom, A., Moncrieff, J., Aubinet, M., Bernhofer, C., Jensen, N., Vesala, T., Granier, A., Schulze, E.-D., Lindroth, A., Dolman, A., Jarvis, P., Ceulemans, R. and Valentini, R. (2001), 'Productivity overshadows temperature in determining soil and ecosystem respiration across European forests', *Global Change Biology* **7**, 269–278.
- Janssens, I. and Pilegaard, K. (2003), 'Large seasonal changes in Q₁₀ of soil respiration in a beech forest', *Global Change Biology* **9**, 911–918.
- Jones, C. (1986), *CERES-Maize: A simulation model of maize growth and development.*, Texas A&M University Press.
- Kaimal, J., Clifford, S. and Lataitis, R. (1989), 'Effect of finite sampling on atmospheric spectra', *Boundary-Layer Meteorology* **47**, 337–347.
- Kaimal, J. and Finnigan, J. (1994), *Atmospheric boundary layer flows - their structure and measurement*, Oxford University Press, New York.
- Kaimal, J., Wyngaard, J., Izumi, Y. and Cote, O. (1972), 'Spectral characteristics of surface-layer turbulence', *Quarterly Journal of the Royal Meteorological Society* **98**, 563–589.
- Kaufmann, P. and Weber, R. (1996), 'Classification of mesoscale wind fields in the MISTRAL field experiment', *Journal of Applied Meteorology* **35**, 1963–1979.
- Kljun, N., Calanca, P., Rotach, M. and Schmid, H. (2004), 'A simple parameterisation for flux footprint predictions', *Boundary-Layer Meteorology* **112**, 503–523.
- Larcher, W. (1994), *Ökophysiologie der Pflanzen*, Ulmer, Stuttgart.
- Larionova, A., Yevdokimov, I. and Bykhovets, S. (2007), 'Temperature response of soil respiration is dependent on concentration of readily decomposable C', *Biogeosciences* **4**, 1073–1081.
- Laubach, J. and McNaughton, K. (1998), 'A spectrum-independent procedure for correcting eddy fluxes measured with separated sensors', *Boundary-Layer Meteorology* **89**, 445–467.

- Law, B., Thornton, P., Irvine, J., Anthoni, P. and Van Tuyl, S. (2001), 'Carbon storage and fluxes in ponderosa pine forests at different developmental stages', *Global Change Biology* **7**, 755–777.
- Leakey, A., Bernacchi, C., Dohleman, F., Ort, D. and Long, S. (2004), 'Will photosynthesis of maize (*Zea mays*) in the US corn belt increase in future [CO₂] rich atmospheres? An analysis of diurnal courses of CO₂ uptake under free-air concentration enrichment (FACE)', *Global Change Biology* **10**, 951–962.
- Leakey, A., Uribeharrea, M., Ainsworth, E., Naidu, S., Rogers, A., Ort, D. and Long, S. (2006), 'Photosynthesis, productivity, and yield of maize are not affected by open-air elevation of CO₂ concentration in the absence of drought', *Plant Physiology* **140**, 779–790.
- Lee, X. (1998), 'On micrometeorological observations of surface-air exchange over tall vegetation', *Agricultural and Forest Meteorology* **91**, 39–49.
- Lee, X. and Hu, X. (2002), 'Forest-air fluxes of carbon, water and energy over non-flat terrain', *Boundary-Layer Meteorology* **103**, 277–301.
- Lenschow, D. H., Mann, J. and Kristensen, L. (1994), 'How long is long enough when measuring fluxes and other turbulence statistics', *Journal of Atmospheric and Oceanic Technology* **11**, 661–673.
- Leuning, R. (2004), Measurements of trace gas fluxes in the atmosphere using eddy covariance: WPL corrections revisited, in X. Lee, W. Massman and B. Law, eds, 'Handbook of Micrometeorology', Kluwer Academic Publishers, Dordrecht, pp. 119–132.
- Leuning, R. (2007), 'The correct form of the Webb, Pearman and Leuning equation for eddy fluxes of trace gases in steady and non-steady state, horizontally homogeneous flows', *Boundary-Layer Meteorology* **123**, 263–267.
- Lietzke, B. (2008), The role of horizontal CO₂-advection in and above a maize-crop, Master's thesis, University of Basel.
- Lloyd, J. and Taylor, J. (1994), 'On the temperature-dependence of soil respiration', *Functional Ecology* **8**, 315–323.
- Lovett, G., Cole, J. and Pace, M. (2006), 'Is net ecosystem production equal to ecosystem carbon accumulation?', *Ecosystems* **9**, 152–155.
- Maddonni, G., Otegui, M. and Cirilo, A. (2001), 'Plant population density, row spacing and hybrid effects on maize canopy architecture and light attenuation', *Field Crops Research* **71**, 183–193.
- Mahrt, L. (1998), 'Flux sampling errors for aircraft and towers', *Journal of Atmospheric and Oceanic Technology* **15**, 416–429.
- Malhi, Y., McNaughton, K. and von Randow, C. (2004), Low frequency atmospheric transport and surface flux measurements, in X. Lee, W. Massman and B. Law, eds, 'Handbook of Micrometeorology', Kluwer Academic Publishers, Dordrecht, pp. 101–118.
- Massman, W. (2000), 'A simple method for estimating frequency response corrections for eddy covariance systems', *Agricultural and Forest Meteorology* **104**, 185–198.
- Massman, W. and Lee, X. (2002), 'Eddy covariance flux corrections and uncertainties in long-term studies of carbon and energy exchanges', *Agricultural and Forest Meteorology* **113**, 121–144.
- Massman, W. and Tuovinen, J.-P. (2006), 'An analysis and implications of alternative methods of deriving the density (WPL) terms for eddy covariance flux measurements', *Boundary-Layer Meteorology* **121**, 221–227.
- Mauder, M. and Foken, T. (2004), Documentation and instruction manual of the eddy covariance software package TK2, Technical Report 26, Universität Bayreuth.
- McGinn, S. and King, K. (1990), 'Simultaneous measurements of heat, water vapour and CO₂ fluxes above alfalfa and maize', *Agricultural and Forest Meteorology* **49**, 331–349.
- McMillen, R. (1988), 'An eddy-correlation technique with extended applicability to non-simple terrain', *Boundary-Layer Meteorology* **43**, 231–245.
- Moffat, A., Papale, D., Reichstein, M., Hollinger, D., Richardson, A., Barr, A., Beckstein, C., Braswell, B., Churkina, G., Desai, A., Falge,

- E., Gove, J., Heimann, M., Hui, D., Jarvis, A., Kattge, J., Noormets, A. and Stauch, V. (2007), 'Comprehensive comparison of gap-filling techniques for eddy covariance net carbon fluxes', *Agricultural and Forest Meteorology* **147**, 38–50.
- Moncrieff, J., Malhi, Y. and Leuning, R. (1996), 'The propagation of errors in long-term measurements of land-atmosphere fluxes of carbon and water', *Global Change Biology* **2**, 231–240.
- Moncrieff, J., Massheder, J., deBruin, H., Elbers, J., Friborg, T., Heusinkveld, B., Kabat, P., Scott, S., Soegaard, H. and Verhoef, A. (1997), 'A system to measure surface fluxes of momentum, sensible heat, water vapour and carbon dioxide', *Journal of Hydrology* **189**, 589–611.
- Montgomery, R. (1948), 'Vertical eddy flux of heat in the atmosphere', *Journal of Meteorology* **5**, 265–274.
- Moore, C. J. (1986), 'Frequency-response corrections for eddy-correlation systems', *Boundary-Layer Meteorology* **37**, 17–35.
- Obukhov, A. M. (1951), 'Charakteristiki mikrostruktury vetra v prizemnom sloje atmosfery (characteristics of wind microstructure in the atmospheric surface layer)', *Izv. Akad. Nauk SSSR, ser. Geofiz.* **3**, 49–68.
- Oke, T. (1987), *Boundary layer climates*, Routledge, London.
- Oncley, S., Foken, T., Vogt, R., Kohsiek, W., de Bruin, H., Bernhofer, C., Christen, A., van Gorsel, E., Grantz, D., Feigenwinter, C., Lehner, I., Liebethal, C., Liu, H., Mauder, M., Pitacco, A., Ribeiro, L. and Weidinger, T. (2007), 'The energy balance experiment EBEX-2000. part I: Overview and energy balance', *Boundary-Layer Meteorology* **123**, 1–28.
- Panofsky, H. and Dutton, J. (1984), *Atmospheric turbulence - models and methods for engineering applications*, John Wiley & Sons, New York.
- Papale, D., Reichstein, M., Aubinet, M., Canfora, E., Bernhofer, C., Longdoz, B., Kutsch, W., Rambal, S., Valentini, R., Vesala, T. and Yakir, D. (2006), 'Towards a standardized processing of net ecosystem exchange measured with eddy covariance technique: algorithms and uncertainty estimation', *Biogeosciences* **3**, 571–583.
- Papale, D. and Valentini, R. (2003), 'A new assessment of European forests carbon exchanges by eddy fluxes and artificial neural network spatialization', *Global Change Biology* **9**, 525–535.
- Paw U, K., Baldocchi, D., Meyers, T. and Wilson, K. (2000), 'Correction of eddy-covariance measurements incorporating both advective effects and density fluxes', *Boundary-Layer Meteorology* **97**, 487–511.
- Philipona, R., Fröhlich, C. and Betz, C. (1995), 'Characterization of pyrgeometers and the accuracy of atmospheric long-wave radiation measurements.', *Applied Optics* **34**, 1598–1605.
- Raupach, M. (1989), 'A practical lagrangian method for relating scalar concentrations to source distributions in vegetation canopies', *Quarterly Journal of the Royal Meteorological Society* **115**, 609–632.
- Raupach, M., Finnigan, J. and Brunet, Y. (1996), 'Coherent eddies and turbulence in vegetation canopies: The mixing layer analogy', *Boundary-Layer Meteorology* **78**, 351–382.
- Reichstein, M., Falge, E., Baldocchi, D., Papale, D., Aubinet, M., Berbigier, P., Bernhofer, C., Buchmann, N., Gilmanov, T., Granier, A., Grünwald, T., Havrankova, K., Ilvesniemi, H., Janous, D., Knohl, A., Laurila, T., Lohila, A., Loustau, D., Matteucci, G., Meyers, T., Mighletta, F., Ourcival, J.-M., Pumpanen, J., Rambal, S., Rotenberg, E., Sanz, M., Tenhunen, J., Seufert, G., Vaccari, F., Vesala, T., Yakir, D. and Valentini, R. (2005), 'On the separation of net ecosystem exchange into assimilation and ecosystem respiration: review and improved algorithm', *Global Change Biology* **11**, 1424–1439.
- Scheffer, F., Schachtschabel, P., Blume, H.-P., Brümmner, G., Hartge, K. H. and Schwertmann, U. (1998), *Lehrbuch der Bodenkunde*, Ferdinand Enke Verlag, Stuttgart.
- Schimel, D., Melillo, J., Tian, H., McGuire, A., Kicklighter, D., Kittel, T., Rosenbloom, N., Running, S., Thornton, P., Ojima, D., Parton, W., Kelly, R., Sykes, M., Neilson, R. and Rizzo, B. (2000), 'Contribution of increasing CO₂ and climate to carbon storage by ecosystems in the United States', *Science* **287**, 2004–2006.

- Schmid, H. (2002), 'Footprint modeling for vegetation atmosphere exchange studies: a review and perspective', *Agricultural and Forest Meteorology* **113**, 159–183.
- Schotanus, P., Nieuwstadt, F. and DeBruin, H. (1983), 'Temperature-measurement with a sonic anemometer and its application to heat and moisture fluxes', *Boundary-Layer Meteorology* **26**, 81–93.
- Schuepp, P., Leclerc, M., MacPherson, J. and Desjardins, R. (1990), 'Footprint prediction of scalar fluxes from analytical solutions of the diffusion equation', *Boundary-Layer Meteorology* **50**, 355–373.
- Schulze, E.-D., Beck, E. and Müller-Hohenstein, K. (2002), *Pflanzenökologie*, Spektrum Akademischer Verlag, Heidelberg.
- Sharp, R. and Davies, W. (1985), 'Root-growth and water-uptake by maize plants in drying soil', *Journal of Experimental Botany* **36**, 1441–1456.
- Shaw, R. (1977), 'Secondary wind speed maxima inside plant canopies', *Journal of Applied Meteorology* **16**, 514–521.
- Shaw, R., Silversides, R. and Thurtell, G. (1974), 'Some observations of turbulence and turbulent transport within and above canopies', *Boundary-Layer Meteorology* **5**, 429–449.
- Smart, C. (1994), 'Gene expression during leaf senescence', *New Phytologist* **126**, 419–448.
- Stauch, V. and Jarvis, A. (2006), 'A semi-parametric gap-filling model for eddy covariance CO₂ flux time series data', *Global Change Biology* **12**, 1707–1716.
- Steduto, P. and Hsiao, T. (1998a), 'Maize canopies under two soil water regimes. I. Diurnal patterns of energy balance, carbon dioxide flux, and canopy conductance', *Agricultural and Forest Meteorology* **89**, 169–184.
- Steduto, P. and Hsiao, T. (1998b), 'Maize canopies under two soil water regimes. II. Seasonal trends of evapotranspiration, carbon dioxide assimilation and canopy conductance, and as related to leaf area index', *Agricultural and Forest Meteorology* **89**, 185–200.
- Stull, R. (1988), *An introduction to boundary layer meteorology*, Kluwer Academic Publishers, Dordrecht.
- Suyker, A., Verma, S., Burba, G. and Arkebauer, T. (2005), 'Gross primary production and ecosystem respiration of irrigated maize and irrigated soybean during a growing season', *Agricultural and Forest Meteorology* **131**, 180–190.
- Suyker, A., Verma, S., Burba, G., Arkebauer, T., Walters, D. and Hubbard, K. (2004), 'Growing season carbon dioxide exchange in irrigated and rainfed maize', *Agricultural and Forest Meteorology* **124**, 1–13.
- Swinbank, W. (1951), 'The measurement of vertical transfer of heat and water vapor by eddies in the lower atmosphere', *Journal of Meteorology* **8**, 135–145.
- Tjoelker, M., Oleksyn, J. and Reich, P. (2001), 'Modelling respiration of vegetation: evidence for a general temperature-dependent Q₁₀', *Global Change Biology* **7**, 223–230.
- Twine, T., Kustas, W., Norman, J., Cook, D., Houser, P., Meyers, T., Prueger, J., Starks, P. and Wesley, M. (2000), 'Correcting eddy-covariance flux underestimates over a grassland', *Agricultural and Forest Meteorology* **103**, 279–300.
- van Gorsel, E., Leuning, R., Cleugh, H., Keith, H. and Suni, T. (2007), 'Nocturnal carbon efflux: Reconciliation of eddy covariance and chamber measurements using an alternative to the u_{*}-threshold filtering technique', *Tellus B* **59**, 397–403.
- van Wijk, W. and de Vries, D. (1963), *Physics of plant environment*, North-Holland Publishing Co., Amsterdam, chapter Periodic temperature variations in a homogenous soil.
- Verma, S., Baldocchi, D., Anderson, D., Matt, D. and Clement, R. (1986), 'Eddy fluxes of CO₂, water vapor and sensible heat over a deciduous forest', *Boundary-Layer Meteorology* **36**, 71–91.
- Verma, S., Dobermann, A., Cassman, K., Walters, D., Knops, J., Arkebauer, T., Suyker, A., Burba, G., Amos, B., Yang, H., Ginting, D., Hubbard, K., Gitelson, A. and Walter-Shea, E. (2005), 'Annual carbon dioxide exchange in irrigated and rainfed

- maize-based agroecosystems', *Agricultural and Forest Meteorology* **131**, 77–96.
- Verma, S., Kim, J. and Clement, R. (1989), 'Carbon dioxide, water vapor and sensible heat fluxes over a tallgrass prairie', *Boundary-Layer Meteorology* **46**, 53–67.
- Vickers, D. and Mahrt, L. (1997), 'Quality control and flux sampling problems for tower and aircraft data', *Journal of Atmospheric and Oceanic Technology* **14**, 512–526.
- Vleeshouwers, L. and Verhagen, A. (2002), 'Carbon emission and sequestration by agricultural land use: a model study for Europe', *Global Change Biology* **8**, 519–530.
- Vogt, R. (1995), *Theorie, Technik und Analyse der experimentellen Flussbestimmung am Beispiel des Hartheimer Kiefernwaldes*, PhD thesis, University of Basel.
- Vogt, R., Christen, A., Rotach, M., Roth, M. and Satyanarayana, A. (2006), 'Temporal dynamics of CO₂ fluxes and profiles over a central european city', *Theoretical and Applied Climatology* **84**, 117–126.
- Vogt, R. and Reber, S. (1992), 'Das REKLIP-Energiebilanzmessnetz', *Regio Basiliensis - Basler Zeitschrift für Geographie* **108**, 81–92.
- Webb, E., Pearman, G. and Leuning, R. (1980), 'Correction of flux measurements for density effects due to heat and water-vapor transfer', *Quarterly Journal of the Royal Meteorological Society* **106**, 85–100.
- Wieringa, J. (1980), 'A revaluation of the Kansas mast influence on measurements of stress and cup anemometer overspeeding', *Boundary-Layer Meteorology* **18**, 411–430.
- Wilczak, J., Oncley, S. and Stage, S. (2001), 'Sonic anemometer tilt correction algorithms', *Boundary-Layer Meteorology* **99**, 127–150.
- Wilson, J. and Swaters, G. (1991), 'The source area influencing a measurement in the planetary boundary layer: the "footprint" and the "distribution of contact distance"', *Boundary Layer Meteorology* **55**, 25–46.
- Wilson, K., Goldstein, A., Falge, E., Aubinet, M., Baldocchi, D., Berbigier, P., Bernhofer, C., Ceulemans, R., Dolman, H., Field, C., Grelle, A., Ibrom, A., Law, B., Kowalski, A., Meyers, T., Moncrieff, J., Monson, R., Oechel, W., Tenhunen, J., Valentini, R. and Verma, S. (2002), 'Energy balance closure at FLUXNET sites', *Agricultural and Forest Meteorology* **113**, 223–243.
- WMO (2007), 'The state of greenhouse gases in the atmosphere using global observations through 2006', *WMO Greenhouse Gas Bulletin* **3**.
- Wofsy, S., Goulden, M., Munger, J., Fan, S.-M., Bakwin, P., Daube, B., Bassow, S. and Bazzaz, F. (1993), 'Net exchange of CO₂ in a mid-latitude forest', *Science* **260**, 1314–1317.
- Wyngaard, J. (1981), 'The effects of probe-induced flow distortion on atmospheric turbulence measurements', *Journal of Applied Meteorology* **20**, 784–794.
- Wyngaard, J. (1988), 'Flow-distortion effects on scalar flux measurements in the surface-layer - implications for sensor design', *Boundary-Layer Meteorology* **42**(1-2), 19–26.
- Xu, L. and Baldocchi, D. (2004), 'Seasonal variation in carbon dioxide exchange over a mediterranean annual grassland in California', *Agricultural and Forest Meteorology* **123**, 79–96.
- Young, K. and Long, S. (2000), Crop ecosystem responses to climatic change: maize and sorghum, in K. Reddy and H. Hodges, eds, 'Climate change and global crop productivity', CAB International, pp. 107–131.

Curriculum Vitae

Dipl. Geogr. Irene Lehner
October 10, 1975, Solothurn, Switzerland

Post-Doc - since 11/2007

Institute for Atmospheric and Climate Science, ETH Zürich, Switzerland. Group "Land-Climate Interactions" lead by Prof Dr S.I. Seneviratne.

PhD in Meteorology - 06/2008

University of Basel, Switzerland. PhD thesis on "Carbon balance of a rain-fed maize field" supervised by Prof Dr E. Parlow (University of Basel, Switzerland) and Prof Dr C. Bernhofer (TU Dresden, Germany).

Visiting Scientist - 03/2006

One month as visiting scientist at the CSIRO Marine and Atmospheric Research, Canberra, Australia in the working group "Land Air Interactions" (Dr R. Leuning, Dr E. van Gorsel).

Research Assistant - 05/2003 to 03/2007

Institute of Meteorology, Climatology and Remote Sensing, University of Basel, Switzerland (Prof Dr E. Parlow, Dr R. Vogt).

Diploma in Geography - 04/2003

University of Basel, Switzerland. Diploma thesis in meteorology on "Energy Balance of an Irrigated Cotton Field (EBEX2000)" supervised by Prof Dr E. Parlow and Dr R. Vogt. Exams in physical geography (Prof Dr Dr h.c. H. Leser), human geography (Prof Dr R. Schneider-Sliwa), meteorology (Prof Dr E. Parlow) and NLU (Prof Dr P. Nagel, Prof Dr B. Baur).

Scientific Course - 10/2001

Attendance at the "Advanced Short Course on Agricultural, Forest and Micro Meteorology", Bologna, Italy.

Student Research Assistant - 10/2000 to 04/2003

Institute of Meteorology, Climatology and Remote Sensing, University of Basel, Switzerland (Prof Dr E. Parlow, Dr R. Vogt, Prof Dr D. Scherer).

Semester Abroad - 03/2000 to 06/2000

A semester abroad at the Karl-Franzens-University of Graz, Austria.

Placement - 09/1999 to 02/2000

A six month practical training at the German Weather Service, Freiburg i. Br., Germany in the division of biometeorology (Prof Dr G. Jendritzky).

Assistant - 02/1995 to 06/1999

Credit Suisse, Bern and Fribourg, Switzerland.

Matura - 02/1995

Swiss high-school degree with focus on economics and law.